AFFDL-TR-75-137
Volume I

AN AUTOMATED PROCEDURE FOR FLUTTER AND STRENGTH ANALYSIS AND OPTIMIZATION OF AEROSPACE VEHICLES
Volume I. Theory and Application

GRUMMAN AEROSPACE CORPORATION
BETHPAGE, NEW YORK 11714

DECEMBER 1975

TECHNICAL REPORT AFFDL-TR-75-137, Volume I
FINAL REPORT FOR PERIOD MARCH 1972 – DECEMBER 1975

AIR FORCE FLIGHT DYNAMICS LABORATORY
AIR FORCE WRIGHT AERONAUTICAL LABORATORIES
Air Force Systems Command
Wright-Patterson Air Force Base, Ohio 45433

NOTICE

When Government drawings, specifications, or other data are used for any purpose other than in connection with a definitely related Government procurement operation, the United States Government thereby incurs no responsibility nor any obligation whatsoever; and the fact that the government may have formulated, furnished, or in any way supplied the said drawings, specifications, or other data is not to be regarded by implication or otherwise as in any manner licensing the holder or any other person or corporation, or conveying any rights or permission to manufacture, use, or sell any patented invention that may in any way be related thereto.

This report has been reviewed and is approved for publication.

Stephen M. Batill

STEPHEN M. BATILL, CAPTAIN, USAF
Project Engineer
Design Analysis Group
Aerospace Dynamics Branch

FOR THE COMMANDER

Gerald G. Leigh

GERALD G. LEIGH, Lt. Col, USAF
Chief, Structures Division

Copies of this report should not be returned unless return is required by security considerations, contractual obligations, or notice on a specific document.

AIR FORCE - 12 MARCH 1976 - 150

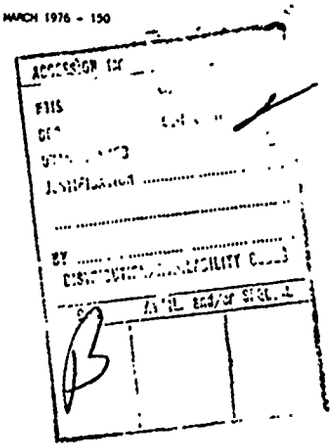

UNCLASSIFIED

SECURITY CLASSIFICATION OF THIS PAGE (When Data Entered)

REPORT DOCUMENTATION PAGE	READ INSTRUCTIONS BEFORE COMPLETING FORM
1. REPORT NUMBER: AFFDL-TR-75-137-Vol-I	2. GOVT ACCESSION NO. / 3. RECIPIENT'S CATALOG NUMBER
4. TITLE (and Subtitle): AN AUTOMATED PROCEDURE FOR FLUTTER AND STRENGTH ANALYSIS AND OPTIMIZATION OF AEROSPACE VEHICLES, Volume I, Theory and Application	5. TYPE OF REPORT & PERIOD COVERED: Final Report, 15 Mar 1972 – Dec 1975
	6. PERFORMING ORG. REPORT NUMBER
7. AUTHOR(s): Keith Wilkinson, Joel Markowitz, Edwin Lerner, Richard Chipman, Dino George	8. CONTRACT OR GRANT NUMBER(s): F33615-72-C-1101
9. PERFORMING ORGANIZATION NAME AND ADDRESS: Grumman Aerospace Corporation, Bethpage, New York 11714	10. PROGRAM ELEMENT, PROJECT, TASK AREA & WORK UNIT NUMBERS: 62201F, AF-1370-01-07
11. CONTROLLING OFFICE NAME AND ADDRESS: Air Force Flight Dynamics Laboratory, Air Force Wright Aeronautical Laboratories, Air Force Systems Command, Wright-Patterson Air Force Base, Ohio 45433	12. REPORT DATE: December 1975
	13. NUMBER OF PAGES: 198
14. MONITORING AGENCY NAME & ADDRESS (if different from Controlling Office)	15. SECURITY CLASS. (of this report): Unclassified
	15a. DECLASSIFICATION DOWNGRADING SCHEDULE

16. DISTRIBUTION STATEMENT (of this Report)

Distribution limited to U.S. Government agencies only; test and evaluation; statement applied 31 December 1975. Other requests for this document must be referred to AF Flight Dynamics Laboratory, FYS, Wright-Patterson AFB, Ohio 45433

17. DISTRIBUTION STATEMENT (of the abstract entered in Block 20, if different from Report)

18. SUPPLEMENTARY NOTES

19. KEY WORDS (Continue on reverse side if necessary and identify by block number)

Structural Analysis
Flutter Analysis
Structural Optimization
Flutter Optimization
Minimum-Weight Design

20. ABSTRACT (Continue on reverse side if necessary and identify by block number)

This volume documents the theoretical developments that are incorporated into a computer program entitled FASTOP (Flutter And STrength Optimization Program). The program is capable of both integrated analysis and efficient (near-minimum weight) sizing of cantilever or free-free lifting surface structures in the presence of strength and flutter-speed constraints. Automated resizing of a finite-element structures model in FASTOP leads to an efficient

(over)

DD FORM 1 JAN 73 1473 EDITION OF 1 NOV 65 IS OBSOLETE

UNCLASSIFIED

SECURITY CLASSIFICATION OF THIS PAGE (When Data Entered)

20. ABSTRACT (Continued)

final design in which three categories of elements exist, viz.: --

- o elements at manufacturing constraints,
- o strength-critical elements (these elements are fully stressed for at least one load condition),
- o flutter-critical elements (these elements, which were resized for flutter without encountering manufacturing or strength constraints, have uniform flutter-velocity derivatives).

The specific analysis and redesign capabilities of FASTOP are summarized below:

Applied Loads - Inertial and aerodynamic (subsonic and/or supersonic)

Structural Analysis and Resizing - Primarily for metallic structures but with limited composite capability

Vibration Analysis - Cantilever or free-free structures

Flutter Analysis - Assumed pressure function and doublet-lattice methods for subsonic flow; Mach-box method for supersonic flow

Flutter Resizing - Applicable to metallic and composite structures

Three examples of structures that were optimized using FASTOP are included to demonstrate the various features of the program.

FOREWORD

This final report was prepared by the Structural Mechanics Section of the Grumman Aerospace Corporation, Bethpage, New York, for the Vehicle Dynamics and Structures Division, Air Force Flight Dynamics Laboratory, Wright-Patterson Air Force Base, Ohio. The work was performed under Contract No. F33615-72-C-1101, which was initiated under Project No. 1370, "Dynamic Problems in Flight Vehicles", Task No. 01, "Aeroelastic Problems". Initially Mr. R. F. Taylor (FYS) and Dr. V. B. Venkayya (FBR) were the Project Monitors of this contract, after which Capt. S. M. Batill (FYS) assumed this position.

The report consists of two volumes. Volume I, entitled "Theory and Application", describes the analysis and redesign procedures provided by a computer program system for minimum-weight design of cantilever or free-free lifting-surface structures subject to combined strength and flutter-speed requirements. Detailed instructions required to use this Flutter And STrength Optimization Program (FASTOP) are provided in Volume II, entitled "Program User's Manual". The report, which covers work conducted between 15 March 1972 and 31 December 1975, was submitted to the Air Force in December 1975.

Dr. W. Lansing was the Program Manager and Mr. K. Wilkinson was the Project Engineer. Principal contributors to the project and their associated areas of responsibility include: Messrs. D. George and G. R. Schriro - Overall Program Integration and Final Checkout; Dr. J. Markowitz - Integration of Flutter Redesign and Strength Redesign Program Functions; Messrs. E. Lerner and J. H. Berman - Evaluation of Candidate Flutter Redesign Procedures; Messrs. R. R. Chipman and M. Chernoff - Development of Integrated Flutter Analysis Module; Dr. W. J. Dwyer - Strength Analysis and Redesign Module; Mr. P. Shyprykevich - Applied Loads Analysis Module; Messrs. M. J. Shapiro and S. Goldenberg - Vibration Analysis Module. The continued assistance and advice of Mr J. Smedfjeld and Capt. S. M. Batill have been greatly appreciated. The authors also wish to acknowledge Mr. W. Mykytow and Dr. L. Berke for initiating this effort and for their valuable suggestions during the course of the project.

TABLE OF CONTENTS

TABLE OF CONTENTS (Continued)

TABLE OF CONTENTS (Continued)

TABLE OF CONTENTS (Concluded)

LIST OF ILLUSTRATIONS

LIST OF ILLUSTRATIONS (Continued)

LIST OF ILLUSTRATIONS (Concluded)

LIST OF TABLES

tion 1

INTRODUCTION

In order to meet the increasingly restrictive budgetary and schedule constraints imposed on aerospace vehicle development programs, considerable attention has been devoted in recent years to automation of the aircraft design process. This effort has largely focused on the refinement and integration of existing analysis tools (e.g., see References 1-1 and 1-2). At the same time, some significant advances have been made in the development of automated redesign procedures as a further means of accelerating the the design cycle (e.g., see Reference 1-3).

The computer program described in this report falls into both of these categories. Its capabilities encompass integrated interdisciplinary analysis as well as enhanced automated redesign for aircraft lifting - surface structures. The analysis capability includes loads prediction, structural analysis, vibration mode determination, and flutter analysis. The redesign procedure minimizes the weight of a lifting - surface structure in the presence of combined strength and flutter-speed constraints. The entire program is known as FASTOP, for Flutter And STrength Optimization Program.

Before describing the specific features of this program, it is valuable to review some of the background and objectives which governed its development.

The strength analysis and redesign module in FASTOP was developed several years ago under a contract sponsored by the Air Force Flight Dynamics Laboratory. This program, known as ASOP (Automated Structural Optimization Program), automatically resizes the gages of a finite-element structures model to achieve a fully stressed (near-minimum-weight) design for specified design load conditions. Prior to the advent of automated strength resizing procedures, the stress analyst was faced with the time consuming task of computing element stresses based on the results of a finite-element analysis, and then manually resizing the preliminary gages of the structures model. This process had to be repeated until an acceptable design was achieved. Consequently the automated resizing capability in ASOP has resulted in a significant reduction in the time required for the strength design of airplane structures.

The major objective in developing FASTOP has been to integrate the aforementioned strength redesign program with a new automated procedure for minimum-weight resizing to satisfy a flutter-speed constraint. This requirement originated from the obvious inefficiencies in existing flutter prevention procedures, wherein the flutter analyst relies largely on judgement in pursuing an adequate flutter "fix". Such an approach often leads to many trial and error studies which are particularly inefficient because of the non-automated interface between the flutter analysis and structural analysis procedures. That is, any stiffness change to be considered in the course of a flutter investigation must be evaluated through manual changes to the input data of the structural analysis program. New stiffness properties, vibration modes, and a flutter speed are then computed on a step-by-step basis via individual computer programs. The time required for each of these tasks and the number of "fixes" to be evaluated obviously increase in proportion to the complexity of the structures model under investigation.

Automation of this interactive strength/flutter redesign process has been accomplished in FASTOP, providing the user with redesign capability for small-or large-scale structures models. Moreover, the flutter redesign procedure, which evolved from an extensive evaluation of candidate approaches, has been demonstrated to achieve a minimum-weight redesign for flutter-critical configurations.

This report describes the various analysis and redesign procedures included in FASTOP. Results obtained from the analysis and resizing of three sample structures are also presented. After first providing an overview of the entire FASTOP system, each of the major analysis and redesign functions is discussed in a separate section. It will be noted that the depth of detail varies in each of these sections. Where adequate documentation of well-known methods already exists, as, for example, in the discussion of the structural analysis methods, considerable reliance is placed on this documentation, and the discussion only summarizes the procedures. On the other hand, even though some other techniques are already documented, it is felt that they may be less familiar to the reader and that he would benefit from having them discussed in detail and included in this volume for completeness. In other instances, where the analysis capability provided in a parti-

cular discipline extends into areas beyond the original intended scope of this contract, as, for example, in the consideration of wing-body aerodynamic interference and in the computation of divergence speed in the flutter analysis section, only a brief discussion of these features is included.

Section 2

OVERVIEW OF THE FASTOP SYSTEM

The FASTOP system provides capability for the analysis and near-minimum-weight structural sizing of a lifting surface to meet strength and flutter-speed requirements. A functional flow diagram of the system is presented in Figure 2.1. The package is comprised of two major programs, each one designed to perform successive analysis and resizing functions in a single computer submission. The Strength Optimization Program (SOP) focuses on basic aspects of static structural analysis and minimum-weight design for strength requirements. It provides for automated calculation of applied loads, performance of conventional strength and flexibility (or stiffness) analysis, and automated resizing of a structural idealization to achieve a fully stressed design. It also prepares data required for direct input to the second major program. The Flutter Optimization Program (FOP) addresses dynamic analysis requirements and provides the redesign capability for achieving a desired value of flutter speed with minimum cost in weight. Using output data from the first program, it proceeds to establish mass matrix input for vibration mode analysis, compute normal mode shapes and frequencies, determine the surface's critical flutter speed, and perform resizing if desired to increase flutter speed. Finally, the second program saves data required for re-entering SOP.

The use of this two-program approach for redesign proceeds as follows. First, using SOP, the structure is sized to satisfy its strength requirements with a fully stressed design. The structural elements after this step can be in either of two categories - fully stressed (i.e., strength-critical) or at a prespecified minimum gage (as dictated, for example, by manufacturing considerations). Then, using FOP, resizing of structural and/or mass-balance variables is performed to increase the critical flutter speed of the surface. No structural elements can be reduced in this step, since this would cause them to fall below the gages previously required by SOP. The structural variables that are increased in the second step, plus any mass-balance variables that have been specified by the user, constitute an initial set of "flutter-critical" elements, i.e., elements whose sizes have been dictated by flutter-speed requirements. The structural variables that have been increased by FOP are now removed from the previous strength-critical and minimum-gage categories.

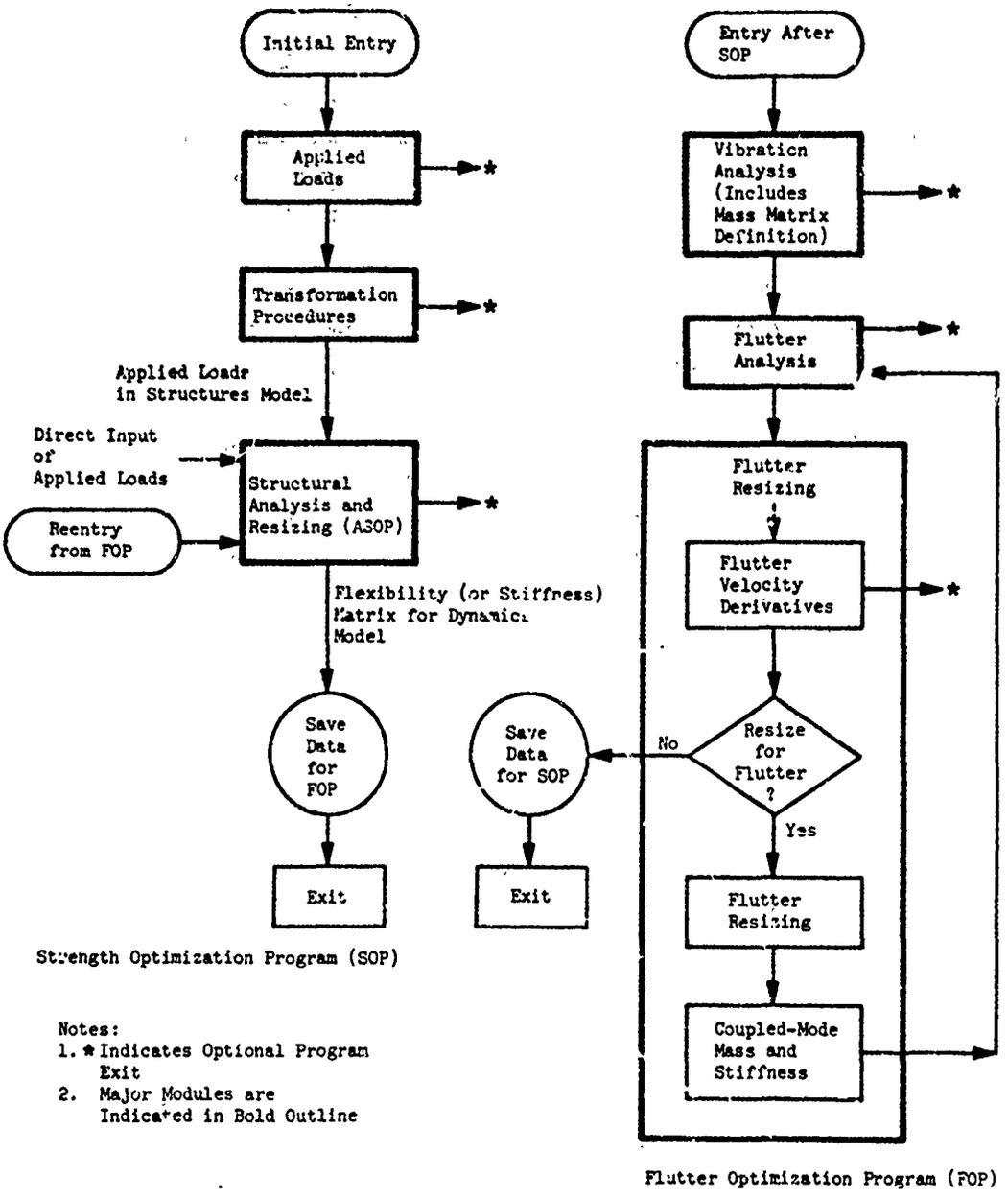

Figure 2.1. Functional Flow Diagram for the FASTOP System

Since the resizing of certain structural elements to achieve an increase in flutter speed may alter the internal load distributions and therefore the resulting gage requirements for strength considerations, SOP is now re-entered. This is the first step toward achieving a minimum-weight design accounting for strength/flutter interaction. In this step, no flutter-critical element, and of course no element at the prescribed minimum gage, can be resized downward, but the remaining elements, which constitute the newly defined set of strength-critical elements, can be either decreased or increased. Again, a reclassification of the various elements into strength-critical, flutter-critical, and minimum-gage categories takes place. For example, if a previously flutter-critical element is resized upward to meet strength requirements, it is now moved into the strength-critical set; similarly, if a previously strength-critical element can be reduced in weight until it reaches its prescribed minimum gage, it is now put into the minimum-gage category.

At this point, FOP is entered for the second time, and the strength/flutter interactive redesign continues. The resizing that can take place in this second pass through FOP is more flexible than that which occurred the first time, in that now there is a set of flutter-critical structural elements that can be resized either upward or downward. Any downward resizing cannot violate the values required by strength or minimum-gage considerations, however. As before, elements in the new sets of strength-critical and minimum-gage variables can only be resized upward, and if this occurs they are reclassified as flutter-critical.

Subsequent interactive application of the two programs proceeds in a manner similar to the second passes until, in the opinion of the user, the process is sufficiently converged. The final design will consist of a set of flutter-critical elements which have nearly uniform flutter-velocity derivatives, a set of strength-critical elements which are fully stressed, and a set of elements which are at the user prescribed minimum gages.

While it is felt that the two-program approach provides the most logical "stop points" needed by the user for appraisal of intermediate results and possible revision of redesign step-size control parameters, it is still possible to use a multiple-step option to exercise the analysis and redesign functions of both programs without interruption. It is also noted (as indicated in Figure 2.1) that provision is made to exit either program after performing

specific analysis or redesign functions, thereby affording the user the opportunity to monitor the results even more closely or, if he wishes, exercise individual portions of the system independently. Finally, if a user observes that flutter resizing occurs in a very local area with only minor interaction with strength requirements, the flutter resizing program can be used several times in succession, using coupled-mode flutter analyses, before returning to another strength resizing step. In this situation it is recommended, however, that SOP be used in an analysis mode to compute a new flexibility (or stiffness) matrix for a new normal-mode calculation after each resizing step; if coupled modes are used, the accuracy of the flutter-velocity derivatives deteriorates rapidly, and improper resizing steps can result.

In both programs, considerable emphasis has been placed on the modular programming concept, so that the system's capability can readily be extended in the future. The analysis and redesign functions of both programs are performed with the following six modules:

- Applied Loads
- Structural Analysis and Resizing
- Transformation Procedures
- Vibration Analysis (Including Mass Matrix Definition)
- Flutter Analysis
- Flutter Resizing

The capabilities of the individual analysis and redesign routines are briefly summarized below:

Applied Loads

Aerodynamic

Maximum number of flight conditions (subsonic and/or supersonic)	8
Maximum number of control surfaces	8
Maximum number of aerodynamic panels	100

Inertial

Maximum number of flight conditions	8
Maximum number of distributed (point) masses	1000
Maximum number of concentrated (mass and inertia) masses	100

Structural Analysis and Resizing

Primarily for metallic structures (limited composites capability)

Maximum allowable number of finite elements to define the structures model	3000
Maximum number of structures model node points	1000
Maximum number of structures model degrees of freedom	6000*
Maximum number of applied load conditions	8

Vibration Analysis

Maximum number of dynamics model degrees of freedom	200

Flutter Analysis

Assumed-pressure-function and doublet-lattice routines for subsonic flow	M=0→0.9
Mach-box routine for supersonic flow	M=1.2→3.0
Maximum number of modes for flutter analysis	20
Maximum number of control surfaces on main surface for doublet-lattice and Mach-box routines	5
Maximum number of aerodynamic panels:	
Doublet-lattice	400
Mach-box	350

Flutter Resizing

Maximum number of elements which can be resized for flutter:	
Structural elements	2000
Mass-balance elements	20

The following sections describe the theory and procedures in each program module. Each section begins with a brief summary to enable the reader to quickly grasp the intent of each analysis and to understand its relationship to the overall system.

*Reduces to 3000 if subsequent flutter resizing uses a free-free vibration model; unchanged for cantilever model.

Section 3

APPLIED LOADS ANALYSIS

3.1 SUMMARY

The applied loads analysis module provides the capability for computing aerodynamic and inertial loads for specified maneuver conditions. The aerodynamic forces are computed by modeling the lifting surface with a distribution of vortices for subsonic flow or with a distribution of sources for supersonic flow. For flight conditions expressed in terms of vehicle load factors and angular accelerations and velocities, inertial loads are computed at a gridwork of concentrated and distributed masses. The aerodynamic and inertial forces are then transformed from their respective math models to the structures model using transformations computed in a separate transformation analysis module described in Section 5. FASTOP also provides the capability for the direct input of known loads in the structures model.

3.2 AERODYNAMIC LOADS

To obtain surface aerodynamic forces, the planform is subdivided into an arbitrary number of small trapezoidal panels (not more than 100) in a fashion dictated by the overall planform geometry and the locations of the control surfaces. The number of panels in the chordwise direction can vary over the span. Using the same panel geometry for all Mach numbers, aerodynamic influence coefficients corresponding to these panels are computed and stored on tape using either subsonic vortex-lattice theory (Reference 3-1) or the supersonic source distribution theory (Reference 3-2). For subsonic flow only, the effect of a fuselage on the lift on the wing can be modelled in this program using the method of images. By multiplying the aerodynamic influence coefficients by prescribed dynamic pressures and downwash distributions, the forces are determined for the selected loading conditions. Provision for various correction factors is included.

3.2.1 Subsonic Influence Coefficients

In subsonic flow, the calculation of aerodynamic influence coefficients is based on the vortex-lattice method of Reference 3-1. If a distribution of vortices is placed on the surface of a planform, the resulting downwash at any point, P_j, is related to the circulations of the vortices by:

$$w(P_j) = \frac{\bar{w}}{U} = \frac{1}{4\pi U} \iint_S \gamma(P)\, K(P_j, P, M)\, dS, \qquad (3.1)$$

where

- P is any point on the planform with coordinates ξ, η, ζ
- P_j is a j^{th} point with coordinates x, y, z
- x, ξ are streamwise coordinates
- y, η are spanwise coordinates
- z, ζ are vertical coordinates
- S is the surface
- w is the downwash angle
- $\bar{w}$ is the downwash velocity
- U is the free stream velocity
- γ is the circulation
- M is the Mach number
- K is the kernel function representing the downwash created at a point due to a unit circulation over a unit area of a vortex sheet.

From the Kutta-Joukowsky theorem, it is known that circulation can be related to the lift and, hence, to the pressure coefficient, C_p. Consequently, the above equation can be written

$$w(P_j) = \frac{1}{8\pi} \iint_S C_p(P)\, K(P_j, P, M)\, dS. \qquad (3.2)$$

In the present method, the given surface is divided into a lattice of I panels, the sides of which parallel the free stream (see Figure 3.1) and over each of which the pressure is assumed constant. Equation (3.2) becomes

$$w(P_j) = \frac{1}{8\pi} \sum_{i=1}^{I} C_{p_i} \iint_{\text{Panel } i} K(P_j, P, M)\, dS. \tag{3.3}$$

With the further assumption that the vortices in each panel are condensed to a single horseshoe vortex, the bound portion of which lies at the quarter chord of the panel, the equation reduces to

$$w(P_j) = \frac{1}{8\pi} \sum_{i=1}^{I} C_{p_i}\, \Delta\xi_i \int_{\text{Panel } i} K(P_j, P(\xi_{\frac{1}{4}}), M)\, dS, \tag{3.4}$$

where $\Delta\xi_i$ is the average chord length of the i^{th} panel and the integration is taken along the quarter-chord of the i^{th} panel. Using the Biot-Savart law, the final integral is evaluated in Reference 3-3, yielding

$$\int_{\text{Panel } i} K(P_j, P(\xi_{\frac{1}{4}}), M)\, dS = E_{ji} = F_{ji} + G_{ji}, \tag{3.5}$$

where

E_{ji} is the downwash at point j induced by a horseshoe vortex of unit strength and length at panel i

F_{ji} is the contribution to E_{ji} due to the trailing vortices

G_{ji} is the contribution to E_{ji} due to the bound vortex.

If it is desired in determining the pressure distribution on a wing to account for the effects of the presence of a fuselage, this is accomplished as in Reference 3-4 by including within the fuselage an image of each horseshoe vortex on the wing (see Figure 3.2). In this idealization, the fuselage is assumed to be a circular cylinder of radius R and the image of a point (x, y) is located at $(x, R^2/y)$. The downwash induced by the point and its image is

$$E_{ji} = (F_{ji} + F'_{ji}) + (G_{ji} + G'_{ji})\,(1 + R^2/y_j^2), \tag{3.6}$$

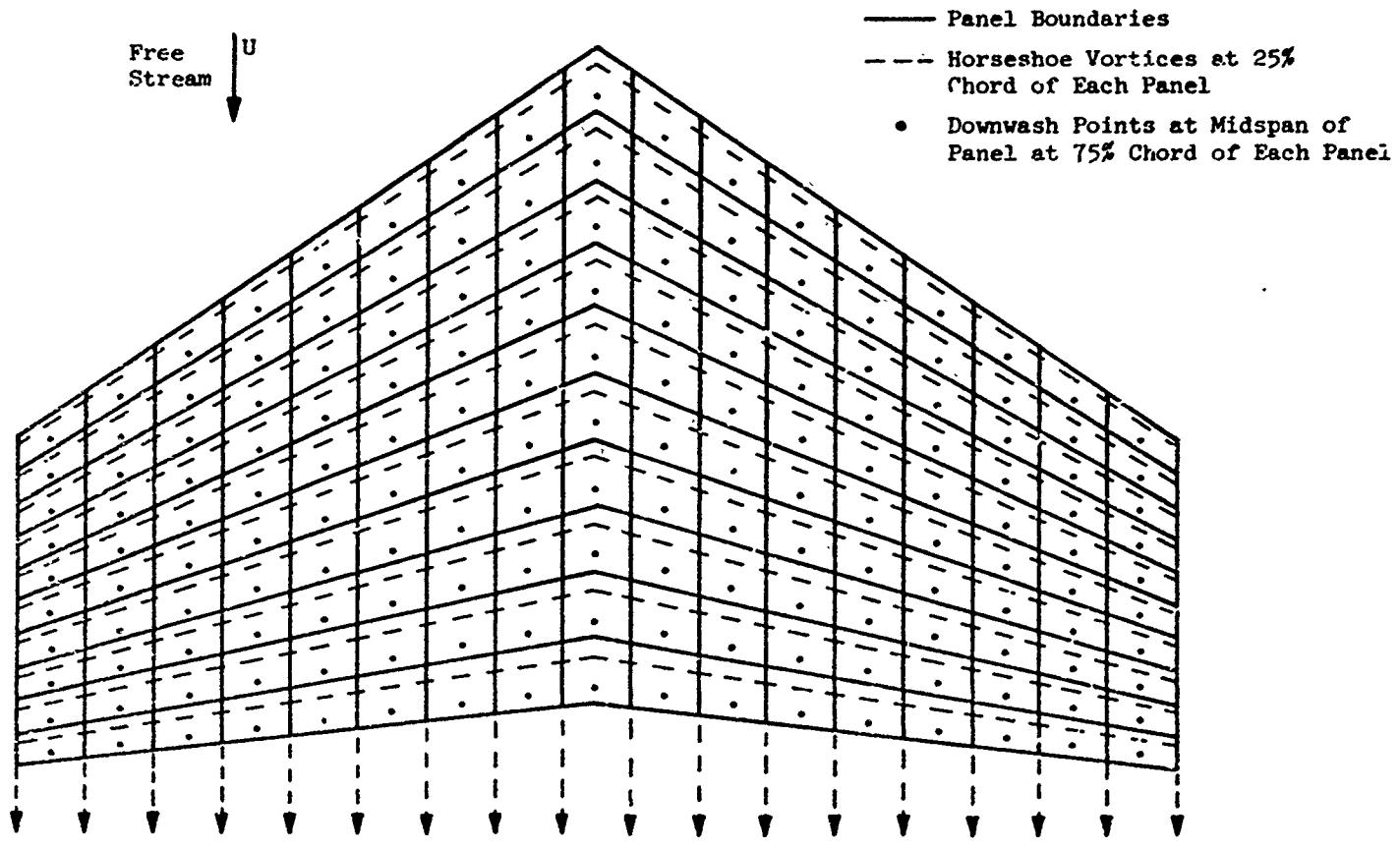

Figure 3.1. Horseshoe Vortices and Downwash Points .

where F'_{ji} and G'_{ji} are due to the image and where the correction factor, $(1 + R^2/y_j^2)$, on the downwash due to the bound vortex is derived from two-dimensional theory.

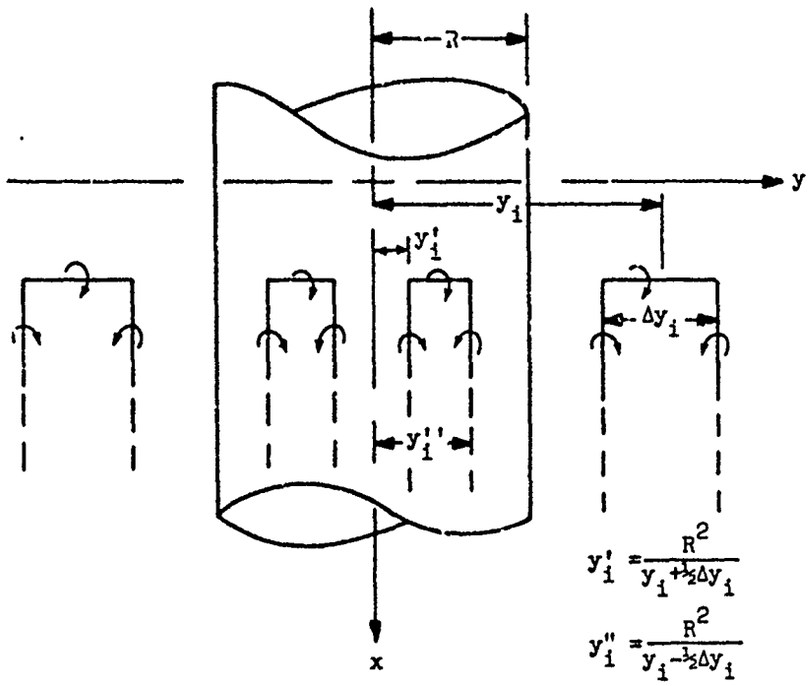

Figure 3.2. Cylinder with a Pair of Horseshoe Vortices and their Images.

Substituting the appropriate value of E_{ji} for the integral in Equation (3.4), one obtains

$$w(P_j) = \frac{1}{8\pi} \sum_{i=1}^{I} C_{p_i} \Delta\xi_i E_{ji}. \tag{3.7}$$

If a point P_j is chosen at the 3/4-chord and midspan of each of the I panels and the above equation is applied at each such point, a system of simultaneous linear equations results, which in matrix notation is

$$\{w\} = \frac{1}{8\pi} \left[\Delta\xi\right] \left[E\right] \left\{C_p\right\}. \tag{3.8}$$

This system can be solved for the pressure distribution:

$$\left\{C_p\right\} = \left[\frac{8\pi}{\Delta\xi}\right]\left[E\right]^{-1} \left\{w\right\}. \tag{3.9}$$

From this equation, an aerodynamic influence coefficient matrix can be defined as

$$\left[AIC\right] = \left[\frac{8\pi}{\Delta\xi}\right]\left[E\right]^{-1} \tag{3.10}$$

The downwash angle distribution, $\{w\}$, used in Equation (3.9) can be considered to consist of contributions, $\{w_1\}$, due to the rigid surfaces inclination to the free stream and contributions, $\{w_2\}$, arising from the deflections of any control surfaces on the surface. The first of these contributions is comprised of three terms

$$\{w_1\} = \{\alpha_e\} + k_2 \{\alpha_2\} + k_3 \{\alpha_3\}, \tag{3.11}$$

where

$\{\alpha_e\}$ is the effective angle of attack of the surface optionally in the presence of a fuselage

$\{\alpha_2\}$ is the distribution of local incremental angles of attack due to camber and twist

$\{\alpha_3\}$ is a distribution of additive corrections to the local incidences based on empirical or experimental data

k_2, k_3 are scalar correction factors also based on empirical or experimental data.

The effective angle of attack equals the sum of the geometric angle of attack of the wing relative to the fuselage and terms due to the fuselage's inclination and the upwash induced by this inclination.

$$\{\alpha_e\} = k_1 \alpha_1 \{1\} + \alpha_f [1 + R^2/y^2] \left[C_1\right] \{1\}, \tag{3.12}$$

where

α_1 is the geometric angle of incidence of the wing relative to the fuselage reference line

α_f is the angle of attack of the fuselage reference line

R is the mean radius of the fuselage

y is the spanwise coordinate of the panel of interest measured from the fuselage centerline

k_1, $\left[C_1\right]$ are scalar corrections factors.

The contribution to the downwash due to N control surface deflections is

$$\{w_2\} = \sum_{n=1}^{N} \left(\delta_{L,n} \left[C_2\right]_n \{U\}_n + k_{4_n} \{\delta_{2,n}\} \right) + \sum_{n=1}^{N} \left(\delta_{R,n} \left[C_2\right]_n \{U\}_n + k_{4_n} \{\delta_{2,n}\} \right), \tag{3.13}$$

where

N is the number of control surfaces

$\delta_{L,n}$, $\delta_{R,n}$ are the rotations of the n^{th} left and right control surfaces respectively

$\{U\}_n$ are fractions ($0 \leq Uj,n \leq 1$) denoting the portion of the j^{th} aerodynamic panel that lies on the n^{th} control surface.

$\{\delta_{2,n}\}$ are additive corrections to the local rotation of the n^{th} control surface

$\left[C_2\right]_n$, k_{4_n} are scalar correction factors.

It should be noted that, in the absence of any correction factor, the downwash distribution on a wing without fuselage or control surfaces is quite simple, namely $\{w\} = \alpha_1 \{1\} + \{\alpha_2\}$.

3.2.2 Supersonic Influence Coefficients

In supersonic flow, aerodynamic influence coefficients are obtained as described in Reference 3-2 using a distribution of sources. The pressure at a point on a planar surface is related to the velocity potential and, thence, to the downwash by

$$C_p(P_j) = \frac{-2}{U} \frac{\partial \varphi (x, y)}{\partial x} = \frac{2}{\pi} \frac{\partial}{\partial x} \iint_S \frac{w}{R} \, d\xi d\eta, \qquad (3.14)$$

C_p is the pressure coefficient

P_j is a j^{th} point with coordinates x and y

x and ξ are streamwise coordinates

y and η are spanwise coordinates

U is the free-stream velocity

φ is the velocity potential

w is the downwash angle at ξ, η

$R = \sqrt{(x - \xi)^2 - \beta^2 (y - \eta)^2}$

$\beta^2 = M^2 - 1$

M is the Mach number

S is the area of integration bounded by the inverse Mach cone emanating from (x, y).

For a surface with supersonic leading and trailing edges, the area of integration is bounded by the leading edge (see Figure 3.3a). Near a side edge of such a surface, however, the potential is influenced by a region off the wing as indicated by S_D in Figure 3.3b. For such a case, Reference 3-5 shows that the effect of this off-wing region is to negate the contribution of the on-wing region S_w' delimited by the leading edge, the side edge and the reflected Mach line. Consequently, only the shaded area S_w need be considered for the integration in Equation 3.13.

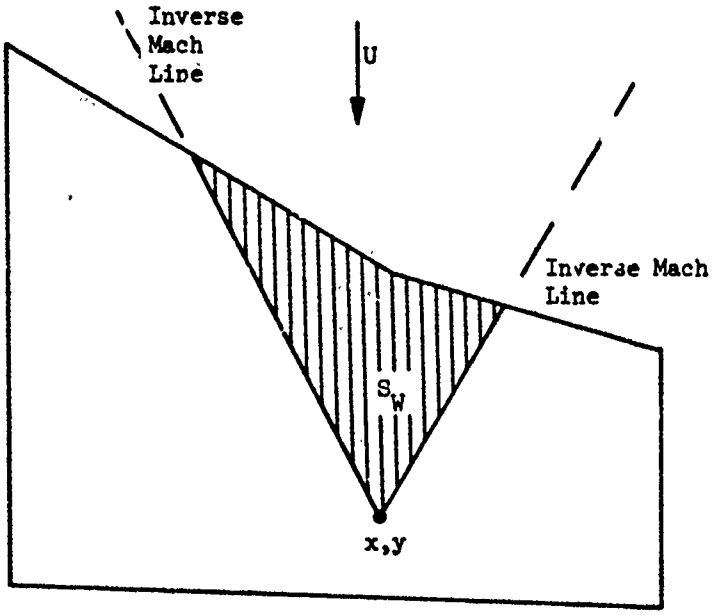

(a) Interior Point

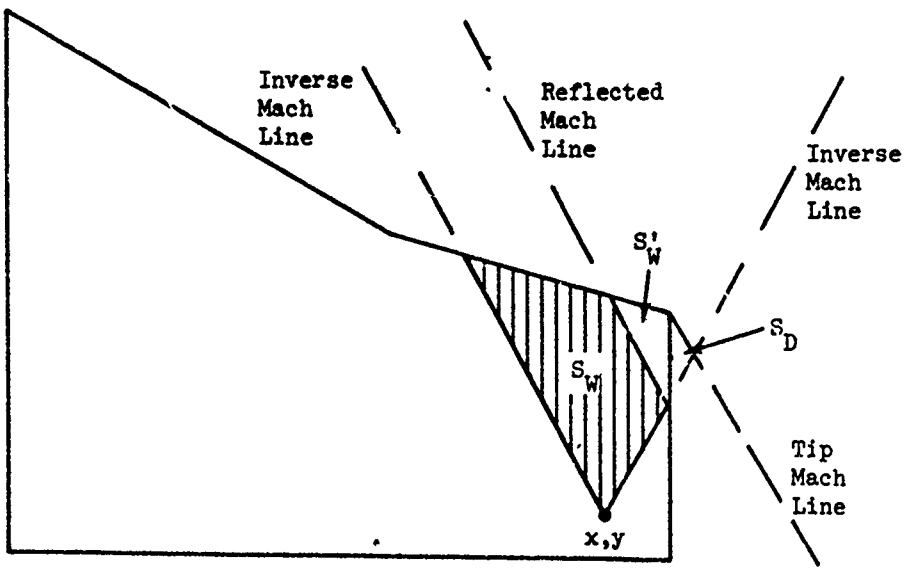

(b) Point near the Tip

Figure 3.3. Areas of Integration on a Wing with Supersonic Leading and Trailing Edges.

This concept can be extended to the case of subsonic leading edges. Referring to Figure 3.4, the areas between the foremost Mach waves, OB' and OD' and the wing leading edges, OEB and OGD, will affect the potential and cancel the influence of the regions BEC, EFH, etc. ahead of the reflected Mach lines BC, EF, etc. Thus, the areas to be considered in the integration are the successively forward quadrilaterals ABCD, CEFG, etc.

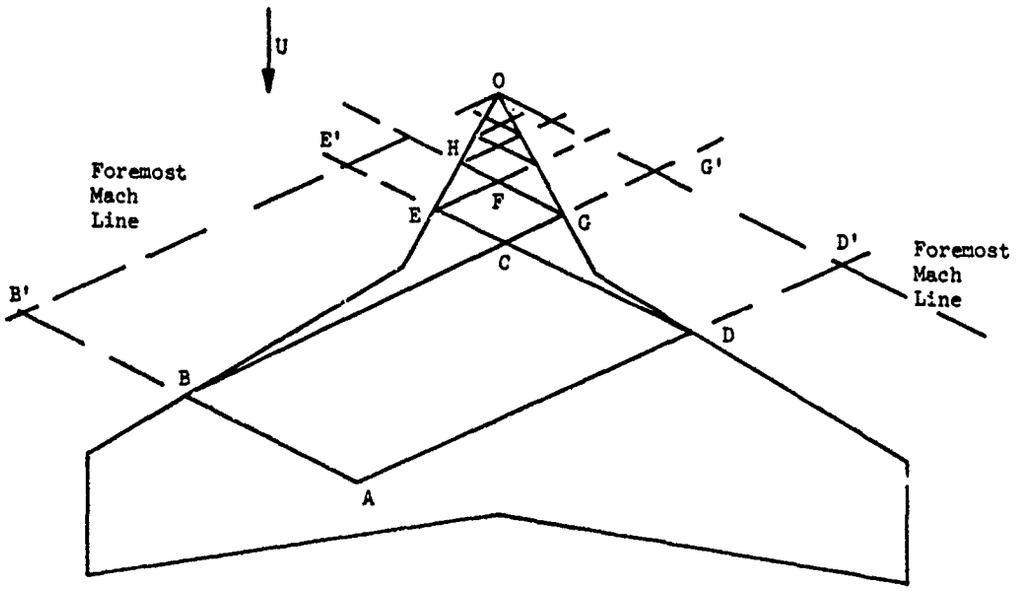

Figure 3.4. Integration Areas for a Wing with Subsonic Leading Edges.

Returning to Equation (3.14) and performing the differentiation indicated, one obtains

$$C_p(P_j) = \frac{2}{\pi}\iint_S \frac{\partial}{\partial x}\left(\frac{w}{R}\right) d\xi d\eta + \frac{2}{\pi}\oint_{T.E.} \frac{w}{R}\, d\eta, \tag{3.15}$$

which can be simplified to

$$C_p(P_j) = \frac{2}{\pi}\iint_S \frac{\partial w}{\partial \xi}\,\frac{d\xi d\eta}{R} + \frac{2}{\pi}\oint_{L.E.} \frac{w}{R}\, d\eta. \tag{3.16}$$

In the above equations, T. E. and L. E. signify that the line integral is to be evaluated along the trailing and leading edges of the area, S, respectively.

To evaluate the above equation, the planform is divided into a number of trapezoidal panels, as was done in the subsonic case. Over each panel, the downwash is assumed to be constant. Consider a typical panel and its neighbors as depicted in Figure 3.5. The contribution to the pressure at (x, y) of the wedge aft of ABC is

$$I_{ACG} = \frac{2}{\pi}\iint_{ACG} \frac{\partial w}{\partial \xi}\,\frac{d\xi d\eta}{R} + \frac{2}{\pi}\oint_{ABC} \frac{w}{R}\, d\eta$$

$$= \iint_{ACG} + \oint_{ABC} = \iint_{ACFD} + \iint_{DFG} + \oint_{ABC}. \tag{3.17}$$

The contribution from the wedge aft of DEF is

$$I_{DFG} = \iint_{DFG} + \oint_{DEF}. \tag{3.18}$$

Subtracting these two equations, one obtains the contribution of the strip ACFD:

$$I_{ACFD} = \iint_{ACFD} + \oint_{ABC} - \oint_{DEF}. \tag{3.19}$$

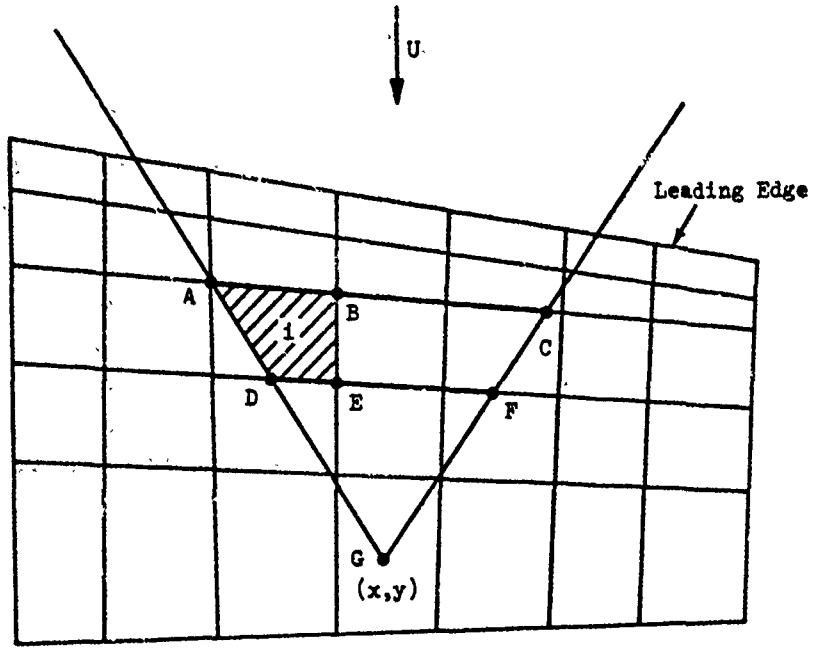

Figure 3.5. Planform Divided into Panels.

This can be broken up into the contributions associated with panel i (shaded in Figure 3.5) and those associated with its spanwise neighbor(s). For panel i, one has:

$$I_i = \iint_{ABED} + \oint_{AB} - \oint_{DE} = \iint_{S_i} + \oint_{L.E._i} - \oint_{T.E._i} , \qquad (3.20)$$

where only those portions of S_i, $L.E._i$ and $T.E._i$ that are within the Mach cone are considered. Since the downwash is assumed constant over each panel, the surface integral in Equation (3.20) equals zero and the net result involves only line integrals along the leading and trailing edges. Hence, Equation (3.16) becomes:

$$C_p(P_j) = \frac{2}{\pi} \sum_{i=1}^{m} w_i \left[\oint_{L.E._i} \frac{d\eta}{R} - \oint_{T.E._i} \frac{d\eta}{R} \right], \tag{3.21}$$

where m is the number of panels within the inverse Mach cone. The remaining integrals are easily evaluated, since the equations for the panel leading and trailing edges are those of straight lines.

For thin airfoils, the magnitude of the downwash on both sides of the surface can be assumed equal to the local angle of attack of the mean surface. Hence, the net pressure coefficient is, merely, twice the value given in Equation (3.21) with the downwash evaluated using Equation (3.11). Fuselage effects are not included, however, since the formulation given previously is not adequate for supersonic flow.

Denoting the two line integrals in Equation (3.21) as A_{ji}, the net pressure becomes

$$C_p(P_j) = \frac{4}{\pi} \sum_{i=1}^{m} w_i A_{ji} + \frac{4}{\pi} \sum_{i=m+1}^{n} w_i \cdot 0, \tag{3.22}$$

where n is the total number of surface panels and the second summation (equal to zero) contains those panels not within the inverse Mach cone emanating from P_j. Applying Equation (3.22) to the center of each panel, one obtains

$$\{C_p\} = [AIC] \{w\}, \tag{3.23}$$

where

$$[AIC] = \frac{4}{\pi} [A] . \tag{3.24}$$

The downwash distribution to be used in Equation (3.23) is specified in accordance with Equations (3.11), (3.12), and (3.13). It is noted that the fuselage radius, R, must be entered as zero for supersonic loads analysis.

3.2.3 Aerodynamic Forces

For a geometrically symmetric planform, pressure coefficients are computed for the left half only, based on an appropriate combination of symmetric and antisymmetric aerodynamic influence coefficients and the specification of the total (generally asymmetrical) downwash angle distribution in terms of symmetrical and antisymmetrical components:

$$\left\{C_p\right\}_L = \left[AIC\right]_{sym.}\left\{w\right\}_{sym.} + \left[AIC\right]_{\substack{anti-\\sym.}}\left\{w\right\}_{\substack{anti-\\sym.}}, \qquad (3.25)$$

where

$$\left\{w\right\}_{sym.} = \tfrac{1}{2}\left[\left\{w\right\}_L + \left\{w\right\}_R\right]$$

$$\left\{w\right\}_{\substack{anti-\\sym.}} = \tfrac{1}{2}\left[\left\{w\right\}_L - \left\{w\right\}_R\right]$$

and L and R denote the left and the right halves, respectively, of the symmetric planform. With the pressure coefficients determined, the total aerodynamic force on each panel is simply

$$\left\{F\right\} = \tfrac{1}{2}\rho U^2\left[S\right]\left\{C_p\right\} \qquad (3.26)$$

where ρ is the air density and $\left[S\right]$ is a diagonal matrix of panel areas. Using the procedures described in Section 5, the aerodynamic forces are finally transformed from the aerodynamics model to the structures model.

3.3 INERTIAL LOADS

Using D'Alembert's principle, rigid-body inertial forces and moments at a point on a body can be written as

$$-\bar{F} = m\ddot{\bar{r}} + m\bar{\omega} \times (\bar{\omega} \times \bar{\rho}) + m\dot{\bar{\omega}} \times \bar{\rho}$$

and $$-\bar{M} = \dot{\bar{H}} + \bar{\omega} \times \bar{H}, \qquad (3.27)$$

where

$\bar{F}$ is the inertial force vector

$\bar{M}$ is the inertial moment vector

$\bar{r}$ is the position vector locating the origin of the reference axes on the body

m is the mass of the point

$\bar{\omega}$ is the angular velocity of the reference axes

$\bar{\rho}$ is the position of the point relative to the reference axes

$\bar{H}$ is the moment of momentum of the point.

Expansion of these equations yields

$$F_{x,\,i} = (x_i - x_o)(Q^2 + R^2)\,m_i + (y_i - y_o)(\dot{R} - PQ)\,m_i$$
$$-(z_i - z_o)(RP + \dot{Q})\,m_i - g\,N_x\,m_i$$

$$F_{y,\,i} = (y_i - y_o)(R^2 + P^2)\,m_i + (z_i - z_o)(\dot{P} - QR)\,m_i$$
$$-(x_i - x_o)(PQ + \dot{R})\,m_i - g\,N_y\,m_i$$

$$F_{z,\,i} = (z_i - z_o)(P^2 + Q^2)\,m_i + (x_i - x_o)(\dot{Q} - RP)\,m_i$$

$$-(y_i - y_o)(QR + \dot{P})\,m_i - g\,N_z\,m_i$$

$$M_{x,\,i} = -I_{xx,\,i}\,\dot{P} - I_{xy,\,i}(PR - \dot{Q}) + I_{xz,\,i}(PQ + \dot{R})$$

$$-I_{yz,\,i}(R^2 - Q^2) - (I_{zz,\,i} - I_{yy,\,i})\,QR$$

$$M_{y,\,i} = -I_{yy,\,i}\,\dot{Q} - I_{yz,\,i}(QP - \dot{R}) + I_{yx,\,i}(QR + \dot{P})$$

$$-I_{zx,\,i}(P^2 - R^2) - (I_{xx,\,i} - I_{zz,\,i})\,RP$$

$$M_{z,\,i} = -I_{zz,\,i}\,\dot{R} - I_{zx,i}(RQ - \dot{P}) + I_{zy,\,i}(RP + \dot{Q})$$

$$-I_{xy,\,i}(Q^2 - P^2) - (I_{yy,\,i} - I_{xx,\,i})\,PQ\,, \qquad (3.28)$$

where

g is the acceleration of gravity

x_i, y_i, z_i, m_i are the coordinates and mass of the i^{th} point

$I_{xx,\,i}$, $I_{yy,\,i}$, etc. are the inertia properties about the center of gravity of the i^{th} point

N_x, N_y, N_z are load factors

P, Q, R are x, y, z components of the angular velocity, $\bar{\omega}$, respectively

x_o, y_o, z_o are the coordinates of the reference point (usually the center of gravity of the airplane).

There are two types of mass data that the user may provide for inertial load computations. The first type, termed "distributed masses", are simply point masses with no rotational inertia properties. Thus the output of the inertial loads routine for distributed masses consists only of forces at the center of gravity of each mass item. Distributed masses are most typically used to define the mass of the finite element structures model (including non-optimum factors where appropriate) and are logically assigned to structures model node points. The inertia properties of the structure are implicit in the node point mass distribution. The second type of mass data, referred to as "concentrated masses", have both mass and inertia properties. In this case the inertial loads routine computes inertial forces and moments at the center of gravity of each mass item. Concentrated masses are used to represent large masses such as engines, stores, etc.

The computed inertial loads acting at the centers of gravity of the various masses are subsequently distributed to the node points of the structures model using the transformation procedures described in Section 5.

3.4 PROVISION FOR DIRECT INPUT OF APPLIED LOADS

For non-maneuver loading conditions (e.g., landing or gust loads) or maneuver loading conditions for which applied loads have been determined directly from test data, separate loading conditions consisting of forces at structural nodes may be prescribed by the user.

Section 4

STRUCTURAL ANALYSIS

4.1 SUMMARY

Structural analysis and strength resizing capability are provided by utilizing the Automated Structural Optimization Program (ASOP) described in detail in Reference 4-1. The analysis procedure employs the matrix displacement method to obtain nodal deflections and internal element corner forces. The corner forces are then converted into forces that are equivalent to those obtained by the matrix force method, and these are subsequently transformed into representative element stress levels. Resizing for strength requirements, in the presence of minimum-gage constraints, is accomplished through the iterative use of ratios of actual-to-allowable stress to satisfy the fully-stressed-design optimality criterion.

The following paragraphs provide a summary of the finite elements that can be used in a structural idealization within FASTOP. The basic aspects of the overall structural analysis procedure are briefly reviewed and the numerical method for solving the structure's load/displacement equations is presented. Further discussion of the redesign aspects of ASOP, in the context of the combined strength-and-flutter optimization problem, is given in Section 10.

4.2 SUMMARY OF AVAILABLE FINITE ELEMENTS

The finite elements available for structural modeling are those that are commonly used in major structural analysis involving metallic construction. With the exception of the plate elements (i.e., the bending triangle and the bending quadrilateral), all of the elements in the following list have stiffness characteristics that are directly proportional to their weight, thus making them available for resizing in FASTOP. Plate elements should be used for analysis only. The elements, which are discussed in Reference 4-1, include

- a uniform bar element
- a uniform beam element having constant radii of gyration in its cross-section
- an anisotropic triangular membrane element

- an anisotropic planar quadrilateral membrane element
- a quadrilateral warped or planar shear panel element
- an anisotropic warped quadrilateral membrane element
- a hinged beam element
- an anisotropic bending triangle element
- an anisotropic bending quadrilateral element
- a combined triangular membrane and bending triangle element
- a combined planar quadrilateral membrane and bending quadrilateral.

4.3 REVIEW OF ANALYSIS PROCEDURE

In applying the matrix displacement method, the analyst first establishes a structural idealization comprised of the above elements, and representing, as closely as possible, the actual topological arrangement of the primary structural members. The required input data is then classified into groups defined as: nodal geometry, member data, boundary conditions, material tables and applied loads. The member data contains both topological data plus member sizes. Using this information, the program assembles the total stiffness matrix [K] by superimposing the element stiffness matrices compatible with a global coordinate system. That is,

$$[K] = \sum_{i=1}^{n} \alpha_i [k_i], \tag{4.1}$$

where α_i is a function of the design parameter t_i and $[k_i]$ is the expanded element stiffness matrix for a unit value of that design parameter with the appropriate boundary conditions applied to it. The $[k_i]$ matrices are calculated only once and stored. In succeeding redesign cycles they are multiplied by the new design parameter and reassembled to form the new [K] matrix.

Applied forces for the various loading conditions are entered by referring them to the node point at which they are applied and to the global coordinate direction in which they act. The forces are then transformed to correspond to a degree-of-freedom numbering scheme associated with the free degrees of freedom in the idealization. The resulting load matrix, [P], is then one in which

the rows correspond to the degrees of freedom and the columns correspond to loading conditions. The equations of nodal equilibrium are thus

$$[K][\Delta] = [P], \tag{4.2}$$

where $[\Delta]$ is the matrix of nodal displacements. This system is solved by using a modified version of the Cholesky algorithm (discussed in the next subsection) and the resulting displacements are then converted into element corner forces, $[q]$, by

$$[q] = [S_1][\Delta], \tag{4.3}$$

in which $[S_1]$ embodies both element stiffness matrices and appropriate force transformations from a global to a local element coordinate system.

The procedure adopted for defining internal stress levels is the "nodal stress method" described in References 4-1 and 4-2. This procedure first converts the element corner forces, $[q]$, into a new system of forces that are equivalent to those obtained by the matrix force method of analysis (i.e., cap loads and shear flows). Then, an approximate strain-compatibility relationship is used at each structural node point to determine the states of stress at the corners of each finite element. Representative single values of stress are then computed at each corner for use in a stress-ratio resizing formula that relates this value of stress to its allowable.

4.3.1 Solution of the Load/Displacement Equations

The solution of Equation (4.2) is accomplished by employing the Cholesky algorithm for decomposition of positive-definite symmetric matrices (see Reference 4-3). This technique is also used elsewhere in the FASTOP system (see Sections 7,8). The overall solution procedure involves the following steps:

First, factor $[K]$ by the Cholesky algorithm such that

$$[K] = [L][L]^T, \tag{4.4}$$

where $[L]$ is a lower triangular matrix. The procedure for obtaining $[L]$ is

based upon the defining relationship, Equation (4.4), and the positive-definite symmetric nature of the stiffness matrix [K]. It first involves the calculation of elements in the first column, given by

$$\ell_{11} = k_{11}^{1/2}$$

$$\ell_{i1} = k_{i1}/\ell_{11} \qquad i > 1,$$

where the ℓ's and k's are the elements of [L] and [K], respectively. Thereafter, each successive column of [L] is computed with the following recursion formulae:

$$\ell_{ij} = 0 \qquad i<j$$

$$\ell_{ii} = (k_{ii} - \sum_{r=1}^{i-1} \ell_{ir}^2)^{1/2} \qquad i>1$$

$$\ell_{ij} = (k_{ij} - \sum_{r=1}^{j-1} \ell_{ir}\,\ell_{jr})/\ell_{jj} \qquad i>j.$$

Equation (4.2) may now be rewritten as

$$[L][L]^T[\Delta] = [P]. \tag{4.5}$$

In the second step, define $[Z] = [L]^T[\Delta]$ and solve

$$[L][Z] = [P] \tag{4.6}$$

for [Z] by successive substitution, starting with the first equation and proceeding downward.

For the final step, solve

$$[L]^T[\Delta] = [Z]$$

for the displacements, [Δ], by successive substitution, starting with the last equation and proceeding upward.

Section 5

TRANSFORMATIONS BETWEEN MATHEMATICAL MODELS

5.1 SUMMARY

Because different mathematical models are employed in performing the major analysis tasks required for the design of a lifting surface, it is necessary, in an integrated system, to provide automated methods that transform data obtained with one model into a suitable form for use in another. The transformation of aerodynamic and inertial applied loads into structural node forces is achieved by using fully automated "load-beaming" procedures that rely on assumed load paths. These same procedures, with some added special capabilities, also provide a basis for establishing a method that transforms flexibility and mass data, defined in terms of a structures model, into a form for use in vibration analysis.

5.2 DEFINITION OF REQUIRED TRANSFORMATIONS

To perform the analyses required for the structural design of a lifting surface, four distinctly different mathematical models are usually employed. For determining applied aerodynamic loads, an aerodynamics model provides a regular planar distribution of points at which angles of attack are specified and forces normal to the plane are calculated. When rigid-body inertial loads are being considered, a weights model is defined, comprised of lumped-mass points representing both structural and nonstructural (i.e., leading- and trailing-edge assemblies, fuel, actuators, etc.) mass items. A structures model, used to define internal load distributions and elastic flexibility, consists of an assemblage of finite elements representing the actual arrangement of primary structural members. To determine the surface's modes of vibration for subsequent flutter analysis, a dynamics model is defined. This model consists of lumped masses having degrees of freedom that are important for the accurate determination of the lowest-frequency vibration-mode characteristics and will usually differ from the weights and structures models.

It is evident that an integrated analysis system must provide the capability for automatically transferring data from one model to the next in the analysis sequence. Since each analysis function, however, utilizes a model tailored to

its own specific discipline, it is also necessary to provide certain data transformations. The automated procedures included in FASTOP provide for

- transformation of loads in the aerodynamics and weights models to equivalent applied loads in the structures model, and
- transformation of flexibility and mass matrices associated with the structures model into similar matrices that are representative of the dynamics model.

All of these transformation are based on principles of "load beaming", that is, assumed relationships that transfer loads in one model to sets of statically equivalent loads in another.

5.3 DESCRIPTION OF BEAMING PROCEDURES

The methods for transferring (or "beaming") forces in the aerodynamics model and forces and moments in the weights model to the structural node points are illustrated in Figures 5.1 and 5.2. Two basic types of beaming are provided. The "eight-point" procedure is designed primarily to transfer applied aerodynamic or inertial loads that act at locations within the geometric boundaries of the primary structure. The "four-point" procedure is intended to transfer loads that act outside the structure, such as at a wing's trailing or leading edge. When using either procedure, transformation matrices are established that express loads at the structures-model node points (in its coordinate system) in terms of unit applied loads in either the aerodynamics or the weights models (in their respective coordinate systems). For aerodynamic forces, provision is made for transferring only forces that act normal to a reference plane; however, for inertial loads, all six components of force and moment may be transferred. The program requires as input the nodal geometries of the pertinent models and correspondence tables that indicate the manner of beaming and the nodes from and to which the loads are to be transferred.

The assumptions made in both procedures are described in the next two subsections. These are followed by a discussion of the use of load beaming as a first step in developing the transformations that are required to convert data from the structures model to the dynamics model. It should be noted in the

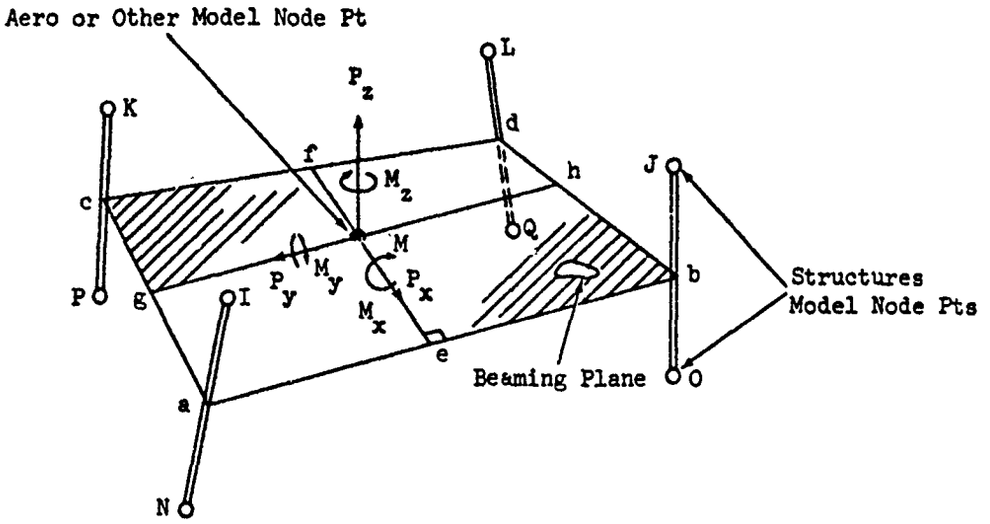

a. Applied Load Point Within Structural Nodes

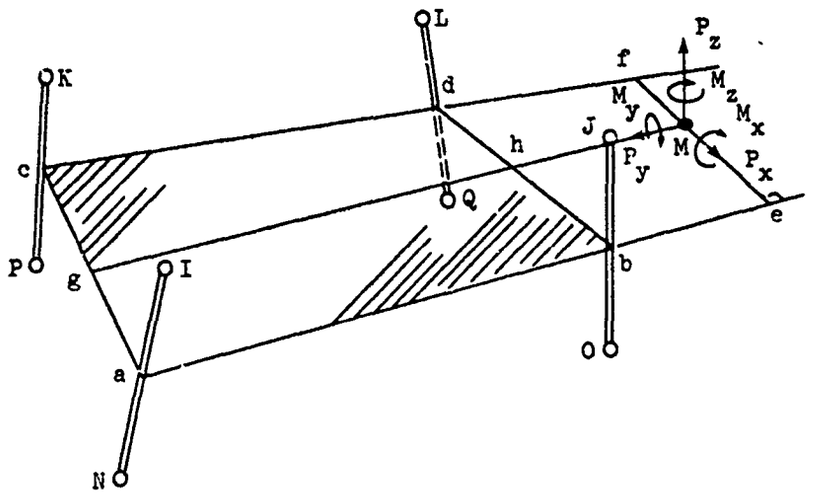

b. Applied Load Point Outside of Structural Nodes

Figure 5.1. Eight-Point Beaming Procedure.

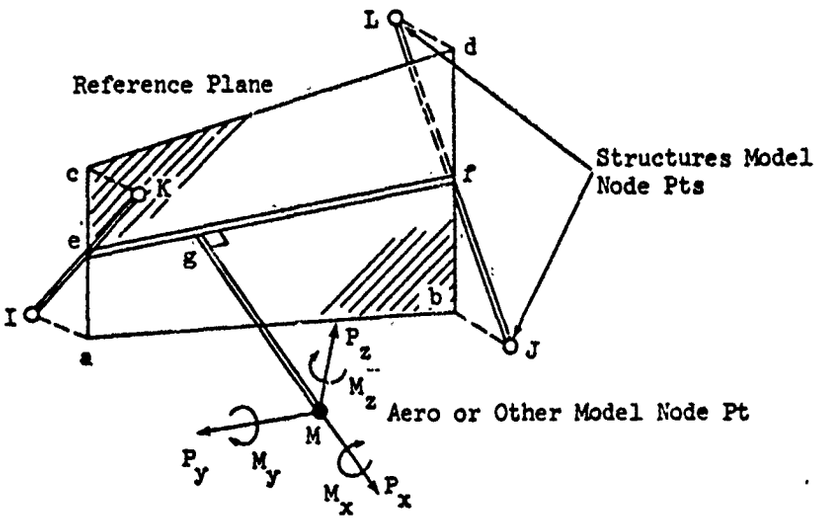

a. Applied Load Point Within Structural Nodes

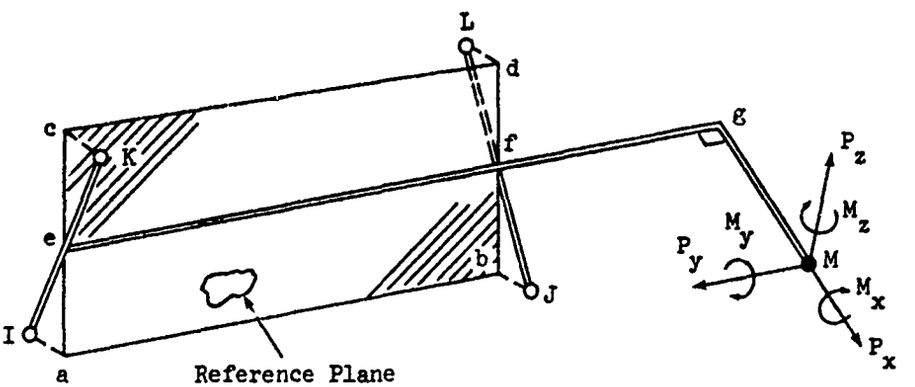

b. Applied Load Point Outside of Structural Nodes

Figure 5.2. Four-Point Beaming Procedure.

following discussions that the x-y coordinate planes of all mathematical models are assumed parallel, even though the coordinate systems may have different origins.

5.3.1 Eight-Point Beaming

Referring to Figure 5.1(a) or (b), point M represents an applied aerodynamic or inertial load point; points I, J, K, L and N, O, P, Q represent the upper and lower cover structural nodes, respectively, to which the applied loads are being transferred. The "beaming plane" contains point M and is parallel to the structures model x-y plane. The line e-f is defined perpendicular to the line a-b, and g-h is parallel to a-b. Thus, e-f, g-h, and a normal to the beaming plane form a local, orthogonal coordinate system.

Unit applied forces and moments are first transformed into components in this local system. Local loads P_x, P_y, P_z, and M_y are first transferred along line e-f to points e and f, under the assumption that e-f acts as simple (pin-ended) beam. Then, using a-b and c-d as simple beams, the loads are transferred to points a, b, c, and d, where they are finally beamed to the structural node points. The local moments M_x and M_z follow a different path; they are first beamed to g and h, and thence to a, b, c, and d by using a-c and b-d as simple beams.

It should be noted that all applied moments are initially transformed into force couples in the first beaming step, and only force components are eventually transferred to the structural node points. Also, forces that are applied parallel to a beam member are distributed to the end points in inverse proportion to the distances from the point of application.

After the forces at the structural node points are determined, they are then rotated into the structural coordinate system.

5.3.2 Four-Point Beaming

As indicated previously, this procedure is particularly applicable to aerodynamic or inertial loads that are applied at points external to the structural idealization. Referring to Figure 5.2(a), point M represents the applied aerodynamic or inertial loading point; points I, J, K and L are the structural node points to which the applied loads are being transferred. The "reference plane"

is parallel to lines connecting I with L and K with J, and contains points e and f which are the mid-points of I-K and J-L, respectively. Points a, b, c, and d are orthogonal projections of the structural node points on the reference plane. The line g-M is perpendicular to line e-f; these two lines and a common normal define a local, orthogonal coordinate system.

Unit applied forces and moments at M are first transformed into this local coordinate system, and then transferred to point g, under the assumption that M-g acts as a beam cantilevered from point g. Next, they are transferred along member e-f to its end points, with this member acting as a beam capable of resisting bending, axial load, and torsion. The torsion-resisting capability at e and f is assumed to be confined to the planes connecting I-K-a-c and J-L-b-d, respectively. The three force components and the concentrated moment at each point, e and f, are then transferred to the structural nodes by assuming that members I-K and J-L are pin-connected at their respective structural node points. Where forces and moments are applied parallel to a member, they are distributed to the end points in inverse proportion to the distances from the point of application.

For the special case where point g lies outside of points e and f, as shown in Figure 5.2(b), the torsional moment about e-f and the axial force acting along this member are assumed to be resisted totally by the more adjacent support point which is f in the illustrative example.

As with the previous beaming procedure, after the forces at the structural node points are determined, they are then rotated into the structural coordinate system.

5.3.3 Special Beaming Features for Use in Defining a Dynamics Model

The preceding beaming procedures are also used in the transformation of flexibility and mass data associated with the structures model into a form compatible with a dynamics model. Specifically, these procedures, along with the special added features discussed next, enable the definition of load paths for transferring inertial loads in the dynamics model to the structural node points. Once these paths have been defined, considerations of virtual work and kinetic energy lead to a means for arriving at rationally determined flexibility and

mass matrices for the dynamics model. These latter steps are fully discussed in Subsection 5.4.

5.3.3.1 Provision for Swept Degrees of Freedom. In dynamics modelling it is often desirable to prescribe degrees of freedom that are parallel to primary structural members rather than the structural coordinate axes. For example, pitching motion of a mass point representing a portion of the trailing edge assembly of a wing might be described about an axis that is parallel to the swept rear beam. To accommodate this type of coordinate rotation, a feature is provided that enables the program user to specify a sweep angle, α, at each dynamic node point, as illustrated in Figure 5.3. (It is noted that these sweep angles are limited to the x-y plane.) The preceding beaming procedures are then used to transfer unit inertial loads in the local swept coordinate systems into structural node point loads in the structural coordinate system.

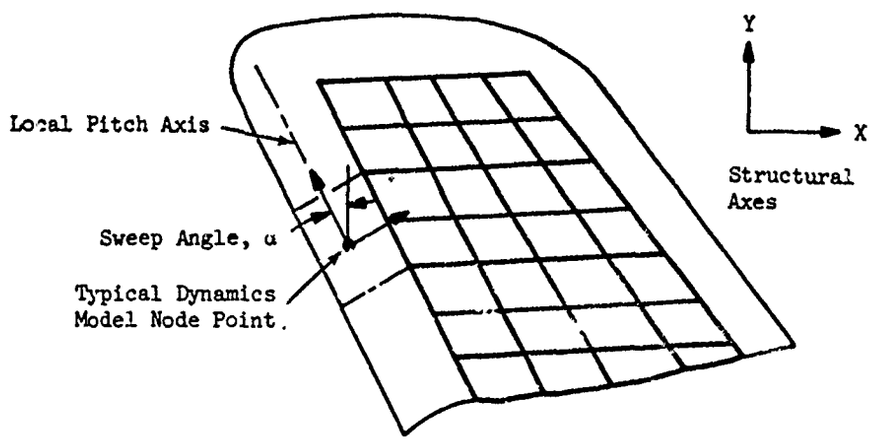

Figure 5.3 Swept Coordinate System for Dynamics Model Degrees of Freedom

5.3.3.2 Direct Load Transfer. This option permits the direct transfer of forces and moments from the dynamics to the structures model when selected degrees of freedom at a node point are identical in both models. It is particularly useful in transferring moments to structures model node points that attach beam elements. This differs from the previous techniques which transfer loads to node points that are assumed to be incapable of sustaining applied moments.

5.3.4 Practical Considerations

In the procedures just discussed, applied loads are transformed from one mathematical model (along assumed load paths) into a statically equivalent set of loads in the structures model. Since the manner in which the user relates the structural node point numbers to the points I through L and N through Q can affect the final load distribution, he should try to use these procedures in ways that enforce the most reasonable load distributions from the viewpoint of local structural characteristics. This point is best illustrated by a simple example.

Consider an applied wing tip pitching moment that is to be transferred by four-point beaming to structural nodes 11, 12, 13, and 14, and assume that the user has assigned these node numbers to I, J, K, and L as illustrated in Figure 5.4(a). In accordance with the procedure outlined previously, the beaming member e-f will be essentially horizontal, and the structural nodes will therefore receive the applied moment as approximately vertical forces. On the other hand, if the node numbers are assigned to I, J, K, and L as illustrated in Figure 5.4(b), the member e-f will be approximately vertical and will deliver horizontal forces to the structural nodes. If the structural tip assembly is attached to the primary structure with continuous rows of fasteners along the upper and lower covers, it would be more logical to assign the node numbers in accordance with the second case.

Some further recommendations are required with regard to defining load beaming from the dynamics model to the structures model. The dynamics model load beaming matrix is used to transform the structural stiffness matrix to a dynamic flexibility matrix using a procedure discussed in Subsection 5.4.1. This flexibility matrix is subsequently inverted in the process of calculating

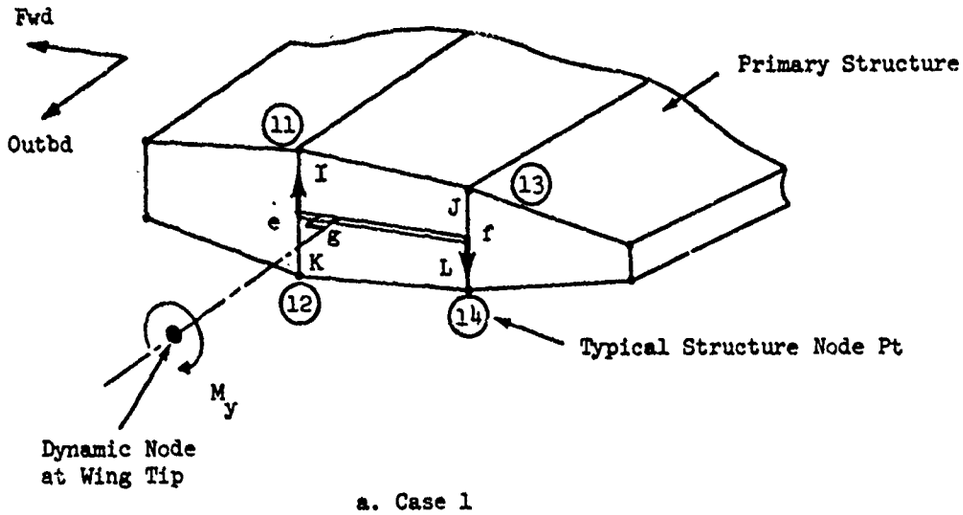

a. Case 1

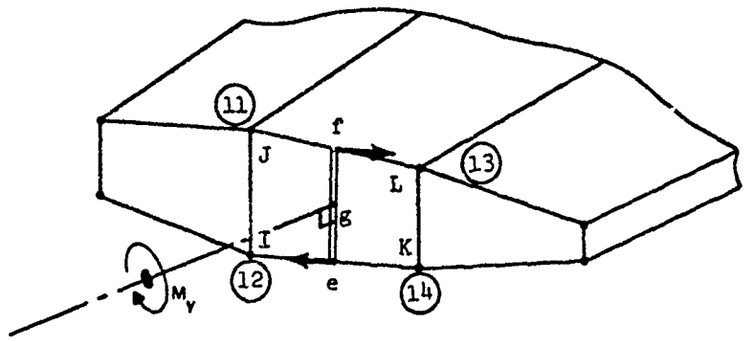

b. Case 2

Figure 5.4. Effect of Node Number Designation on Load Distribution

matrix $[B]^T$, which transforms dynamics model displacements to structures model displacements (see Equation 5.7). The dynamics model flexibility matrix must, therefore, be non-singular. A singular flexibility matrix can occur if the the number of structural degrees of freedom designated for load beaming is less than the corresponding number of dynamic degrees of freedom that are being created. The user must therefore avoid over-utilization of structural degrees of freedom in any zone of the structures model.

The user should also follow the general rule of designating dynamics nodes which are adjacent to structures nodes. This will ensure correct accounting of the incremental dynamic mass matrix prescribed by Equation 6.2. Choice of a completely arbitrary dynamics model grid, in which dynamics loads are distributed to a large number of structures nodes, can lead to a singularity in the updated dynamic mass matrix computed by Equation 6.1. An example of the recommended procedure is illustrated in Figure 11.4 where it is noted that dynamic node points are coincident in the X-Y plane with structures nodes and are positioned vertically between the upper and lower covers.

5.4 TRANSFORMATIONS REQUIRED TO DEFINE A DYNAMICS MODEL

The following procedure is employed to transform flexibility and mass data from the structures model to the dynamics model. It assumes that the previously discussed beaming procedures have first been employed to develop a transformation matrix, [T], that relates forces (or moments) in the dynamics model, $\{F_D\}$, to forces (or moments) in the structure model $\{F_s\}$; that is,

$$\{F_s\} = [T]\{F_D\}. \tag{5.1}$$

5.4.1 Flexibility Transformation

From the concept that virtual work is invariant under a coordinate transformation, it follows that if forces relate in accordance with Equation (5.1), then displacements relate as

$$\{\Delta_D\} = [T]^T \{\Delta_s\}, \tag{5.2}$$

where $\{\Delta_D\}$ and $\{\Delta_s\}$ are displacements in the dynamic and structural degrees of freedom, respectively.

The displacements in the structure are related to applied forces by the structural flexibility matrix, $[K_s]^{-1}$; that is,

$$\{\Delta_s\} = [K_s]^{-1} \{F_s\}. \tag{5.3}$$

Substituting $\{F_s\}$ from Equation (5.1) into Equation (5.3), premultiplying by $[T]^T$, and then making use of Equation (5.2), enables us to write

$$\{\Delta_D\} = [T]^T [K_s]^{-1} [T] \{F_D\}. \tag{5.4}$$

This equation gives dynamics model displacements in terms of forces in the same model, and we may thus define the dynamics model flexibility matrix, [A], as

$$[A] = [T]^T[K_s]^{-1}[T]. \tag{5.5}$$

Provision in made in FASTOP for the automated computation of this flexibility matrix and its transfer to the vibration analysis module discussed in Section 7. For the special case, however, where the degrees of freedom of the dynamics model correspond exactly with those of the structures model, the preceding transformation process may be bypassed. In this instance, the structural stiffness matrix, discussed previously in Section 5, is transferred to and used directly for vibration analysis.

5.4.2 Mass Transformation

The relationship between structural node displacements and displacements in the dynamic degrees of freedom may be obtained by substituting Equations (5.1) and (5.4) into Equation (5.3) and making use of Equation (5.5):

$$[\Delta_s] = [K_s]^{-1}[T] [A]^{-1}[\Delta_D]. \tag{5.6}$$

By defining the displacement transformation matrix

$$[B]^T = [K_s]^{-1}[T][A]^{-1}, \tag{5.7}$$

and requiring that the kinetic energy of the structures model be preserved in the dynamics model, we may obtain a consistently defined mass matrix for the dynamics model, as follows:

$$\text{Kinetic Energy} = 1/2\ \{\dot{\Delta}_s\}^T[M_s]\{\dot{\Delta}_s\}, \tag{5.8}$$

where $[M_s]$ is a mass matrix corresponding to the structures model. Substituting the velocity form of Equation (5.6) into Equation (5.8), and making use of Equation (5.7), yields

$$\text{Kinetic Energy} = 1/2\ \{\dot{\Delta}_D\}^T[B][M_s][B]^T\ \{\dot{\Delta}_D\}, \tag{5.9}$$

where the inner triple product is the desired dynamics model mass matrix, $[M_D]$; that is,

$$[M_D] = [B]\ [M_s]\ [B]^T. \tag{5.10}$$

In the event that the degrees of freedom of the structures and dynamics models are identical, the computation of [B] may be bypassed, with the mass matrix of the structures model being used directly in subsequent vibration analysis. Further discussion on the calculation of the structures model mass matrix, in conjunction with the options for defining dynamics model data, is presented in Section 6.

5.4.3 Computational Considerations

Equations (5.5) and (5.7) show that the inverse of the structural stiffness matrix, $[K_s]^{-1}$, is present in the expressions for the dynamic flexibility matrix [A] and the transformation matrix [B]. As equation solving routines are more efficient than inversion routines, the following computational procedure was incorporated into FASTOP.

First, a new matrix [Y] is defined by the relation

$$[Y] = [K_s]^{-1}\ [T], \tag{5.11}$$

or equivalently,

$$[K_s]\ [Y] = [T]. \tag{5.12}$$

In view of Equation (5.11), Equations (5.5) and (5.7) can be put in the form

$$[A] = [T]^T [Y], \tag{5.13}$$

and

$$[A] [B] = [Y]^T . \tag{5.14}$$

Within FASTOP, Equation (5.12) is solved for [Y], which is then used in Equation (5.13) to compute [A]. Then, having [A] and [Y], Equation (5.14) is solved for [B].

Section 6

MASS MATRIX DEFINITION

6.1 SUMMARY

Two alternate approaches are available for the computation of the dynamics model mass matrix required for vibration analysis. One approach requires that initial mass input data be specified by the user while the other is fully automated and calculates initial mass data using the structural model idealization.

6.2 INITIAL DYNAMICS MODEL MASS MATRIX SUPPLIED BY THE USER

In this approach, the dynamics model mass matrix, $[M_D]$, is considered to be the sum of a constant mass matrix, $[\bar{M}_D]$, associated with the initial design, plus a variable mass matrix, $[\Delta\bar{M}_D]$, which reflects the accumulated design changes beyond the starting design; that is,

$$[M_D] = [\bar{M}_D] + [\Delta\bar{M}_D]. \tag{6.1}$$

The task of generating $[\bar{M}_D]$ for the initial design is usually the responsibility of a weights engineer, who must account for the presence of structural members, fixed mass items (equipment, overhanging structure, etc.), initial mass-balance weights, and all of the nonoptimum components (fasteners, joints, etc.) which contribute to the total weight of the real aircraft structure. Based upon the weights and locations of all these items, the weights engineer must develop a single representative dynamics model mass matrix for direct input to the system.

Computation of the incremental dynamics model mass matrix, $[\Delta\bar{M}_D]$, is automated within FASTOP. Inasmuch as all redesign beyond $[\bar{M}_D]$ involves structural members and/or mass balances, both of which are determined in the structures model, it is natural to first compute the incremental mass matrix in the structures model, $[\Delta\bar{M}_s]$, and then transform the result to the dynamics model; that is,

$$[\Delta\bar{M}_D] = [B]\,[\Delta\bar{M}_s]\,[B]^T, \tag{6.2}$$

where $[B]$ is the transformation matrix previously defined in Section 5.4.2.

Computation of the diagonal matrix $[\Delta\bar{M}_s]$ is straightforward. If the current gage of a structural member differs from its starting value, the incremental weight of that member (including any nonoptimum factor specified by the user) is computed and then distributed equally among its attaching structural node points. For each such node, this "nodal weight" is then assigned to each of the translational degrees of freedom in $[\Delta\bar{M}_s]$ associated with that node. The procedure is essentially identical for a mass-balance variable, except that the incremental weight is applied entirely to the single structural node at which the mass balance is located. Finally, $[\Delta\bar{M}s]$ is complete when all the structural members and mass balances have been considered.

6.3 FULLY AUTOMATED COMPUTATION OF DYNAMICS MODEL MASS MATRIX

In the event that time or personnel are not sufficient to generate the initial input mass data required by the preceding approach, a fully automated mass calculation procedure is available. At any stage of design (starting or otherwise), the fully automated method obtains a dynamics model mass matrix, $[M_D]$, by first computing a mass matrix, $[M_s]$, in the structures model and then transforming the result by

$$[M_D] = [B]\,[M_s]\,[B]^T. \tag{6.3}$$

The computation of $[M_s]$ is identical to that of $[\Delta M_s]$ in the first procedure, except that here total weights of structural members and mass balances are used, rather than incremental weights beyond the starting design. Also, the user has the option of inserting fixed mass additions to $[M_s]$ (not necessarily diagonal) before transforming to the dynamics model.

Section 7
VIBRATION ANALYSIS

7.1 SUMMARY

The procedure for computing modes of vibration begins with the transformation of the familiar structural-vibration form of the eigenvalue problem into a special symmetric form. This is followed by a further transformation to tridiagonal form by Householder's method (Reference 7-1, page 290). A Sturm sequence technique (Reference 7-1, page 300) is then employed to determine the eigenvalues, and inverse iteration (Reference 7-1, page 321) is used to calculate the eigenvectors. This procedure has proved to be both efficient and accurate for problems where the solution may be achieved directly in core.

7.2 TRANSFORMATION OF EIGENVALUE PROBLEM TO A SPECIAL SYMMETRIC FORM

The first step in the solution procedure is to transform the structural-vibration eigenvalue problem into the form

$$[D]\{Y\} = \lambda\{Y\}, \tag{7.1}$$

where

$[D]$ = a real symmetric matrix having only real roots

$\{Y\}$ = an eigenvector of the transformed problem

λ = a real eigenvalue $(= 1/\omega^2)$

ω = a natural frequency in radians/sec.

This transformation can take either of two forms depending on whether the initial structural representation is in terms of a stiffness matrix or a flexibility matrix. It should be noted that the eigenvalue, λ, is defined here as $1/\omega^2$ since the solution procedure to be defined subsequently will determine the higher eigenvalues with greatest accuracy.

7.2.1 Stiffness Matrix Formulation

The eigenvalue problem for the stiffness matrix formulation may be written as

$$[M]\{X\} = \lambda[K]\{X\}, \tag{7.2}$$

where

$[M]$ = the mass matrix of the dynamics model idealization

$[K]$ = the stiffness matrix of the dynamics model idealization

$\{X\}$ = an eigenvector in dynamics model coordinates

and the definition of λ is the same as for Equation (7.1). Factoring the stiffness matrix into

$$[K] = [L][L]^T \tag{7.3}$$

by Cholesky decomposition, discussed previously in Section 4.3.1, and substituting into Equation (7.2) yields

$$[M]\{X\} = \lambda[L][L]^T\{X\}, \tag{7.4}$$

where the factorization of Equation (7.3) requires that $[K]$ be nonsingular. Letting

$$\{Y\} = [L]^T\{X\} \tag{7.5a}$$

or

$$\{X\} = [L]^{-T}\{Y\}, \tag{7.5b}$$

and premultiplying Equation (7.4) by $[L]^{-1}$ gives

$$[L]^{-1}[M][L]^{-T}\{Y\} = \lambda\{Y\} \tag{7.6}$$

or

$$[D]\{Y\} = \lambda\{Y\}, \tag{7.7}$$

where $[D] = [L]^{-1}[M][L]^{-T}$. It should be noted that $[D]$ is symmetric since $[M]$ is always symmetric.

After the eigenvalue problem of Equation (7.7) is solved, as discussed subsequently, the eigenvectors are transformed back to the dynamics model coordinate system using Equation (7.5b).

7.2.2 Flexibility Matrix Formulation

The eigenvalue problem for the flexibility matrix formulation is

$$[M]\{X\} = \lambda [A]^{-1}\{X\} \tag{7.8}$$

or

$$[A][M]\{X\} = \lambda \{X\}, \tag{7.9}$$

where $[A] = [K]^{-1}$ = the flexibility matrix, and $[M]$, $[K]$, $\{X\}$, and λ are the same as defined previously. Factoring the mass matrix into

$$[M] = [L][L]^T \tag{7.10}$$

and substituting into Equation (7.9) yields

$$[A][L][L]^T\{X\} = \lambda \{X\}. \tag{7.11}$$

Making the same substitution for $\{X\}$ as defined by Equation (7.5b), but, in this case using $[L]$ as defined above, and premultiplying by $[L]^T$, yields

$$[L]^T[A][L]\{Y\} = \lambda \{Y\} \tag{7.12}$$

or

$$[D]\{Y\} = \lambda \{Y\}, \tag{7.13}$$

where

$$[D] = [L]^T[A][L].$$

Here again, symmetry is preserved in the transformation, and the eigenvectors are transformed by Equation (7.5b).

7.3 COMPUTATION OF VIBRATION MODES FOR A CANTILEVER STRUCTURE

Computation of vibration modes for a cantilever structure proceeds as described previously in Section 7, where the formulation of the eigenvalue problem employs either the structural stiffness matrix (Equation 7.2) or the dynamics model flexibility matrix (Equation 7.9) of the supported structure. The former approach is taken where degrees of freedom of the dynamics model correspond exactly with those of the structures model.

7.4 COMPUTATION OF VIBRATION MODES FOR A FREE-FREE STRUCTURE

Although the computation of free-free modes also uses the stiffness or flexibility matrix of the supported structure, the formulation of the free-free eigenvalue problem requires relaxation of the fixed support points to allow rigid-body motion of the structure. The analytical procedures are described below. In the following discussion a hypothetical "plug" is defined which is assumed to be rigidly interconnected to all the fixed support points of the structures model; the plug mass properties represent that portion of the configuration not included in the dynamics model of the flexible structure.

Figure 7.1 shows an unsupported (free-free) configuration consisting of a rigid "plug" section connected at points A and B to flexible structure; local flexibilities can exist at A and B.

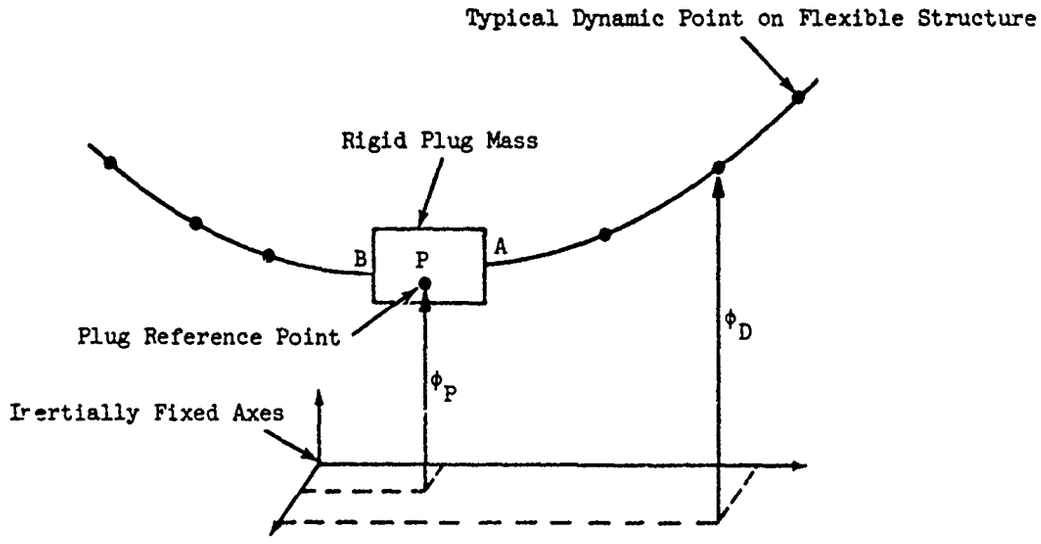

Figure 7.1. Unsupported Configuration for Free-Free Analysis

The vibration equation for this unsupported system may be written as:

$$-\omega^2 \left[\begin{array}{c|c} M_D & 0 \\ \hline 0 & M_P \end{array}\right] \left\{\begin{array}{c} \phi_D \\ \hline \phi_P \end{array}\right\} + \left[\begin{array}{c|c} K_D & K_{DP} \\ \hline K_{PD} & K_P \end{array}\right] \left\{\begin{array}{c} \phi_D \\ \hline \phi_P \end{array}\right\} = \left\{\begin{array}{c} 0 \\ \hline 0 \end{array}\right\}, \qquad (7.14)$$

where

$\{\phi_D\}$ is a vector of absolute displacements of dynamic points on the flexible structure.

$\{\phi_P\}$ is a vector of absolute displacements of the plug reference point.

$[M_D]$ is the dynamic mass matrix of the flexible structure alone; this matrix was discussed in Sections 6.2 and 6.3.

$[M_P]$ is the mass matrix of the plug alone.

$[K_D]$ is the stiffness matrix for dynamic degrees of freedom of the flexible structure excluding the plug; that is, this matrix defines forces at dynamic points on the flexible structure due to displacements at those points alone.

$[K_P]$ is the stiffness matrix for the plug degrees of freedom; that is, this matrix defines the forces acting on the plug due to motion of the plug alone.

$[K_{DP}]$ is the stiffness matrix defining forces at dynamic points on the flexible structure due to plug motion alone.

$[K_{PD}]$ is the stiffness matrix defining forces on the plug due to motion of the flexible structure alone.

Now, the absolute motion of the flexible structure $\{\phi_D\}$ is due to both rigid-body motion of the entire configuration and flexible (or relative) motion, $\{\phi_{DR}\}$. Accordingly, if the plug motions are chosen to prescribe the rigid-body motions, it follows that

$$\left\{\begin{array}{c} \phi_D \\ \hline \phi_P \end{array}\right\} = \left[\begin{array}{c|c} I & \lambda_D \\ \hline 0 & I \end{array}\right] \left\{\begin{array}{c} \phi_{DR} \\ \hline \phi_P \end{array}\right\}, \qquad (7.15)$$

where $[\lambda_D]$ defines the displacements of the dynamic points on the structure due to unit rigid-body motions. The basic vibration equation can now be recast in terms of $\{\phi_{DR}\}$ and $\{\phi_P\}$ by first substituting Equation (7.15) into Equation (7.14) and then premultiplying the result by the transpose of the transformation matrix in Equation (7.15). The result is

$$-\omega^2 \left[\begin{array}{c|c} M_D & M_{DA} \\ \hline M_{AD} & M_A \end{array}\right] \left\{\begin{array}{c} \phi_{DR} \\ \hline \phi_P \end{array}\right\} + \left[\begin{array}{c|c} K_D & K_{DA} \\ \hline K_{AD} & K_A \end{array}\right] \left\{\begin{array}{c} \phi_{DR} \\ \hline \phi_P \end{array}\right\} = \left\{\begin{array}{c} 0 \\ \hline 0 \end{array}\right\} , \tag{7.16}$$

where

$$\left.\begin{aligned} [M_{DA}] &= [M_D][\lambda_D] \,, \quad [M_{AD}] = [\lambda_D]^T [M_D] \\ [M_A] &= [\lambda_D]^T [M_D][\lambda_D] + [M_P] \end{aligned}\right\} \tag{7.17a}$$

and

$$\left.\begin{aligned} [K_{DA}] &= [K_D][\lambda_D] + [K_{DP}] \\ [K_{AD}] &= [\lambda_D]^T [K_D] + [K_{PD}] \\ [K_A] &= [\lambda_D]^T [K_D][\lambda_D] + [\lambda_D]^T [K_{DP}] + [K_{PD}][\lambda_D] + [K_P] \,. \end{aligned}\right\} \tag{7.17b}$$

However, $[K_{DA}]$, $[K_{AD}]$ and $[K_A]$ must all be zero because rigid-body motion alone (as prescribed by $\{\phi_P\}$) cannot induce restoring forces from the stiffness matrix of the free-free system. The same conclusion can be reached in another manner. Consider, for example, the two terms present in the expression for $[K_{DA}]$ in Equation (7.17b). These two terms respectively define the forces acting at dynamic points on the structure due to (a) rigid-body motion of the flexible structure alone (see Figure 7.2a), and (b) motion of the plug alone (see Figure 7.2b). As these two force systems are negatives of each other, $[K_{DA}]$ must vanish. Matrices $[K_{AD}]$ and $[K_A]$ can be shown to vanish in a similar manner.

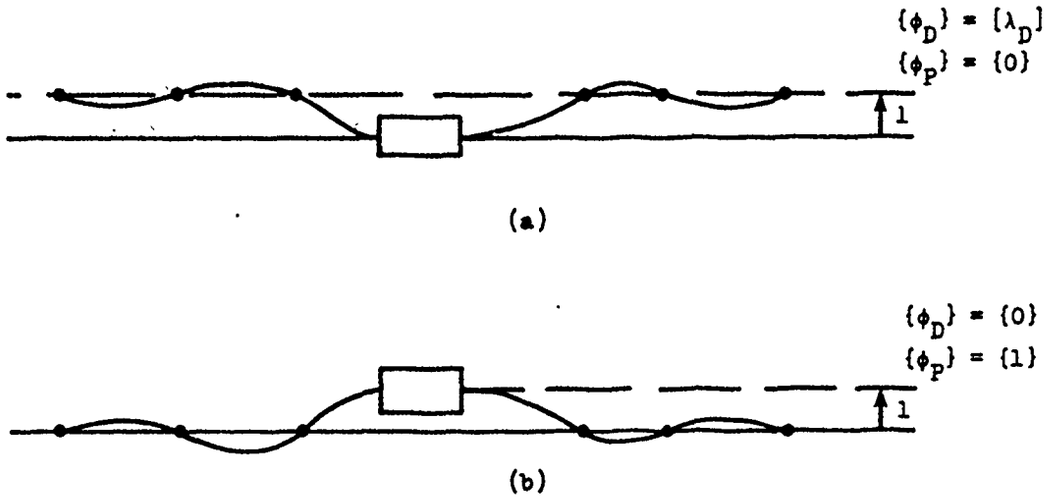

Figure 7.2. Rigid-Body Motions of Structure Alone and Plug Alone

Thus, Equation (7.16) may be rewritten as

$$-\omega^2 \left[\begin{array}{c|c} M_D & M_{DA} \\ \hline M_{AD} & M_A \end{array}\right] \left\{\begin{array}{c} \phi_{DR} \\ \hline \phi_P \end{array}\right\} + \left[\begin{array}{c|c} K_D & 0 \\ \hline 0 & 0 \end{array}\right] \left\{\begin{array}{c} \phi_{DR} \\ \hline \phi_P \end{array}\right\} = \left\{\begin{array}{c} 0 \\ \hline 0 \end{array}\right\}. \tag{7.18}$$

It follows from Equation (7.18) that the rigid-body coordinates $\{\phi_P\}$ are expressable in terms of the relative coordinates $\{\phi_{DR}\}$; that is

$$\{\phi_P\} = -\left[M_A\right]^{-1} \left[M_{AD}\right] \{\phi_{DR}\}. \tag{7.19}$$

Finally, if Equation (7.19) is substituted into Equation (7.18), the vibration equation for the free-free structure in terms of relative coordinates becomes

$$-\omega^2 \left[M_{DFF}\right] \{\phi_{DR}\} + \left[K_D\right] \{\phi_{DR}\} = \{0\}, \tag{7.20}$$

where

$$\left[M_{DFF}\right] = \left[M_D\right] - \left[M_{DA}\right] \left[M_A\right]^{-1} \left[M_{AD}\right]. \tag{7.21}$$

Equation (7.21) defines the mass matrix $\left[M_{DFF}\right]$ for a free-free vibration analysis regardless of which of the two alternate approaches is used to obtain the dynamics model mass matrix $\left[M_D\right]$ (see Sections 6.2 and 6.3). Of course, the plug mass matrix $\left[M_P\right]$ must be supplied. If the flexibility approach is used, Equation (7.20) may be written in the form

$$\left(-\omega^2 \left[A_D\right] \left[M_{DFF}\right] + \left[I\right]\right) \left\{\phi_{DR}\right\} = 0, \tag{7.22}$$

where $\left[A_D\right]$ is the flexibility matrix for dynamic degrees of freedom of the flexible structure excluding the plug (see Equations 7.8 and 7.9).

After the $\{\phi_{DR}\}$ are generated in the solution of Equation (7.20) or Equation (7.22) using the eigenvalue solution procedures described previously, the associated plug motions can be obtained from Equation (7.19) and the absolute displacements of the dynamic points on the structure may be computed from Equation (7.15). The generalized mass matrix for the free-free system may then be obtained from the relation

$$\left[M\right] = \begin{Bmatrix}\phi_D\\ \phi_P\end{Bmatrix}^T \left[\begin{array}{c|c} M_D & 0 \\ \hline 0 & M_P \end{array}\right] \begin{Bmatrix}\phi_D\\ \phi_P\end{Bmatrix}. \tag{7.23}$$

In the event that the degrees of freedom of the structures and dynamics model are identical, matrix $\left[\lambda_D\right]$ is replaced by matrix $\left[\lambda_S\right]$ which defines the displacements of the structures points due to unit rigid-body motions. The matrix $\left[\lambda_S\right]$ is always required if flutter-velocity derivatives are to be computed for a free-free vibration model (see Subsection 9.3.1).

Section 8

FLUTTER ANALYSIS

8.1 SUMMARY

This module of the FASTOP package determines the oscillatory pressures and the generalized aerodynamic forces for the lifting surface to be analyzed, given a set of normal mode shapes and frequencies. Additionally, given the generalized masses corresponding to the modes, the program solves the flutter equation to determine the flutter speed and values of modal damping and frequency as functions of air speed.

Generalized aerodynamic forces are computed using either the subsonic assumed-pressure-function procedure (kernel function), the supersonic Mach-box method or the subsonic doublet-lattice procedure. In determining the flutter speed, these aerodynamic forces are required at many different reduced frequencies; consequently, to save computing time, these forces are determined at the required reduced frequencies by interpolation, using a small number of directly calculated aerodynamic forces as a basis.

The flutter solutions are obtained by use of either the conventional k-method or an improved version of the p-k method of Reference 8-1. To allow the user to study the flutter mechanism, several parameter variations have been automated. For redesign purposes, the eigenvectors and their associated row vectors are determined at the flutter speed when the p-k method is selected.

8.2 AERODYNAMICS ROUTINES

Three oscillatory lifting-surface aerodynamics routines, each based on linearized potential flow theory, are included:

(1) a subsonic assumed-pressure-function program (kernel function) for analyzing one or more planar, noninteracting, lifting surfaces;

(2) a supersonic Mach-box program for analyzing one or several planar, noninteracting, lifting surfaces;

(3) a subsonic doublet-lattice program for analyzing a general configuration of multiple interacting nonplanar surfaces and slender bodies.

To minimize the required input data preparation, all of these programs have been written or modified to provide automated geometry definition and modal interpolation of vibration data. The latter either may be obtained on a magnetic tape (or disk) from the vibration analysis program described in Section 7 or may be user-supplied on input data cards. With the former method of providing the vibration data, the user has the option of eliminating modal data not needed in the flutter analysis. To conserve computer machine time, the program can be instructed to save the aerodynamic influence coefficients on magnetic tape for subsequent reanalysis with altered vibration modes.

The following is a brief theoretical discussion of the aerodynamics routines and the associated options.

8.2.1 Subsonic Assumed-Pressure-Function Program

In the subsonic regime, aerodynamic forces are computed using the assumed-pressure-function method of Reference 8-2. For the general nonplanar case, the pressure on a harmonically oscillating surface, such as shown in Figure 8.1, is related to the downwash by the following integral equation derived

U is the free stream velocity

h,α are the normal displacement and the streamwise slope of the surface

ω is the harmonic frequency of oscillation

ρ is the air density

t is time

K is the kernel function specifying the normalwash angle at P_j due to a unit pressure at P

k is the reduced frequency = $\omega b_o/U$

b_o is the reference semichord

M is the Mach number.

This can be rewritten as

$$w(P_j) = \frac{1}{4\pi\rho U^2} \iint_S p(P)K(P_j, P, k, M)d\xi d\sigma$$

or

$$w(P_j) = \frac{1}{8\pi}\iint_S C_p(P)K(P_j, P, K, M)d\xi d\sigma, \qquad (8.2)$$

and for planar surfaces can be written as

$$w(x,y) = \frac{1}{8\pi} \iint_S Cp(\xi,\eta)K(x-\xi, y-\eta,k,M)d\xi d\eta, \qquad (8.3)$$

where

w is the normal or downwash angle = $\tilde{w}/U$

C_p is the differential pressure coefficient = p/q

q is the dynamic pressure = $\frac{1}{2}\rho U^2$.

In the program, the planform coordinates (x,y) and (ξ,η) are normalized with respect to the root semichord, b_o. These nondimensional coordinates $(\tilde{x},\tilde{y})$ and $(\tilde{\xi},\tilde{\eta})$ are, in turn, transformed into the coordinates of a square planform, $(\underline{x}, \underline{y})$ and $(\underline{\xi},\underline{\eta})$ as shown in Figure 8-2. After transformation of coordinates, the integral equation becomes

$$w(x,y) = \frac{1}{b_o}\left(\frac{\partial h}{\partial \tilde{x}} + ikh\right)$$

$$= \frac{1_o}{8\pi {b_o}^2} \int_{-1}^{1}\int_{-1}^{1} C_p(\underline{\xi},\underline{\eta})K(\tilde{x}-\tilde{\xi}, \tilde{y}-\tilde{\eta},k,M)b(\underline{\eta})d\underline{\xi}d\underline{\eta}, \qquad (8.4)$$

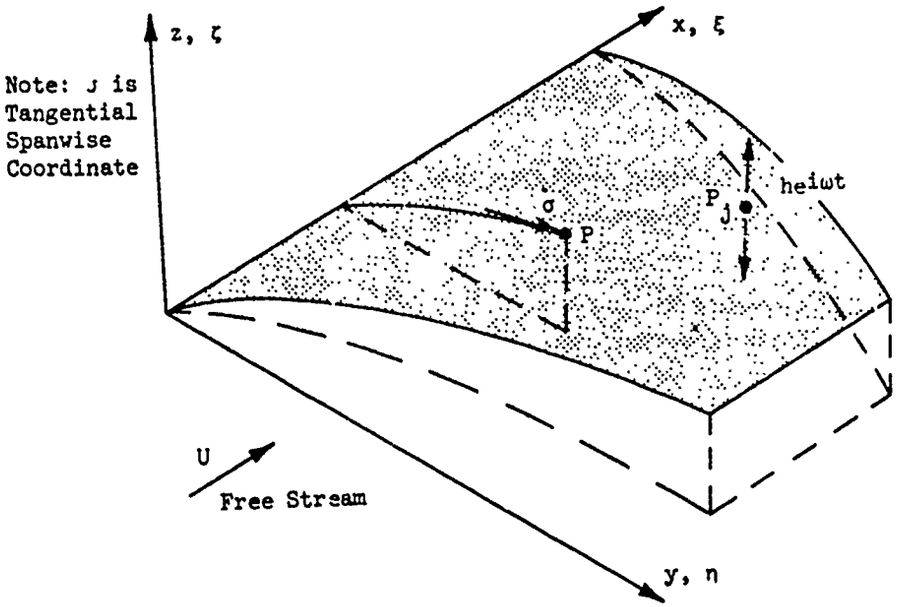

Figure 8.1. Nonplanar Harmonically Oscillating Surface.

from linear potential theory:

$$\bar{w}(P_j) \cdot e^{i\omega t} = \frac{e^{i\omega t}}{4\pi\rho U} \iint_S p(P) K(P_j, P, k, M)\, d\xi d\sigma, \tag{8.1}$$

where

P is any point on the surface, the coordinates of which are ξ, η, ζ

P_j is a j^{th} point, the coordinates of which are x, y, z

x,ξ are streamwise coordinates

y,η are spanwise coordinates

z,ζ are vertical coordinates

σ is the tangential spanwise coordinate
(equivalent to η for a planar surface)

S is the total lifting surface area

p is the pressure difference between the upper and lower covers of the surface

$\bar{w}$ is the complex normal wash = $U\alpha + i\omega h$

U is the free stream velocity

h,α are the normal displacement and the streamwise slope of the surface

ω is the harmonic frequency of oscillation

ρ is the air density

t is time

K is the kernel furction specifying the normalwash angle at P_j due to a unit pressure at P

k is the reduced frequency = $\omega b_o/U$

b_o is the reference semichord

M is the Mach number.

This can be rewritten as

$$w(P_j) = \frac{1}{4\pi\rho U^2} \iint_S p(P)K(P_j, P, k, M)d\xi d\sigma$$

or

$$w(P_j) = \frac{1}{8\pi}\iint_S C_p(P)K(P_j, P, K, M)d\xi d\sigma, \qquad (8.2)$$

and for planar surfaces can be written as

$$w(x,y) = \frac{1}{8\pi} \iint_S C_p(\xi,\eta)K(x-\xi, y-\eta,k,M)d\xi d\eta, \qquad (8.3)$$

where

w is the normal or downwash angle = $\bar{w}/U$

C_p is the differential pressure coefficient = p/q

q is the dynamic pressure = $\frac{1}{2}\rho U^2$.

In the program, the planform coordinates (x,y) and (ξ,η) are normalized with respect to the root semichord, b_o. These nondimensional coordinates $(\tilde{x},\tilde{y})$ and $(\tilde{\xi},\tilde{\eta})$ are, in turn, transformed into the coordinates of a square planform, $(\underset{\sim}{x}, \underset{\sim}{y})$ and $(\underset{\sim}{\xi},\underset{\sim}{\eta})$ as shown in Figure 8-2. After transformation of coordinates, the integral equation becomes

$$w(x,y) = \frac{1}{b_o}\left(\frac{\partial h}{\partial \underset{\sim}{x}} + ikh\right)$$

$$= \frac{1_o}{8\pi b_o^2} \int_{-1}^{1}\int_{-1}^{1} C_p(\underset{\sim}{\xi},\underset{\sim}{\eta})K(\tilde{x}-\tilde{\xi}, \tilde{y}-\tilde{\eta},k,M)b(\underset{\sim}{\eta})d\underset{\sim}{\xi}d\underset{\sim}{\eta}, \qquad (8.4)$$

Planform (in real coordinates)

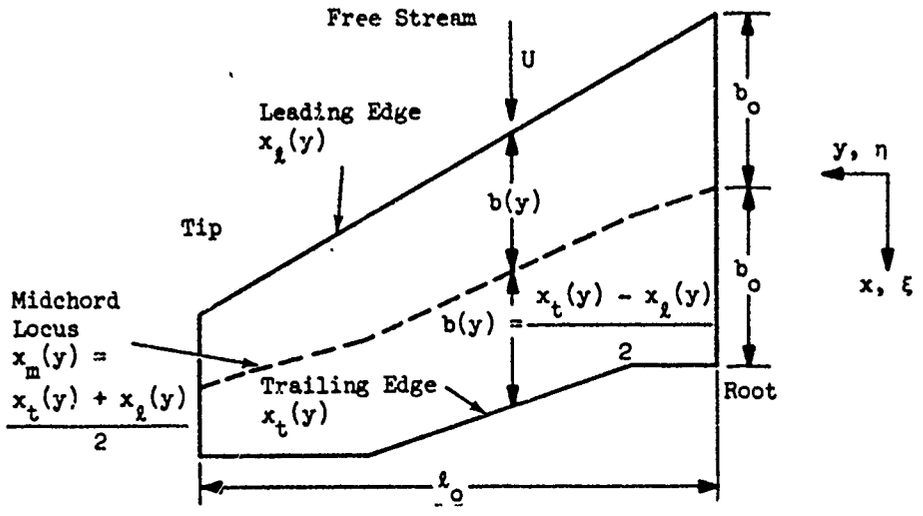

Transformations to Nondimensional Coordinates

$$\tilde{x} = x/b_o \qquad \tilde{\xi} = \xi/b_o$$
$$\tilde{y} = y/b_o \qquad \tilde{\eta} = \eta/b_o$$

Transformations to Normalized Nondimensional Coordinates

$$\underset{\sim}{x} = \frac{x - x_m(y)}{b(y)} \qquad \underset{\sim}{\xi} = \frac{\xi - \xi_m(\eta)}{b(\eta)}$$

$$\underset{\sim}{y} = y/l_o \qquad \underset{\sim}{\eta} = \eta/l_o$$

The above transformations convert the planform into a unit square.

Figure 8.2. Coordinate Systems Used in the Assumed-Pressure-Function Approach.

where

l_o is the semispan

b_o is the root semichord

$b(\eta)$ is the local semichord.

In the above equation, the planform has been assumed symmetrical about y = o as indicated by the limits of spanwise integration. Equation (8.4) must now be solved for the unknown pressure coefficient distribution, $C_p\ (\xi,\eta)$, in terms of the known downwash distribution. The solution procedure requires that the pressure distribution be expressed as a series of terms, each of which is the product of an unknown constant coefficient and a specific loading function. The unknown constant coefficients are then moved outside the integral and the remaining integration is performed. To assure that the series can represent the pressure correctly, the loading functions are chosen to satisfy the following boundary conditions:

- A square-root singularity at the planform leading edge
- A zero at the trailing edge
- A zero at the planform tip (or outboard edge)
- An infinite slope at the tip.

A suitable series expression satisfying these conditions, which is used in Reference 8-2 and in this program, is

$$C_p\ (\xi,\eta) = \frac{8l_o}{b(\eta)}\sqrt{\frac{1-\xi}{1+\xi}}\cdot\sqrt{1-\eta^2}\sum_{j=1}^{J}\eta^{2(j-1)+\delta}$$

$$\cdot\left(a_{1,j}+\sum_{i=2}^{I}a_{i,j}\,\xi^{i-2}\,(1+\xi)\right), \qquad (8.5)$$

where

$a_{i,j}$ are the, as yet, undetermined pressure series coefficients

δ = 0 for a symmetrical distribution of airloads about the root and

= 1 for an antisymmetrical distribution

I is the number of terms in the chordwise series

J is the number of terms in the spanwise series.

After substituting the series expression for the differential pressure into Equation (8.4) and removing the unknown constants from the integral, the remaining chordwise integrations are of the form:

$$I_d = \int_{-1}^{1} (1-u)^{\alpha}(1+u)^{\beta} f_d(u)\,du, \qquad (8.6)$$

where

$u = \xi$

$\alpha = \frac{1}{2}$ and $\beta = -\frac{1}{2}$

$f_d(u)$ is an appropriate polynomial of degree d.

In the spanwise direction, the integrals also are of the above form but with different values of α and β. Inspection of Equation (8.5) shows the leading spanwise factor to be $\sqrt{1 - \eta^2}$; however, the kernel function, K, of Equation (8.4) contains a factor of $1/(1 - \eta^2)$. Consequently, the product of the pressure series and the kernel function has a factor of $1/\sqrt{1 - \eta^2}$ making the appropriate values of α and β: $\alpha = \beta = -\frac{1}{2}$ in the spanwise integral.

These integrals are evaluated using the Gauss-Mehler quadrature of Reference 8-3 (pages 312-357) to give

$$I_d = \sum_{q=1}^{Q} H(u_q)\, f_d(u_q), \qquad (8.7)$$

where

Q is the number of integration points

H are weighting functions given in rows two and four of Table 8.1

u_q are integration points given in rows two and four of Table 8.1.

With this method, if the integrand can be exactly represented by the product of a simple singular function, such as $1/\sqrt{1-u^2}$, and a polynomial of degree $d = 2Q-1$, then using the Q integration points would produce the integral with no error. Although the true integrand cannot be represented exactly with a finite number of terms in the polynomial part, by choosing enough integration points, the error may be made as small as desired.

TABLE 8.1. GAUSS-MEHLER QUADRATURE FORMULAE

For $\int_{-1}^{1} (1-u)^{\alpha}(1+u)^{\beta} f_d(u)du = \sum_{q=1}^{Q} H(u_q) f_d(u_q)$

α	β	H (weighting function)	U_q (integration point)
$\frac{1}{2}$	$\frac{1}{2}$	$\frac{\pi}{Q+1}(1-u_q^2)$	$-\cos\left(\frac{q\pi}{Q+1}\right)$
$\frac{1}{2}$	$-\frac{1}{2}$	$\frac{2\pi}{2Q+1}(1-u_q)$	$-\cos\left(\frac{2q-1}{2Q+1}\pi\right)$
$-\frac{1}{2}$	$\frac{1}{2}$	$\frac{2\pi}{2Q+1}(1+u_q)$	$-\cos\left(\frac{2q\pi}{2Q+1}\right)$
$-\frac{1}{2}$	$-\frac{1}{2}$	$\frac{\pi}{Q}$	$-\cos\left(\frac{2q-1}{2Q}\pi\right)$

After the integrations are performed, Equation (8.4) can be written

$$w(\tilde{x},\tilde{y}) = \sum_{i=1}^{I}\sum_{j=1}^{J} L_{i,j}(\tilde{x},\tilde{y})\, a_{i,j},$$

$$= \sum_{n=1}^{N} L_n(\tilde{x},\tilde{y})\, a_n, \qquad (8.8)$$

where

$a_n = a_{i,j}$, $N = I \times J$

$L_n = L_{i,j}$ = the result of the integration of the product of the kernel function and the i,j^{th} pressure series term.

When Equation (8.8) is applied at a set of points on the wing (called collocation points), a resulting system of linear equations relating the downwash at these points to the unknown coefficients is formed:

$$w(P_c) = \sum_{n=1}^{N} L_n(P_c) \cdot a_n$$

or

$$\underset{(Cx1)}{\{w\}} = \underset{(CxN)}{\left[L\right]} \underset{(Nx1)}{\{a\}}, \tag{8.9}$$

where

P_c is the c^{th} collocation point

C is the total number of collocation points.

The locations of the collocation points are chosen so that the error that would result from calculating the lift based on fitting a polynomial thru the collocation points is minimized. Reference 8-2 shows that in the chordwise direction, this loading is calculated from

$$\int_{-1}^{1} \sqrt{\frac{1+\underline{x}}{1-\underline{x}}}\; f(\underline{x})\, d\underline{x}, \tag{8.10}$$

where $f(\underline{x})$ is a polynomial. In the spanwise direction, the integral is of the form

$$\int_{-1}^{1} \sqrt{1-\underline{y}^2}\; g(\underline{y})\, d\underline{y}, \tag{8.11}$$

where $g(\underline{y})$ is a polynomial. Since these integrals are of the same form as Equation (8.6), Gaussian quadrature can again be used. In the streamwise case, Equation (8.10), $\alpha = -\frac{1}{2}$ and $\beta = +\frac{1}{2}$, while in the spanwise case of Equation (8.11) $\alpha = \beta = +\frac{1}{2}$. Hence, the proper choice of collocation points can be found in the first and third rows of Table 8.1.

The kernel function, K, of Equation (8.4) possesses a singularity as $\tilde{y} \to \tilde{\eta}$ and $\tilde{x} \to \tilde{\xi}$. Consequently, the collocation and integration points must not be allowed to coincide. From the above discussion and Table 8.1, the chordwise locations of these points are:

$$\underline{\text{integration points}} \qquad u_i = -\cos\left(\frac{2i-1}{2I_x+1}\right), \; i = 1,\ldots,I_x$$

$$\underline{\text{collocation points}} \qquad u_c = -\cos\left(\frac{2c\,\pi}{2C_x+1}\right) \quad c = 1,\ldots,C_x, \tag{8.12}$$

where

I_x is the total number of chordwise integration points

C_x is the total number of chordwise collocation points.

In the spanwise direction, the locations are:

$$\underline{\text{integration points}} \quad u_i = -\cos\left(\frac{2i-1}{2I_y}\pi\right), \; i = 1,\ldots,I_y$$

$$\underline{\text{collocation points}} \quad u_c = -\cos\left(\frac{c\pi}{C_y+1}\right), \; c = 1,\ldots,C_y \qquad (8.13)$$

where

I_y is the total number of spanwise integration points

C_y is the total number of spanwise collocation points.

With a choice of $I_y = C_y+1$ as in Reference 8-2, the points are distinct. In the current program, I_y can be chosen differently as will be described later.

Equation (8.9) can be written for each mode to be used in the analysis; hence, for several modes

$$\underset{(C\times NM)}{[w]} = \underset{(C\times N)}{[L]}\,\underset{(N\times NM)}{[a]}, \qquad (8.14)$$

where NM is the total number of modes. In Reference 8-2, the total number of collocation points, C, must equal the total number of undetermined pressure series coefficients, N. With such a restriction, $[L]$ is a square matrix and Equation (8.14) can be solved for $[a]$ by simple inversion. For relatively complicated mode shapes, requiring a large number of collocation points, this restriction forces the use of high order polynomials to represent the pressure distribution. Since this can lead to unrealistic convolutions in the calculated pressures, a new procedure has been adopted in the present program which permits the use of fewer polynomial terms. In this approach, the $[L]$ matrix is no longer square $(C>N)$ and Equation (8.14) is solved in a least-square sense as described in Reference 8-4.

A least-square solution to Equation (8.14) consists of a matrix $[a]$ which minimizes

$$\| [w] - [L][a] \| \qquad (8.15)$$

where $\|\ldots\|$ indicates the Euclidean norm - defined as the square root of the sum of the squares of the terms of the array. This is equivalent to minimizing

$$\left([w]^T - [a]^T[L]^T\right)\left([w] - [L][a]\right). \qquad (8.16)$$

for each of the NM columns of $[w] - [L][a]$.

When the rank of $[L]$ equals N, a solution can be obtained hypothetically by

$$[L]^T [L][a] = [L]^T [w]$$
$$[a] = \left([L]^T [L]\right)^{-1} [L]^T [w]. \qquad (8.17)$$

However, $[L]^T [L]$ is frequently ill-conditioned making this direct approach impractical. Reference 8-4 shows that this problem can be avoided by first decomposing $[L]$ by an orthogonal transformation $[T]$, formed by the continued product of Householder transformations (Reference 8-5), such that

$$\underset{(CxC)}{[T]}\underset{(CxN)}{[L]} = \begin{bmatrix} \tilde{R} \\ \hline 0 \end{bmatrix}_{(CxN)}, \qquad (8.18)$$

where $[\tilde{R}]$ is an NxN upper triangular matrix. Applying this transformation to both sides of Equation (8.14), one obtains

$$\begin{bmatrix} \tilde{R} \\ \hline 0 \end{bmatrix} [a] = [T][w]. \qquad (8.19)$$

Upon extraction of the first N rows, Equation (8.19) becomes

$$[\tilde{R}]\,[a] = [I\,|\,0][T][w], \qquad (8.20)$$

where $[I]$ is an NxN identity matrix. Since $\tilde{R}$ is an upper triangular matrix, this equation is easily solved by the back solution part of any linear-system-solver (see Reference 8-3, pp 428-429). It can be shown that the solution of this equation is, indeed, a least squares solution to Equation 8.14. This is done by showing that it can be reduced to Equation 8.17. To reduce the computing time required in subsequent re-analyses made with revised modal data, the user can save the matrices $[T]$ and $[T]\cdot[L]$ for future use. In subsequent analyses, new $[w]$ matrices are generated and a system analogous to Equation 8.20 is formed:

$$[I\,|\,0] \cdot ([T] \cdot \underset{old}{[L]}) \cdot \underset{new}{[a]} = [I\,|\,0] \cdot \underset{old}{[T]} \cdot \underset{new}{[w]}, \qquad (8.21)$$

from which pressure series coefficients, $[a]$, can be determined for the new modes.

Once the pressure series coefficients have been determined, the normalized generalized air forces are computed by

$$\bar{Q}_{rs} = \frac{1}{\omega^2} Q_{rs} = \frac{-1}{\omega^2} \iint_{S/2} h_r(x,y)\, p_s(x,y)\, dx\, dy, \tag{8.22}$$

where

Q_{rs} is the generalized air force in the r^{th} mode due to the pressure from the s^{th} mode

$S/2$ indicates integration over one half of the planform

h_r is the deflection distribution in the r^{th} mode

p_s is the pressure distribution in the s^{th} mode.

This can be rewritten as

$$\bar{Q}_{rs} = \frac{-b_{oo}^2}{2k^2} \iint_{S/2} h_r(x,y)\, C_{p_s}(x,y)\, dx\, dy. \tag{8.23}$$

Transforming to nondimensional coordinates and substituting Equation 8.5, this becomes

$$\bar{Q}_{rs} = \frac{-4b_o^3 l_{oo}^2}{k^2} \sum_{j=1}^{J} \int_{-1}^{0} \sqrt{1-\underline{y}^2}\; \underline{y}^{2(j-1)+\delta}$$

$$\cdot \int_{-1}^{1} \sqrt{\frac{1-\underline{x}}{1+\underline{x}}} \left(a_{1,j}^{(s)} + \sum_{i=2}^{I} a_{i,j}^{(s)} (\underline{x}+1)\underline{x}^{i-2} \right) h^{(r)}(x,y)\, d\underline{x}\, d\underline{y}. \tag{8.24}$$

This integration is performed using the appropriate Gauss-Mehler quadrature formulae previously described. The number of integration points used in the chordwise integration is twice the number of chordwise collocation points, C_x, and in the spanwise integration equals the number of collocation points, C_y.

Important considerations in using the assumed-pressure function program are the choices of the number of terms in the pressure polynomial, the number of integration points, and the number of collocation points. For Equation 8.14 to have a unique solution, the number of collocation points in both the chordwise and spanwise directions must be equal to or greater than the number of polynomial terms chosen to represent the pressure distribution in

the respective directions; i.e.,

$$C_x \geq I \text{ and}$$
$$C_y \geq J. \tag{8.25}$$

Furthermore, for chordwise and spanwise integrations of the product of the pressure and the kernel function to be satisfactory, Reference 8-2 advises that the number of integration points in each direction should obey the relationships

$$I_x \geq C_x \text{ and}$$
$$I_y \geq C_y+1. \tag{8.26}$$

To increase accuracy, more integration points can be used in the present program than the minimum recommended. In Reference 8-6, it is shown that the excess chordwise integration points can cause numerical difficulties if their number is not chosen carefully to avoid close proximity between the collocation and integration points. It suggests the following formula to govern the choice:

$$I_x = (C_x + \tfrac{1}{2}) \cdot (2NC-1), \tag{8.27}$$

where NC is a positive integer and I_x is taken as the truncated integer value of the expression. In the present program, the user selects C_x and NC as data after which the program itself computes I_x from the above equation. Additionally, the user supplies C_y and a positive integer, NS, as data; and the program computes the number of spanwise integration stations by the formula:

$$I_y = NS\ (C_y+1). \tag{8.28}$$

One final empirical guideline suggested in Reference 8-6 to obtain converged results is to choose the number of collocation points to satisfy the ratio

$$\frac{C_x}{C_y} \simeq \frac{\sqrt{1-M^2}\ (A.R.)}{\cos \Lambda_m} \tag{8.29}$$

where

M is the Mach number

A.R. is the aspect ratio

Λ_m is the sweep of the wing midchord at the root.

8.2.2 Supersonic Mach-Box Program

For the supersonic regime, the aerodynamics program used is a modified version of the Mach-box procedure described in Reference 8-7. For a harmonically oscillating planar surface, the pressure is related to the velocity potential, and thence to the downwash distribution, by

$$p(x, y) = 2\rho \left(U \frac{\partial}{\partial x} + i\omega\right) \varphi(x, y)$$

$$= \frac{-2\rho}{\pi} \left(U \frac{\partial}{\partial x} + i\omega\right) \iint_S \bar{w}(\xi, \eta) \cdot e^{\frac{-i\omega M^2}{U\beta^2}(x-\xi)} \cdot \frac{\cos \frac{\omega M}{U\beta^2} R}{R} \, d\xi \, d\eta$$

$$\text{or} \quad C_p(x,y) = \frac{-4}{\pi} \left(\frac{\partial}{\partial x} + i \frac{\omega}{U}\right) \iint_S w(\xi, \eta) \cdot e^{-i \frac{\omega M^2}{U\beta^2}(x-\xi)} \cdot \frac{\cos \frac{\omega M}{U\beta^2} R}{R} \, d\xi \, d\eta, \tag{8.30}$$

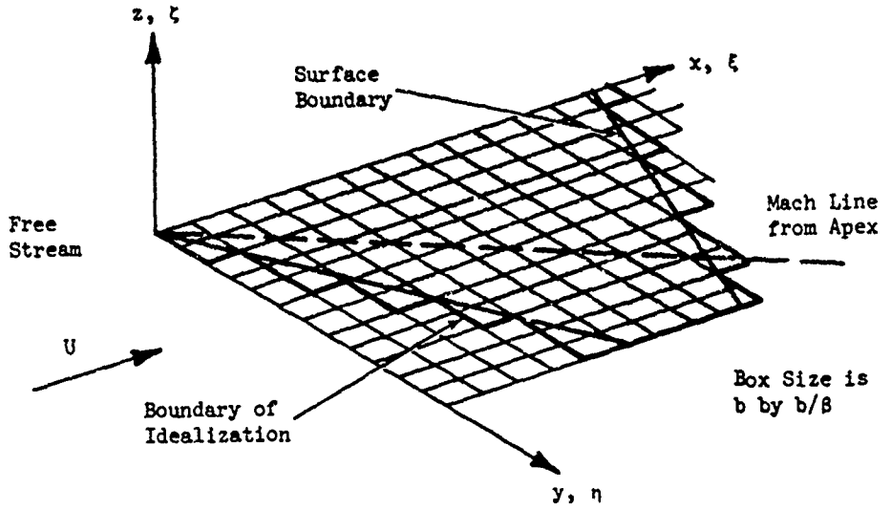

Figure 8.3. Mach Box Grid for a Lifting Surface.

where

x, ξ	are streamwise coordinates
y, η	are spanwise coordinates
p	is the differential pressure between the upper and lower covers of the surface
ρ	is the air density
U	is the free stream velocity
ω	is the frequency of oscillation
φ	is the velocity potential
S	is the lifting surface area bounded by the inverse Mach cone emanating from (x, y)
$\bar{w}$	is the complex downwash velocity $= U\alpha + i\omega h = Uw$
h, α	are the deformation and slope of the surface
M	is the Mach number
β	$= \sqrt{M^2-1}$
R	$= \sqrt{(x-\xi)^2 - \beta^2 (y-\eta)^2}$
C_p	is the differential pressure coefficient $= p/\frac{1}{2}\rho U^2$.

With the exception of special cases, the integral cannot be evaluated in closed form; hence, a numerical approach is required. In Reference 8-7, the area, S, is divided into elementary small rectangular boxes having their diagonals parallel to the Mach lines as shown in Figure 8.3. The rectangles are subsequently converted to squares through the coordinate transformations

$$\underline{\text{Streamwise}} \qquad \tilde{x} = x/b,$$

$$\tilde{\xi} = \xi/b,$$

$$\underline{\text{Spanwise}} \qquad \tilde{y} = \beta y/b$$

$$\tilde{\eta} = \beta\eta/b, \tag{8.31}$$

where b is the streamwise dimension of a box and b/β is the spanwise dimension.

Assuming the downwash is constant over each of these "Mach boxes," Equation (8.30) can be rewritten as:

$$C_p(\tilde{x}, \tilde{y}) = \frac{-4}{\pi}\sum_j w_j \left[\frac{1}{b}\frac{\partial}{\partial \tilde{x}} + i\frac{\omega}{U}\right] \cdot \iint_{S_j} e^{-i\tilde{k}(\tilde{x}-\tilde{\xi})} \cdot \frac{\cos\frac{\tilde{k}\tilde{R}}{M}}{\tilde{R}\cdot b} \frac{b^2}{\beta}\, d\tilde{\xi}\, d\tilde{\eta},$$

$$C_p(\tilde{x}, \tilde{y}) = \frac{-4}{\beta\pi}\sum_j w_j \left(\frac{\partial}{\partial \tilde{x}} + ik\right) \iint_{S_j} e^{-i\tilde{k}(\tilde{x}-\tilde{\xi})} \cos\frac{\tilde{k}\tilde{R}}{M} \cdot \frac{d\tilde{\xi}\, d\tilde{\eta}}{\tilde{R}}, \tag{8.32}$$

or $$C_p(\tilde{x}, \tilde{y}) = \sum_j w_j C_j(\tilde{x}, \tilde{y}), \tag{8.33}$$

where

S_j is the j^{th} box within the inverse Mach cone emanating from $(\tilde{x}, \tilde{y})$

$k = \frac{b\omega}{U}$

$\tilde{k} = \left(\frac{M}{\beta}\right)^2 k$

$\tilde{R} = \sqrt{(\tilde{x}-\tilde{\xi})^2 - (\tilde{y}-\tilde{\eta})^2}$

b is the streamwise box size

w_j is the downwash on the j^{th} box

C_j is the j^{th} pressure influence coefficient for point $(\tilde{x}, \tilde{y})$, i.e., the pressure at the point due to a unit downwash on the j^{th} box.

Two methods have been classically used to perform the complex integration over the box area. The first, developed in Reference 8-8, uses a mean value of the exponential and cosine terms when a box is far removed from the point $(\tilde{x}, \tilde{y})$ and a series expansion up to k^2 when a box is close. Although these approximations simplify the integration, they introduce significant errors, when the reduced frequency, k, is high. For a more exact evaluation, a second method, a Bessel function series representation of the integral, is presented in Reference 8-7.

The method used in the current program is different from both of these two in that Gaussian quadrature is used to evaluate the integral. With this technique, singularities that occur in the integrand when the box area is cut or touched by the inverse Mach cone emanating from the point $(\tilde{x}, \tilde{y})$ - see Figure 8.4a - can be accurately accounted for as described below. In fact, if the integrand could be represented exactly by the product of a simple singular function, such as $1/\sqrt{1-y}$, and a polynomial of order 2N-1, then using N integration points would produce the integral with no error. Although the true integrand cannot be represented exactly in the above manner, by taking enough integration points the error may be made as small as desired.

First, the pressure influence coefficient of Equation (8.32) is rewritten by performing a change of variables:

$$C_j(\tilde{x},\tilde{y}) = -\frac{4}{\beta\pi}\left(\frac{\partial}{\partial\Delta x} + ik\right)\int_{m-\frac{1}{2}}^{m+\frac{1}{2}}\int_{\ell-\frac{1}{2}}^{\ell+\frac{1}{2}} e^{-ik\tilde{\Delta}x}\cdot\cos\frac{\tilde{k}\tilde{R}}{M}\cdot\frac{d\Delta x}{\tilde{R}}\,d\Delta y,$$

$$= -\frac{4}{\beta\pi}\,ik\int_{m-\frac{1}{2}}^{m+\frac{1}{2}}\int_{\ell-\frac{1}{2}}^{\ell+\frac{1}{2}} e^{-i\tilde{k}\Delta x}\cdot\cos\frac{\tilde{k}\tilde{R}}{M}\cdot\frac{d\Delta x\,d\Delta y}{\tilde{R}}$$

$$-\frac{4}{\beta\pi}\,e^{-i\tilde{k}\left(\ell+\frac{1}{2}\right)}\int_{m-\frac{1}{2}}^{m+\frac{1}{2}}\cos\frac{\tilde{k}\tilde{R}_{\ell+\frac{1}{2}}}{M}\cdot\frac{d\Delta y}{\tilde{R}_{\ell+\frac{1}{2}}}$$

$$+\frac{4}{\beta\pi}\,e^{-i\tilde{k}\left(\ell-\frac{1}{2}\right)}\int_{m-\frac{1}{2}}^{m+\frac{1}{2}}\cos\frac{\tilde{k}\tilde{R}_{\ell-\frac{1}{2}}}{M}\cdot\frac{d\Delta y}{\tilde{R}_{\ell-\frac{1}{2}}}, \qquad (8.34)$$

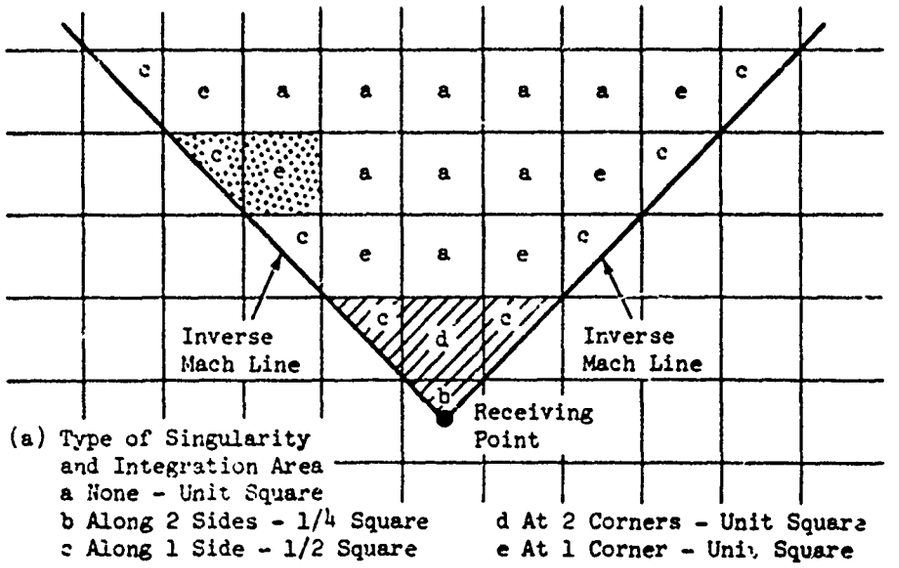

(a) Type of Singularity and Integration Area
a None - Unit Square
b Along 2 Sides - 1/4 Square
c Along 1 Side - 1/2 Square
d At 2 Corners - Unit Square
e At 1 Corner - Unit Square

(b) Local Mach Box Coordinates for Arbitrary Receiving Point

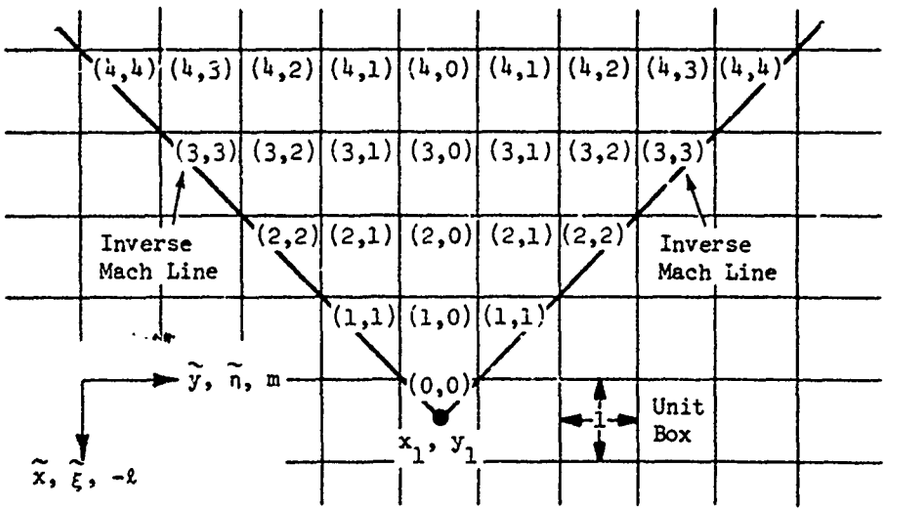

Box Centers:

$\Delta x = \tilde{x} - \tilde{\xi}$ $\quad \ell = \Delta x_c = \tilde{x} - \tilde{\xi}_c$

$\Delta y = \tilde{y} - \tilde{\eta}$ $\quad m = |\Delta y_c| = |\tilde{y} - \tilde{\eta}_c|$

Figure 8.4. Singularities and Coordinate System for Mach Box Formulation.

where

$\Delta x = \tilde{x} - \tilde{\xi}$

$\Delta y = \tilde{y} - \tilde{\eta}$

ℓ,m are the components of the distance between the j^{th} box center and the point $(\tilde{x}, \tilde{y})$ - see Figure 8.4b.

$$\tilde{R}_{\frac{1}{2}} = \sqrt{(\ell + \tfrac{1}{2})^2 - (\tilde{y} - \tilde{\eta})^2}$$

$$\tilde{R}_{-\frac{1}{2}} = \sqrt{(\ell - \tfrac{1}{2})^2 - (\tilde{y} - \tilde{\eta})^2}$$

Next, the two single and one double integrations are performed using various quadrature formulae of Reference 8-9. Referring to Figure 8.4a, five cases can arise depending on how the sending box is cut by the inverse Mach cone from $(\tilde{x}, \tilde{y})$:

(a) Box not touched: $\ell \geq 2$, $m \leq \ell - 2$.

(b) Box at apex of the cone: $\ell = 0$, $m = 0$.

(c) Box split by the cone: $\ell = m$, $m > 0$.

(d) Box touched at two corners by the cone: $\ell = 1$, $m = 0$.

(e) Box touched at one corner by the cone: $\ell > 1$, $m = \ell - 1$.

In case (a), since there is no singularity, the following quadrature formula (Equation 25.4.30, Reference 8-9) may be used for both the spanwise and chordwise integrations:

$$\int_a^b f(y)\, dy = \frac{b-a}{2} \sum_{i=1}^{n} H_i \cdot f(y_i), \tag{8.35}$$

where

$y_i = \frac{b-a}{2} x_i + \frac{b+a}{2}$

x_i is the i^{th} zero of the Legendre polynomial, P_n

H_i, the weighting function at the i^{th} quadrature point,
$= 2/(1 - x_i^2) \left[P_n'(x_i)\right]^2$.

In case (b), the integration is to be performed only on the triangular area of a quarter-box. Hence, reversing the order of integration in Equation (8.34), the limits of the double integral become $\int_0^{\frac{1}{2}} \int_{-\Delta x}^{\Delta x}$, while the limits of the single integral are $\int_{-\frac{1}{2}}^{\frac{1}{2}}$. Since R = 0 at the limits, Δx and $-\Delta x$, and since $R_{\frac{1}{2}} = R_{-\frac{1}{2}} = 0$ at the limits $\frac{1}{2}$ and $-\frac{1}{2}$, the spanwise integrals have singularities and a different quadrature formula (Equation 25.4.39, Reference 8-9) is used:

$$\int_a^b \frac{f(y)\,dy}{\sqrt{(y-a)\,(b-y)}} = \sum_{i=1}^{n} H_i \; f(y_i), \tag{8.36}$$

where

$$y_i = \frac{b-a}{2} x_i + \frac{b+a}{2}$$

$$x_i = \cos (2i-1) \frac{\pi}{2n}$$

$$H_i = \pi/n.$$

After the spanwise integration is performed, Formula (8.35) is used in the chordwise direction.

For case (c), the integration is done over a triangular half-box where the limits of the integrals become $\int_{\ell-\frac{1}{2}}^{\ell+\frac{1}{2}} \int_{\ell-\frac{1}{2}}^{\Delta x}$ and $\int_{\ell-\frac{1}{2}}^{\ell+\frac{1}{2}}$ Since the spanwise integrals here have singularities at the upper limits only, the appropriate quadrature formula (Equation 25.4.37, Reference 8-9) is:

$$\int_a^b \frac{f(y)\,dy}{\sqrt{b-y}} = \sqrt{b-a} \sum_{i=1}^{n} 2 \, H_i^{(2n)} \; f(y_i), \tag{8.37}$$

where

$y_i = a + (b-a)(1-x_i^2)$

x_i is the i^{th} pos. zero of the Legendre polynomial, P_{2n}.

$H_i^{(2n)}$ are the Gaussian weights of order 2n.

Again, Formula (8.35) is used in the chordwise integration.

For case (d), an integration is first performed over the triangular shaded area in Figure 8.4a (comprising boxes b, c, and d) using the quadrature formulae for case (b). Then by subtracting the previously derived pressure influence coefficients for boxes b and c, the desired integral over d is achieved.

Finally, for case (e), the integral for an aggregate area (see dotted area in Figure 8.4a) consisting of a triangle on the Mach line and the subject area is determined; and from it the integral for a triangle is subtracted. When the spanwise integrations are performed, Equation (8.37) is employed, while Equation (8.35) is used in the chordwise direction.

For case (a) and all chordwise integrations, the present program uses six integration points for the quadrature. In the spanwise integrations, six points are used when $k < \frac{4}{3}(\frac{\beta}{M})^2$, while twelve points are employed when $k \geq \frac{4}{3}(\frac{\beta}{M})^2$.

At a given Mach number and reduced frequency, the pressure influence coefficients are functions of only ℓ and m - the separation between the sending and receiving box centers. Consequently, influence coefficients are computed by the above formulae only once for each admissable ℓ, m pair ($\ell \geq 0$, $m \leq \ell$) and are used repeatedly where needed.

The pressure on any box is a function of the downwash of only those boxes within the inverse Mach cone emanating from its box center. For a surface, the edges of which are all supersonic, the pressure is, furthermore, only influenced by boxes on the planform. If any of the surface edges are subsonic, however, there are regions adjacent to these edges which do affect the pressure of some areas on the planform. To account for this effect, the concept (Reference 8-10) of a permeable "diaphragm" is introduced in these regions. This permeable sheet does not alter the flow nor can it sustain pressure. It

is bounded by the surface edge and the Mach lines emanating from the corners of the lifting surface - see Figure 8.5.

The relationship between the pressure and downwash on the combination of the lifting surface and the diaphragm area can be written:

$$\begin{Bmatrix} P_W \\ P_D \end{Bmatrix} = \begin{bmatrix} C_{WW} & C_{WD} \\ C_{DW} & C_{DD} \end{bmatrix} \begin{Bmatrix} w_S \\ w_D \end{Bmatrix}, \tag{8.38}$$

where

P_W is the pressure on the wing boxes

P_D is the pressure on diaphragm boxes

C_{WW} are the influence coefficients giving pressures on the wing boxes due to downwash on the wing boxes

C_{WD} are the influence coefficients giving pressures on the wing boxes due to downwash on the diaphragm boxes

C_{DW} are the influence coefficients giving pressures on the diaphragm boxes due to downwash on the wing boxes

C_{DD} are influence coefficients giving pressures on the diaphragm boxes due to downwash on the diaphragm boxes

w_S is the known downwash on the wing boxes

w_D is the unknown downwash on the diaphragm boxes.

Since the pressure on any diaphragm box is zero, then

$$\left[C_{DW}\right]\left\{w_S\right\} + \left[C_{DD}\right]\left\{w_D\right\} = \left\{0\right\}, \tag{8.39}$$

and the unknown diaphragm downwash can be evaluated by

$$\left\{w_D\right\} = -\left[C_{DD}\right]^{-1}\left[C_{DW}\right]\left\{w_S\right\} \tag{8.40}$$

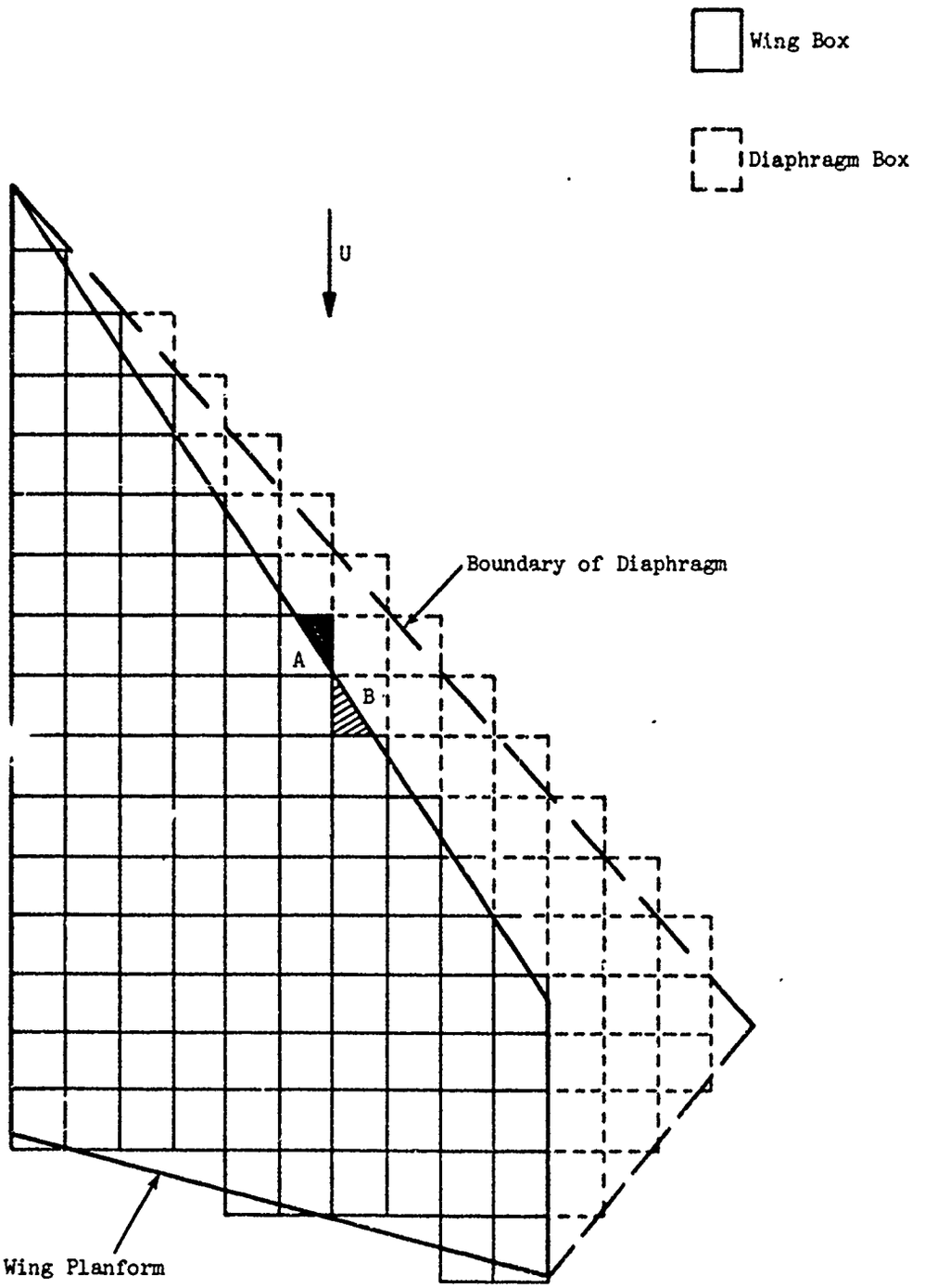

Figure 8.5. Box Allocation for Subsonic Leading Edge

Substituting this result into Equation (8.38), yields the final expression for the pressures on the wing boxes:

$$\{P_W\} = [AIC]\{w_S\} \tag{8.41}$$

where

$$[AIC] = [C_{WW}] - [C_{WD}][C_{DD}]^{-1}[C_{DW}] \tag{8.42}$$

For maximum computer efficiency, the actual calculation of the pressures, P_W, is generally performed in a different manner from that implied by Equation (8.41). The calculation of the aerodynamic influence coefficient matrix, $[AIC]$ leads to either extensive use of core in storing matrices or a large number of I/O operations if the matrices are stored on data devices. If there is no need for saving the $[AIC]$ array for future use, the machine operations can be appreciably reduced by computing the pressures as follows:

$$\left.\begin{array}{lll} (1) & \{X\} = [C_{DW}]\{w_S\} & \\ (2) & \{Y\} = [C_{DD}]^{-1}\{X\} & \\ (3) & \{Z\} = [C_{WD}]\{Y\} & \\ (4) & \{P_W\} = [C_{WW}]\{w_S\} - \{Z\} & \end{array}\right\} \tag{8.43}$$

In this way, core storage requirements are minimized, since only a vector need be stored in going from one step to another.

Once the oscillatory pressures are computed, the normalized generalized aerodynamic forces are computed by

$$\bar{Q}_{rs} = \frac{-b^2\rho}{2k^2} \iint_{S/2} h_r(x, y)\, C_{p_s}(x,y)\, dx\, dy. \tag{8.44}$$

Since the boxes are assumed to be very small, the integration can be replaced by a summation over every box on the planform:

$$\bar{Q}_{rs} = -\frac{b^2\rho}{2k^2} \sum_j h_r^{(j)}\, C_{p_s}^{(j)}\, A^{(j)}, \tag{8.45}$$

where

$h_r^{(j)}$ is the deflection of the j^{th} box in the r^{th} mode

$C_{p(s)}^{(j)}$ is the pressure coefficient of the j^{th} box in the s^{th} mode

$A^{(j)}$ is the area of the j^{th} surface box.

It should be noted that each box area is b^2/β. The program automatically establishes the gridwork of boxes: From a user specified number of boxes desired, the program calculates the box size necessary for the boxes to cover the planform and diaphragm and to align with the inboard and outboard planform edges. Consequently, no boxes overhang the planform side-edges. (Referral to Figure 8.5 here and in the remaining discussion may be helpful.) Each box is designated as either a wing box or diaphragm box depending on whether its center lies on or off the wing, respectively. In general, boxes do overhang the leading and trailing planform edges causing, in effect, a jagged representation of these edges. For most configurations, this jaggedness has been found to have little effect on the accuracy of the computed generalized aerodynamic forces, providing that the box grid is not too coarse. It follows that

since pressure is assumed constant over each box, wing boxes that overlap the planform edges support a force on their off-wing portion as well as the portion actually lying on the surface. This results in a computed force in excess of the correct amount. However, diaphragm boxes that overlap the planform edges support no force on either the on- or off-wing portions and, hence, result in a deficit in the computed wing forces that tends to balance the excess obtained from overhanging wing boxes. In Figure 8.5, this balance is illustrated for one representative pair of boxes. The shaded area is the off-wing portion of wing box A while the crosshatched area is the roughly balancing on-wing portion of diaphragm box B.

When a highly swept surface is analyzed for a relatively low Mach number, the number of forward diaphragm boxes can become so great as to cause an appreciable increase in computing time. However, the downwash in the diaphragm region decreases very rapidly in the forward streamwise direction. To save computing time, the present program takes this rapid decay of diaphragm downwash into account and allows the user to request a box-elimination option whereby the diaphragm boxes are ignored forward of a user specified distance ahead of the leading edge.

In the program, provision is made for computing aerodynamic force coefficients and center-of-pressure locations. The user may use this facility to compare known steady state data with computed values to determine the number of boxes required for a satisfactory solution. Another approach is to vary the number of boxes and look for convergence in the stability coefficients.

8.2.3 Subsonic Doublet-Lattice Program

For the added capability in the subsonic regime of analyzing control surface configurations, multiple interfering surfaces and interfering surface-body configurations, the doublet-lattice program of Reference 8-11 is used. The formulation of this method is different from the assumed-pressure-function method but starts with same integral equation relating the wash normal to a harmonically oscillating surface to the lifting pressure:

$$w(P_j) = \frac{1}{8\pi} \iint_S C_p(P) \quad K(P_j, P, k, M)\, d\xi\, d\sigma\,, \qquad (8.2)$$

where

P is any point on the planform, the coordinates of which are ξ, η, ζ

P_j is a j^{th} point, the coordinates of which are x, y, z

x, ξ are streamwise coordinates

y, η are spanwise coordinates

z, ζ are vertical coordinates

σ is the tangential spanwise coordinate

w is the normalwash angle = $\frac{\bar{w}}{U} = \alpha + i \frac{k}{b_o} h$

C_p is the differential pressure coefficient

K is the kernel function relating the normalwash at P_j to the a unit pressure at P

M is the Mach number

b_o is the reference semichord

h is the vertical displacement of the surface

α is the streamwise slope of the deformed surface

k is the reduced frequency

S is the surface area of all lifting surfaces included in the analysis.

If the surface is divided into J elements over which the pressure is assumed constant, the previous equation becomes

$$w(x, y, z) = \frac{1}{8\pi} \sum_{j=1}^{J} C_{p_j} \iint_{\substack{\text{ELEMENT} \\ j}} K(x-\xi, y-\eta, z-\zeta, \omega, M)\, d\xi\, d\sigma. \qquad (8.46)$$

Next, the pressure is assumed to arise from a loaded line at the $\frac{1}{4}$-chord of each element. As illustrated in Figure 8.6, this is equivalent to an unsteady horseshoe vortex whose bound portion lies along the $\frac{1}{4}$-chord of the element. The resulting expression is:

$$w(x, y, z) = \frac{1}{8\pi} \sum_{j=1}^{J} C_{p_j} \Delta\xi_j \int_{\substack{\text{ELEMENT} \\ j}} K(x-\xi_{\frac{1}{4}}, y-\eta, z-\zeta, \omega, M)\, d\sigma, \qquad (8.47)$$

where $\Delta\xi_j$ is the length of the average chord of element j, and the integration is taken along the $\frac{1}{4}$-chord line of the j^{th} element.

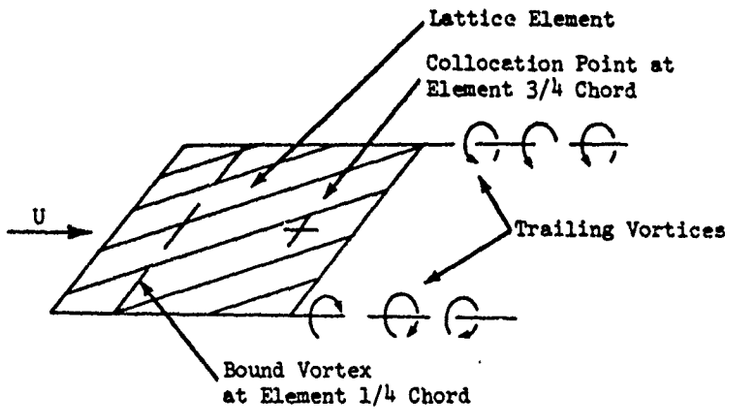

Figure 8.6. Horseshoe Vortex Element Used in Doublet-Lattice Method.

If the downwash is calculated at points located at the 3/4-chord midspan of each of the J elements and the above equation is satisfied at each of these points, the following set of equations holds for i = 1 to J:

$$w_i = \frac{1}{8\pi} \sum_{j=1}^{J} C_{p_j} \Delta\xi_j \int_{\substack{\text{ELEMENT} \\ j}} K\,(x_i-\xi_1,\ y_i-\eta,\ z_i-\zeta,\ \omega,\ M)\ d\sigma. \quad (8.48)$$

This can be written in matrix form as:

$$\{w\} = [D]\ \{C_p\}, \quad (8.49)$$

where D_{ij} relates the downwash at the i^{th} point to the pressure over the j^{th} element. By solving this set of linear equations, the pressure distribution over the surface is calculated.

Because the doublet lattice method is not explicitly fitting pressure functions on a planform as is done in the assumed-pressure-function method, multiple aerodynamically interacting surfaces can be modelled by simply defining lattice elements on each surface. In this case, Equation (8.48) still holds, but J is now the number of elements on all surfaces.

To account for aerodynamic interaction between bodies and surfaces, Reference 8-11 describes a method of modelling each body by axial doublets along the body axis and by panels of unsteady horseshoe vortex elements on the body surface in the vicinity of each lifting surface with which the body might interact (see Figure 8.7, for example). The strength of each axial doublet is calculated by slender body theory. The incremental downwash on the panels on the body surfaces and on the lifting surfaces caused by these axial doublets is then computed and subtracted from the prescribed downwash for these surfaces. Equation (8.49) becomes

$$\begin{bmatrix} D_{SS} & D_{SI} \\ D_{IS} & D_{II} \end{bmatrix} \begin{Bmatrix} C_{p(S)} \\ C_{p(I)} \end{Bmatrix} = \begin{Bmatrix} w_S \\ w_I \end{Bmatrix} - \begin{bmatrix} F_{SB} \\ F_{IB} \end{bmatrix} \{C_{p(B)}\}, \quad (8.50)$$

where

$C_{p(S)}$ is the pressure coefficient distribution on the lifting surfaces

$C_{p(I)}$ is the pressure coefficient distribution on the interacting body surfaces

$C_{p(B)}$ is the pressure coefficient distribution on the slender-body axial elements

w_S is the downwash distribution prescribed on the lifting surfaces

w_I is the downwash distribution prescribed on the interacting body surfaces

F_{SB} is the downwash distribution on the lifting surfaces caused by unit pressure coefficients along the slender bodies

F_{IB} is the downwash distribution on the interacting body surfaces caused by unit pressure coefficients along the slender bodies

D_{SS} is the downwash distribution on the lifting surfaces caused by unit pressure coefficients on the lifting surfaces

D_{SI} is the downwash distribution on the lifting surfaces caused by unit pressure coefficients on the interacting body surfaces

D_{IS} is the downwash distribution on the interacting body surfaces caused by unit pressure coefficients on the lifting surfaces

D_{II} is the downwash distribution on the interacting body surfaces caused by unit pressure coefficient on the interacting body surfaces.

Since $\left\{C_{p_{(B)}}\right\}$ was calculated from the downwash and geometry of each body using slender-body theory, the only unknowns in this matrix equation are $\left\{C_{p_{(S)}}\right\}$ and $\left\{C_{p_{(I)}}\right\}$. This set of equations is solved for these pressure distributions by a standard linear system solution algorithm using Gaussian triangularization and back solution (see Reference 8-3, pp 428-429).

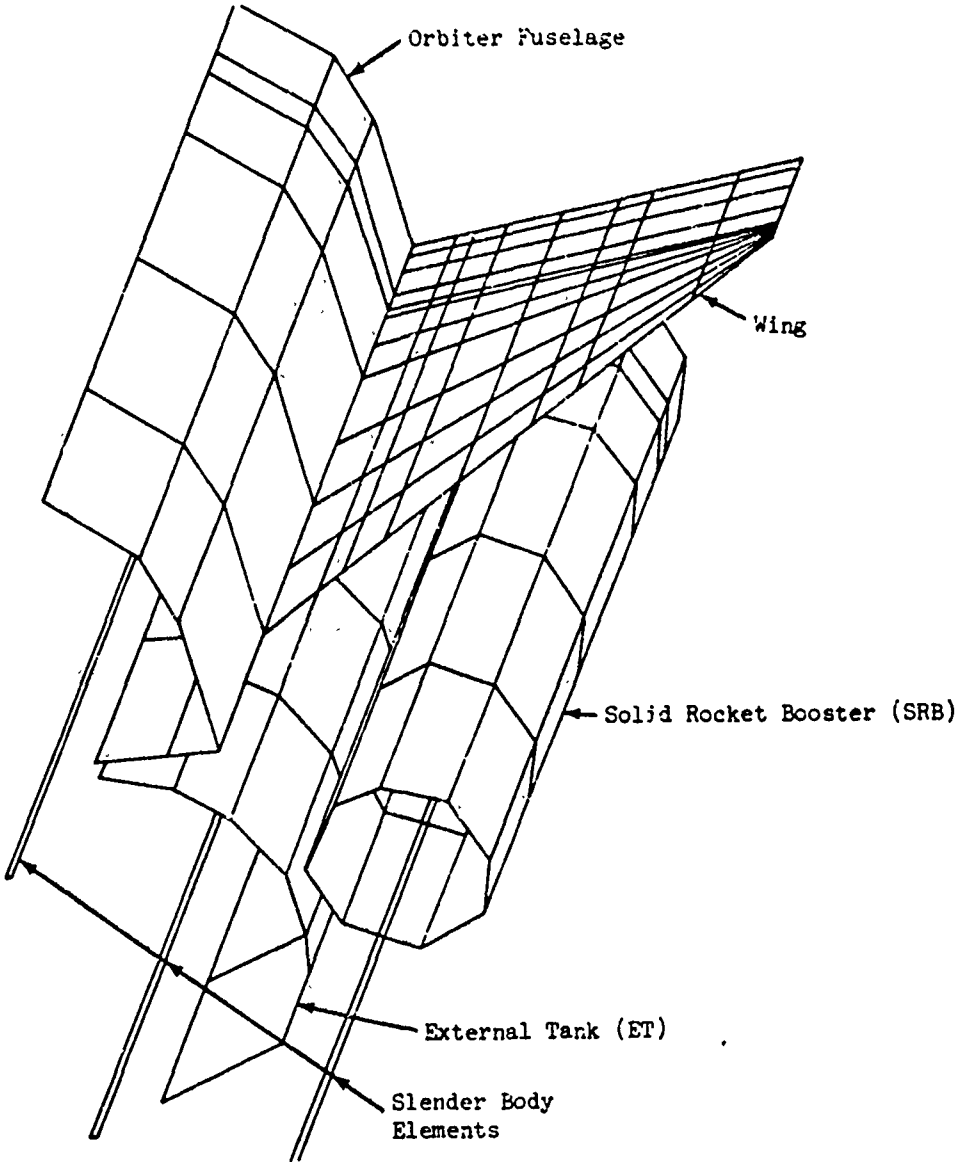

Figure 5.7. Aerodynamic Model of a Space Shuttle Using the Doublet-Lattice Method.

As in the Mach-box method, generalized aerodynamic forces arising from lifting surface pressures are calculated by

$$\bar{Q}_{rs} = \frac{b^2\rho}{2k^2} \sum_{j=1}^{J} h_r^{(j)} C_{p_s}^{(j)} A^{(j)}, \tag{8.45}$$

where, here, $A^{(j)}$ is the area of the j^{th} element. This can be rewritten in matrix form for all N modes as:

$$\underset{(NXN)}{\left[\bar{Q}\right]} = -\frac{b^2\rho}{2k^2} \underset{(NXJ)}{\left[h\right]} \underset{(JXJ)}{\left[A\right]} \underset{(JXN)}{\left[C_p\right]} \tag{8.51}$$

where $\left[A\right]$ is a diagonal matrix. When interacting bodies are present, three generalized forces are present:

$$\left[\bar{Q}\right] = \left[\bar{Q}_S + \bar{Q}_I + \bar{Q}_B\right] \tag{8.52}$$

The first arises from the product of deformations, pressures and areas of the lifting surface elements; the second from the product of those of the interacting body surface elements; and the third from the product of those of the body elements - the appropriate areas in this last case are the products of the body element diameters and lengths.

To obtain satisfactory pressure distributions, the lifting surface must be divided into strips of elements whose edges are parallel to the free stream. An example is shown in Figure 8.8. Additionally, element edges should lie along surface edges, fold lines and control surface hinge lines. Three guidelines should be observed in subdivision:

(1) The leading and trailing edges of adjacent pairs of elements should be aligned and located at a constant percent of the strip chord when possible.

(2) The dimensions of elements should be decreased in the directions and regions of large gradients in pressure and/or downwash, such as near hinge lines, leading edges and wing tips.

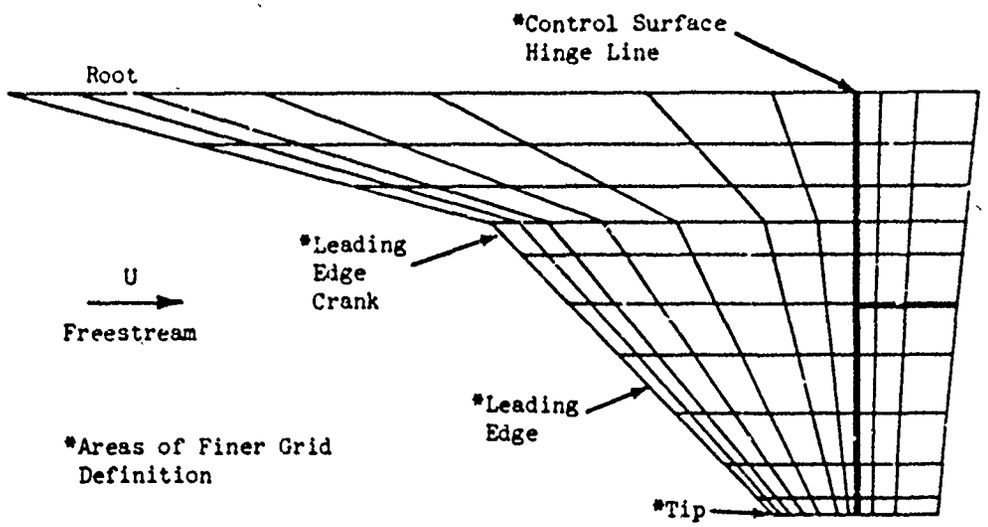

Figure 8.8. Doublet-Lattice Modeling of a Delta Wing with Cranked Leading Edge and Two Control Surfaces.

(3) The aspect ratio of each element should be unity or less. However, this is not always possible, especially in regions where a large pressure gradient is expected. This is evident in the example shown in Figure 8.7.

The optimum configuration is predicated by the need for keeping the number of elements to a minimum and at the same time generating generalized air force terms that are satisfactory for flutter analysis. It may be necessary to test a number of trial configurations and compare results before making a final analysis with a fixed element layout.

8.2.4 Modal Interpolation

For each of the above aerodynamics routines, the normalwash angle is required at specified aerodynamic grid points on the lifting surface:

$$w_{ij} = \frac{\bar{w}_{ij}}{U} = \alpha_{ij} + i \frac{k}{b_o} h_{ij}, \qquad (8.53)$$

where α_{ij} and h_{ij} are the streamwise slope and the displacement of point i in the j^{th} vibration mode. Since the modal data from the vibration analysis is specified on a dynamics grid which, in general, does not coincide with the aerodynamics grid, an interpolation is required. The procedure used consists of representing the dynamics grid as a set of spanwise oriented lines connecting node points at which modal deflections are specified. These deflections are interpolated along the lines to each spanwise station at which aerodynamic grid points lie and then are interpolated chordwise along each such station to each aerodynamic grid point. This scheme is illustrated in Figure 8.9.

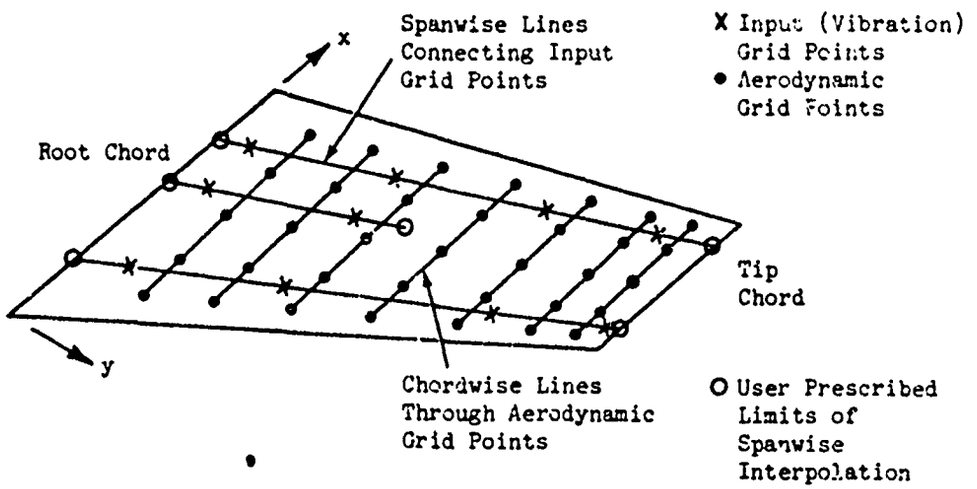

Figure 8.9. Modal Interpolation Scheme.

In a variation of this scheme, available as a program option, modal streamwise slopes, as well as deflections, are specified as input data along a single spanwise line. The program then creates a second line parallel to and at a specified streamwise distance from the specified line and transforms the modal slopes and deflections to a set of deflections along each line:

$$\left\{\begin{array}{c} h_1 \\ \hline h_2 \end{array}\right\} = \left[\begin{array}{c|c} I & 0 \\ \hline I & \delta \end{array}\right] \left\{\begin{array}{c} h_1 \\ \hline \alpha_1 \end{array}\right\} \tag{8.54}$$

where

$\{h_1\}$ and $\{\alpha_1\}$ are the deflections and streamwise slopes prescribed along the first line

$\{h_2\}$ are the deflections computed along the second line

$[I]$ is an identity matrix

$[\delta]$ is a diagonal matrix having the specified separation between the lines as each of its diagonal terms.

Using this set of lines and deflections, the interpolation proceeds according to the original scheme.

For a surface with a control surface or some other special region across the boundaries of which the modal deflections are not continuous, an option is available whereby the interpolation is performed over the main surface and over the control surface(s) separately using separate sets of lines and node points. In this manner, modal discontinuities across the boundaries are preserved.

The calculations performed in the above schemes use the Lagrangian interpolation formula of Reference 8-3, pages 60-68. Accordingly, a polynomial, $g(x)$, is determined as an approximation to a function, $f(x)$, the value of which is known at each of N+1 points, $\{x_0, x_1, \ldots, x_N\}$. This polynomial is computed by

$$g(x) = \sum_{k=0}^{N} \frac{(x-x_0) \cdots (x-x_{k-1})(x-x_{k+1}) \cdots (x-x_N)}{(x_k-x_0) \cdots (x_k-x_{k-1})(x_k-x_{k-1}) \cdots (x_k-x_N)} f(x_k), \tag{8.55}$$

In the present program, the polynomial, $g(x)$, is limited to degree N = 3 to minimize convolutions in the approximation. Consequently, in cases for which the modal deformations are specified at more than four points spanwise or chordwise, the approximation is a piecewise-continuous cubic polynomial. As a program option, the user can further restrict the polynomial to a linear or parabolic function in regions where extrapolation is needed either spanwise or chordwise.

8.2.5 Multiple Surface Capabilities

In the doublet-lattice procedure, multiple aerodynamically interacting surfaces may be treated as described in Section 8.2.3. Although the Mach box procedure and the assumed-pressure-function procedures do not account for interaction effects, these methods may be used to analyze a multiple surface vehicle where aerodynamic interaction is not present. This is achieved by calculating the generalized aerodynamic force contributions for each of the vehicle lifting surfaces and adding these together before passing them to the flutter solution routine. Additionally, the user can request that the aerodynamic forces of a particular surface be multiplied by a specified scalar before the addition is made, so that empirical knowledge of the actual lift of a surface as compared to its calculated value may be reflected.

8.3 GENERALIZED AERODYNAMIC FORCE INTERPOLATION

For a flutter analysis, generalized aerodynamic forces are required at several reduced velocities. To reduce the computation time needed to obtain these forces, interpolation is used to determine the generalized aerodynamic forces at all desired reduced velocities from forces directly computed at a small set of selected, reference reduced velocities. A separate interpolation is performed on the real and on the imaginary part of each term of the generalized aerodynamic force matrix. As in the modal interpolation of section 8.2.4, Lagrangian interpolation (Reference 8-3, pages 60-68) is used and the approximating function is limited to a piecewise continuous second- or third-order polynomial.

In the present program, the user supplies a goodness-of-fit tolerance and six reference reduced velocities ordered by increasing value and distributed over the range required in the subsequent flutter analysis: $\{v_1, v_2, \ldots v_6\}$ Using generalized forces computed at three of these six, a generalized aerodynamic matrix at a fourth is determined by interpolation and compared with a matrix of generalized forces directly computed at that reduced velocity. The comparisons are performed for various arrays, C, formed from combinations of the terms of the generalized force matrix and take the form of the test:

$$\frac{\text{abs}\left(\| C \|_{\text{computed}} - \| C \|_{\text{interpolated}}\right)}{\| C \|_{\text{computed}}} \leq \text{tolerance}, \qquad (8.56)$$

where $\| C \|$ is the Euclidean norm - defined as the square root of the sum of the squares of the terms of array, C. This test is made separately for C chosen as:

(1) the entire generalized force matrix, $\left[\bar{Q}\right]$

(2) a vector of the main diagonal terms of $\left[\bar{Q}\right]$

and (3) each successive two-by-two matrix formed about the main diagonal of $\left[\bar{Q}\right]$.

If any of the above tests fail, the computed forces at the fourth reduced velocity are added to the interpolation basis; and tests are made at a fifth reduced velocity. The procedure is continued for a sixth reduced velocity if necessary. A summary of the tests performed is presented below in Table 8.2.

TABLE 8.2. TESTS PERFORMED FOR GOODNESS-OF-FIT IN GENERALIZED AERODYNAMIC FORCE INTERPOLATION

TEST	INDICES OF COMPUTED ARRAYS USED FOR INTERPOLATION	INDEX OF TESTED ARRAY	TEST FAILURE LEADS TO
A	1, 3, 6	2	Test B
B	1, 2, 3, 6	4	Test C
C	2, 3, 4, 6	5	Use of all computed array in the actual interpolation

After the goodness-of-fit tests have been made, the procedure for obtaining generalized forces at any selected reduced velocity is summarized in Table 8.3.

TABLE 8.3. GENERALIZED AERODYNAMIC FORCE INTERPOLATION PROCEDURE IN VARIOUS REDUCED VELOCITY RANGES

RANGE	TEST A PASSED	TEST B PASSED	TEST C PASSED	TEST C FAILED
$v < v_1$	Extrapolation using parabolic fit through $\bar{Q}_1, \bar{Q}_3, \bar{Q}_6$	Extrapolation using parabolic fit through $\bar{Q}_1, \bar{Q}_2, \bar{Q}_3$		
$v_1 \le v \le v_2$	Interpolation using parabolic fit through $\bar{Q}_1, \bar{Q}_3, \bar{Q}_6$	Interpolation using cubic fit through $\bar{Q}_1, \bar{Q}_2, \bar{Q}_3, \bar{Q}_6$	Interpolation using cubic fit through $\bar{Q}_1, \bar{Q}_2, \bar{Q}_3, \bar{Q}_4$	
$v_2 \le v \le v_3$				
$v_3 \le v \le v_4$			Interpolation using cubic fit through $\bar{Q}_2, \bar{Q}_3, \bar{Q}_4, \bar{Q}_6$	Interpolation using cubic fit through $\bar{Q}_2, \bar{Q}_3, \bar{Q}_4, \bar{Q}_5$
$v_4 \le v \le v_5$				Interpolation using cubic fit through $\bar{Q}_3, \bar{Q}_4, \bar{Q}_5, \bar{Q}_6$
$v_5 \le v \le v_6$				
$v_6 < v$	Extrapolation using parabolic fit through $\bar{Q}_1, \bar{Q}_3, \bar{Q}_6$	Extrapolation using parabolic fit through $\bar{Q}_2, \bar{Q}_3, \bar{Q}_6$	Extrapolation using parabolic fit through $\bar{Q}_3, \bar{Q}_4, \bar{Q}_6$	Extrapolation using parabolic fit through $\bar{Q}_4, \bar{Q}_5, \bar{Q}_6$

* Note: $v_i = (1/k)_i$ ordered by increasing reduced velocity

In choosing the reference reduced velocities, the following considerations should be observed:

(1) For the computed aerodynamic forces to be most accurate, the lowest reduced velocity should be as high as possible consistent with the range of values needed for the flutter solutions.

(2) Generally, the first and sixth reference reduced velocities should span the expected range of v for which generalized aero forces are to be calculated. This precaution eliminates the need for extrapolation.

(3) The reference reduced velocities should emphasize regions where flutter is expected.

8.4 FLUTTER SOLUTION PROCEDURES

There are two solution options available to the user for the flutter analysis:

(1) the conventional k-method, using the QR algorithm (Reference 8-12, pages 515-568) to determine eigenvalues.

(2) the p-k-method, using a determinant iteration procedure with a quadratic predictor (Reference 8-12, page 435) to determine eigenvalues.

Generalized aerodynamic forces required at various reduced velocities in these analyses are usually determined by the interpolation procedure described in Section 8.3. However, if the user desires, directly computed aerodynamic forces can be used in the k-analysis. To help the analyst study the flutter mechanism, various options such as the automatic preparation of plots of modal structural damping and frequency as functions of airspeed are available.

If the redesign capability of FASTOP is to be used, the p-k flutter analysis must be selected, in which case various items such as the flutter vectors are computed.

8.4.1 Flutter Equation

The basic differential equation for a lifting surface in oscillatory motion is:

$$\left[M\right]\left\{\ddot{q}\right\} - \left[Q\right]\left\{q\right\} + \left[K\right]\left\{q\right\} = 0, \tag{8.57}$$

where

$\left[M\right]$ is the generalized mass matrix,

$\left[Q\right]$ is the generalized aerodynamic force matrix,

$\left[K\right]$ is the generalized stiffness matrix,

$\left\{q\right\}$ is the generalized coordinate vector.

The generalized aerodynamic force matrix equals the product of the aerodynamic matrix, $\left[A\right]$, and the dynamic pressure, $\frac{1}{2}\rho U^2$, where an element of $\left[A\right]$ is defined as:

$$A_{rs} = \iint_S h_r(x, y)\, C_{p_{(s)}}(x, y)\, dS, \tag{8.58}$$

where $h_r(x, y)$ is the deflection distribution in the r^{th} mode, $C_{p_{(s)}}(x, y)$ is the pressure coefficient distribution in the s^{th} mode, and the integration is performed over the lifting surface area, S. Hence, Equation (8.57) can be rewritten as

$$\left[M\right]\left\{\ddot{q}\right\} - \frac{\rho U^2}{2}\left[A\right]\left\{q\right\} + \left[K\right]\left\{q\right\} = 0. \tag{8.59}$$

If structural damping is present in the system, the generalized stiffness array should be modified as:

$$\left[\bar{K}\right] = \left[I + iG\right]\left[K\right], \tag{8.60}$$

where $[G]$ is a diagonal matrix of modal damping and $[I]$ is the identity matrix. The stiffness in the j^{th} mode is then

$$\bar{K}_{jj} = \left(1 + i\, g_{s(j)}\right) K_{jj}, \tag{8.61}$$

where $g_{s(j)}$ is the hysteretic or structural damping in the j^{th} mode. Then Equation (8.59) becomes

$$[M]\{\ddot{q}\} - \frac{\rho U^2}{2}[A]\{q\} + [\bar{K}]\{q\} = 0. \tag{8.62}$$

For harmonic motion, the generalized coordinates may be written as $\{q\} = \{\bar{q}\}\, e^{\lambda t}$, where $\bar{q}$ is time independent and λ may contain damping. Equation (8.62) can then be rewritten as:

$$\left[\lambda^2 [M] - \frac{\rho U^2}{2}[A] + [\bar{K}]\right]\{\bar{q}\} = 0. \tag{8.63}$$

8.4.2 k-Method

In the "American approach" (or k-method), since the conventional aerodynamic theories are valid only for undamped oscillations, the aerodynamic matrix is computed for a chosen reduced frequency, k, and the λ is considered to be undamped ($\lambda = i\omega$):

$$\left[-\omega^2 [M] - \tfrac{1}{2}\rho U^2 [A(k)] + [\bar{K}]\right]\{\bar{q}\} = 0. \tag{8.64}$$

This equation may be rewritten as

$$\left[\frac{1}{\omega^2}[\bar{K}] - [M] - \frac{\rho b^2}{2k^2}[A(k)]\right]\{\bar{q}\} = 0, \tag{8.65}$$

where the reduced frequency is defined as

$$k = \frac{b\omega}{U}, \tag{8.66}$$

where

b is a reference semichord

ω is the frequency of oscillation

U is the velocity of the free stream.

Now, an unknown hysteretic structural damping term, g, is introduced to bring the system into neutral stability. Applying this damping to the j^{th} diagonal term of the stiffness matrix of Equation (8.65) results in:

$$\bar{K}'_{jj} = \frac{1}{\omega^2}\left(1 + ig_{s(j)} + ig\right) K_{jj}. \tag{8.67}$$

For small values of damping $\left(g \cdot g_{s(j)} << 1\right)$, this j^{th} on-diagonal term may be approximated by

$$\bar{K}'_{jj} \approx \left(\frac{1 + ig}{\omega^2}\right)\left(1 + ig_{s(j)}\right) K_{jj}, \tag{8.68}$$

$$= \lambda \left(1 + ig_{s(j)}\right) K_{jj} = \lambda \bar{K}_{jj}, \tag{8.69}$$

where

$$\lambda = \frac{1}{\omega^2}(1 + ig). \tag{8.70}$$

Substitution in Equation (8.65) yields

$$\left[\lambda \left[\bar{K}\right] - \left[M\right] - \frac{\rho b^2}{2k^2}\left[A(k)\right]\right]\left\{\bar{q}\right\} = 0. \tag{8.71}$$

Defining the aerodynamic term as $\bar{Q}(k)$, this becomes

$$\left[\lambda \left[\bar{K}\right] - \left[M + \bar{Q}(k)\right]\right]\left\{\bar{q}\right\} = 0. \tag{8.72}$$

Solving this equation for each eigenvalue, λ, one obtains the values of the unknown damping and the accompanying ω of the system. A positive value of the damping means that structural damping must be added to the system to bring it to neutral stability; i.e., the system is unstable. A negative value has the opposite interpretation.

A flutter analysis by the k-method begins with the calculation (or interpolation) of generalized aerodynamic forces, $\left[\bar{Q}(k)\right]$, for a chosen set of reduced frequencies. Using the QR algorithm of Reference 8-12, pages 515-568, eigenvalues are determined from Equation (8.72) for each reduced frequency. Using Equations (8.70) and (8.66), the reduced frequency and the real and imaginary parts of each eigenvalue are converted to a frequency, a required damping, and a free stream velocity. By plotting these dampings and frequencies as functions of these velocities, the critical flutter speed (the lowest nonzero velocity at which $g = 0$) and the accompanying flutter frequency are determined.

Having derived the eigenvalues of Equation (8.72), the eigenvectors are determined using an inverse iteration procedure (Reference 8-12, pages 619-625). These are used to establish the uniqueness of the eigenvalues in a routine using the Gershgorin theorem (Reference 8-12, pages 638-646).

Because of the assumptions implicit in this approach, the subcritical damping and frequency trends are generally inaccurate. Occasionally, the method produces a multiple valued function of damping vs. velocity, making it difficult to order the roots in a routine to automatically determine the flutter speed. The advantage of this approach, however, is its speed; solutions to linear eigenvalue problems are relatively easy to compute.

8.4.3 p-k Method

An alternate approach to the solution of the flutter equation, which gives better subcritical trends and does not lead to double valued functions of damping vs. velocity, is the p-k method of Reference 8-1. The generalized coordinates are assumed to be damped harmonic functions; hence, Λ becomes

$$\Lambda = \sigma + i\omega$$

or

$$\Lambda = \frac{Uk}{b}(\gamma + i) = \frac{U}{b}p, \tag{8.73}$$

where ν is the damping coefficient equal to $\frac{1}{2\pi} \ln \frac{a_{n-1}}{a_n}$ (with a_n and a_{n-1} as the amplitudes of successive cycles of oscillation). Equation (8.63) then becomes

$$\left[\left(\frac{U}{b}\right)^2 p^2 \left[M\right] + \left[\bar{K}\right] - \frac{\rho U^2}{2}\left[A(k)\right]\right]\left\{\bar{q}\right\} = 0, \tag{8.74}$$

where the available constant amplitude (undamped) aerodynamic theories must be used to compute the aerodynamic matrix.

Unlike the k-method, an air speed U is now selected for which Equation (8.74) will be solved. The characteristic equation for the eigenvalues, p, is then written as

$$F(p, k) = \left|\left(\frac{U}{b}\right)^2 p^2 \left[M\right] + \left[\bar{K}\right] - \frac{\rho U^2}{2}\left[A(k)\right]\right| = 0. \tag{8.75}$$

In Reference 8-1, this equation is solved for p by the iterative Regula Falsi method. However, it is noted in that reference that this algorithm, which uses a linear predictor, occasionally exhibits nonconvergence. Consequently, in the present program this algorithm is replaced by Muller's method (Reference 8-12, pages 435-438), which employs a quadratic predictor. This means that each root estimate is a function of the most recent three estimates.

In preparing data for the p-k solution option, the user - by specifying an initial airspeed, an airspeed increment and the total number of airspeeds for which solutions are desired - defines the velocity range over which the flutter solution is to be determined. At the initial velocity, the program makes three estimates of each root, calculates corresponding generalized aerodynamic forces and computes F, the flutter determinant of Equation (8.75), for each estimate. After fitting a quadratic to the three F's, the program determines the value of the root for which this quadratic equals zero. This value becomes the next estimate of the root. Using the three most recent root estimates, this iteration is continued, determining new estimates. When the iteration has converged, the process is concluded for this root and begun for the next.

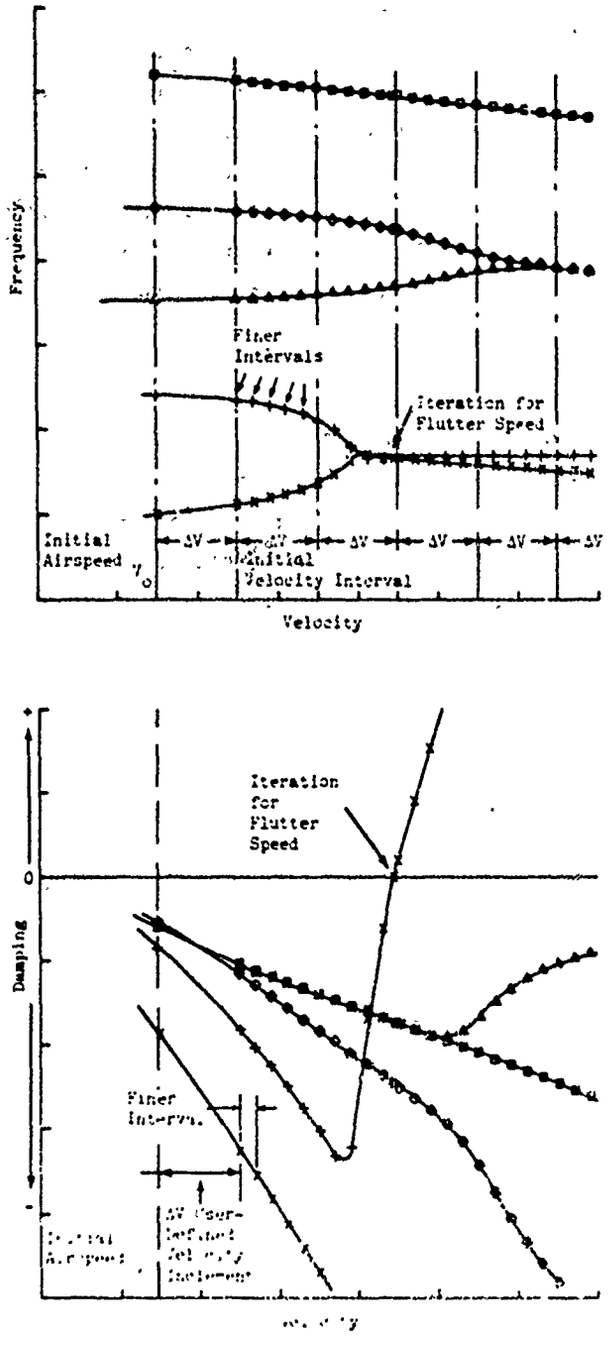

Figure 8.10. Typical p-k Flutter Solution.

Solutions are determined for each specified velocity in the user-defined range, using roots determined at the previous velocity as initial estimates at the next velocity. Optionally, the user can instruct the program to obtain the initial estimates by extrapolation from roots at the previous two velocities. Whenever significant changes in the slope of the damping or frequency are detected over the user-defined interval, the program automatically obtains solutions at finer velocity increments. (See Figure 8.10.) Finally, when a sign reversal in the damping part of the root occurs between consecutive velocities, the program initiates a search to determine the velocity for which the damping is zero, i.e., the flutter speed.

8.4.4 Flutter Analysis Features and Options

To help the user study the flutter mechanism, the program allows for the variation, in a single computer submission, of the stiffness of a chosen mode and of the number of normal modes (from an original set) included in the analysis. Furthermore, the flutter results - root damping and frequency as functions of airspeed - are presented in graphical (print-plot) form as an integral part of the computer listing. In addition, there is provision for obtaining CALCOMP plots of the flutter solution.

Another option is the provision for listing modal components of the eigenvectors (flutter vectors) for a given velocity or reduced velocity range (depending upon whether the p-k or k method is used for the solution). If requested by the user, the equivalent physical-coordinate vectors at the locations specified by input vibration data are also calculated and displayed.

Optionally, the user can make changes to the terms of the flutter equation by adding structural damping and by revising the generalized inertial or stiffness matrices.

A divergence analysis can also be performed, using the aerodynamic forces derived from a non-oscillatory condition. In which case, Equation (8.59) becomes:

$$\frac{-\rho U^2}{2}\left[A\ (k=0)\right]\left\{q\right\} + \left[K\right]\left\{q\right\} = 0. \qquad (8.76)$$

Both $[A]$ and $[K]$ are real matrices and the eigenvalue to be determined by the QR algorithm is U^2 in this case. If no positive eigenvalues exist, i.e., if $U^2 \leq 0$, the surface does not diverge; otherwise the divergence speed is the square root of the lowest positive eigenvalue.

8.4.5 Flutter Vectors for Redesign

When redesign is to be done in FASTOP, the flutter vector (among other quantities) is required. The flutter vector is the eigenvector of Equation (8.74) for the critical root at the flutter speed - the lowest non-zero speed at which the damping (the real part of the root) is zero. As described in Section 8.4.3, the program automatically searches to determine the flutter speed. The eigenvalue p, of the critical root at this speed is determined and the corresponding eigenvector, $\{u\}$ (the flutter vector), is found by the inverse iteration technique (Reference 8-12, pages 619-625).

By transposing the flutter matrix of Equation (8.75) and determining another eigenvector for p, the associated row vector, $\{v\}^T$, is obtained. Subsequently, the following parameter is formed for use in the computation of the flutter derivatives (see Section 9):

$$C = \frac{\text{Re}\left[\{v\}^T\left[\frac{\partial \bar{Q}}{\partial k}\right]\{u\}\right] + 2/k}{\text{Im}\left[\{v\}^T\left[\frac{\partial \bar{Q}}{\partial k}\right]\{u\}\right]} \quad , \tag{8.77}$$

where $\bar{Q}$ was defined by Equations (8.71) and (8.72). The derivative $\frac{\partial \bar{Q}}{\partial k}$ is obtained by differentiation of the generalized aerodynamic force interpolation polynomial, described in Section 8.3.

Section 9

RESIZING FOR COMBINED FLUTTER AND STRENGTH REQUIREMENTS

9.1 SUMMARY

Several methods for sizing the finite elements of a lifting-surface structural idealization to achieve minimum weight design under combined strength and flutter-speed requirements were developed and evaluated. Two basic categories were considered: methods based on a combination of energy principles and optimality criteria, and procedures employing numerical-search techniques. Drawing upon the experience gained from studies of both of these basic methods, a resizing algorithm was developed that employs a uniform-flutter-velocity-derivative optimality criterion for flutter-critical elements and the fully-stressed-design criterion for strength-critical elements. The final result is a practical, automated approach for dealing with large-scale idealizations having both structural and mass-balance design variables.

This section provides a summary of the major findings from the evaluation of the candidate flutter resizing methods and the factors that led to the selection of the final algorithm, which is discussed in detail. A more complete description of the methods examined, their underlying theory and assumptions, and the results they produced for a representative example wing structure are presented in Reference 9-1.

9.2 EVALUATION OF FLUTTER RESIZING ALGORITHMS

For a structure subjected to a single flutter-speed constraint, and no other constraints such as those imposed by strength and minimum-manufacturing-gage requirements, it can be shown that for a minimum-weight design, the derivatives of the critical flutter speed, V_f, with respect to the design variable weights, m_i, must be equal; that is

$$\frac{\partial V_f}{\partial m_i} = \text{constant} \qquad (9.1)$$

for all "i" structural finite elements and mass-balance weights.

This "optimality criterion" provides a standard of local optimality under the limited condition of a single design constraint. However, realistic structural

designs involve many constraints in combination (e.g., strength, flutter speed, minimum manufacturing gages) and their respective, separately-governing optimality criteria must be blended into a composite criterion. Moreover, to be of real value, it must be possible to satisfy such a composite criterion by a practical and efficient resizing procedure. These considerations have strongly influenced the development of the combined flutter/strength resizing algorithm in FASTOP.

The finally selected approach evolved from an extensive study of two classes of optimization methods. The first included optimality-criteria methods based on energy concepts; the second emphasized direct weight reduction by employing numerical-search methods. For comparison purposes, all of the candidate procedures were applied to the intermediate-complexity-wing structure described in Subsection 11.2.1. The objective was to resize an initial fully stressed, strength-governed design to achieve a 30% increase in flutter speed with a minimum increase in weight. The following paragraphs summarize these study efforts and provide the background that led to the final resizing algorithm.

9.2.1 Energy-Based Optimality-Criteria Methods

Although it was recognized early in the study that optimum resizing to increase flutter speed should aim toward achieving uniformity among the flutter-velocity derivatives of all resized elements, it was not evident that a simple resizing equation could be formulated for satisfying this criterion. Because of the rather complicated nature of the expression for these derivatives, as previously developed by Rudisill and Bhatia in Reference 9-2, it was felt that it would be difficult, if not impossible, to devise such an equation. Yet, it was reasoned that for practical resizing of very large structural idealizations, some flutter-resizing procedure that embodied the same basic simplicity as the fully-stressed-design approach for strength resizing should be developed, even if it was necessary to compromise the correct optimality criterion. Along these lines, several procedures based on approximate optimality criteria and simple energy-based resizing equations were conceived and examined. The hope here was that even if the correct criterion was not satisfied, the resulting design would still be efficient, although not optimum.

The two simplest versions of these approximate methods were identified as the "torsion mode fully stressed design" and the "flutter mode fully stressed

design" procedures. They were selected for study mainly because they could be integrated very simply into an existing fully-stressed-design program by the mere addition of pseudo-load conditions, acting along with the actual applied loading conditions, in the resizing process. The first was based on assumed proportionality between the fundamental torsional frequency and the flutter-speed, and attempted, in an approximate way, to optimize for torsional frequency. It used a properly scaled set of inertial loads in the torsion mode as a single additional pseudo-loading condition. The second method used a set of inertial-plus-aerodynamic loading conditions based on the complex flutter mode. In both methods, resizing for strength and flutter-speed requirements was performed simultaneously, so that interaction between the two requirements due to internal load redistribution was achieved automatically.

Two somewhat more sophisticated, but still approximate, procedures sought to achieve "uniform frequency derivatives in the torsion mode" and "uniform mean-strain-energy density in the flutter mode." The first of these approaches still relied on assumed proportionality between flutter speed and torsional frequency, but treated the frequency-optimization problem in a more exact way than in the previous torsion-mode fully-stressed-design approach. The second method, which received previous attention by Siegel in Reference 9-3, resized all flutter-critical elements so as to obtain equal values of average strain energy per unit weight during a flutter-oscillation cycle.

Three of the above methods led to converged designs that satisfied the requirement of a 30% flutter-speed increase with approximately the same increase in structural weight. One method (the one which attempted to achieve uniform frequency derivatives in the torsion mode) behaved so poorly that resizing was aborted before reaching the desired flutter speed. To evaluate the final results for the converged designs, the flutter-velocity derivatives of the elements that were resized to meet the flutter-speed requirement were calculated and examined for uniformity. The conclusion was discouraging in that no tendency toward uniformity existed, and no confidence could be placed in any of the methods. Concurrently, results from parallel studies (discussed in the next subsection) that used numerical-search techniques in conjunction with flutter-velocity derivatives confirmed the existence of significantly lighter designs than those obtained with the previously discussed approximate optimality-criteria methods.

Although none of the preceding methods were acceptable in themselves, the knowledge gained from their development became extremely valuable. All of the methods employed energy-type concepts -- both in establishing their approximate optimality criteria and in obtaining simple and effective resizing formulae for satisfying these criteria. It then became evident that by extending these energy concepts, it was possible to cast the expression for the exact flutter-velocity derivatives of Reference 9-2 into a new form that was identifiable in terms of generalized energy quantities. Moreover, it was also possible to obtain a simple strain-energy-based resizing formula for achieving the desired state of uniform flutter-velocity derivatives among structural elements.

When the formula was applied to the example wing structure, the final design achieved the required 30% increase in flutter speed with a weight increase of only about one-fourth of that required by the previous methods. Also, it was observed that at each intermediate design step in the overall resizing process, the flutter-velocity derivatives of the flutter-critical elements exhibited a high degree of uniformity, thereby demonstrating that the resizing formula embodied excellent convergence characteristics. Nevertheless, since the method relied on strain-energy-related quantities, an additional or more general redesign formula was needed to consider mass-balance variables. The numerical-search methods discussed next, as well as the final method selected for use in FASTOP, have the capability for dealing with mass balance.

9.2.2 Numerical Search Procedures

Paralleling the evaluation of the energy-based methods was the development and study of several numerical-search procedures that all employed the previously referenced expression for the precise flutter-velocity derivatives. A major distinction between these procedures and those already discussed is that the numerical-search methods do not rely on the definition and enforcement of an optimality criterion. Instead, concepts of travel in design space are employed to seek out a near-minimum-weight design that satisfies the flutter-speed constraint without compromising strength requirements.

Of the four numerical-search procedures studied, the first two were in the category of procedures for initially achieving the desired flutter speed. The latter two were techniques for minimizing structural weight after the flutter speed target was achieved. A complete resizing method required that procedures

in both categories be used sequentially.

In the first category, the "flutter-velocity-gradient redesign" procedure was a straightforward approach that added increments of weight to structural elements in proportion to their flutter-velocity derivatives. The second procedure, "weight-factored-gradient redesign", was a refinement of the first, wherein the incremental weight added to each element was factored by the element's total weight. This was done in order to arrive at the desired flutter-speed constraint surface with a lower-weight design than that obtained in the previous method, which tended to add excessive weight to the lighter structural elements. Both techniques were applied to the intermediate-complexity-wing structure in a step-by-step resizing mode, arriving at the desired flutter speed with much smaller increments of structural weight than any of the previously described approximate optimality-criteria methods.

To then travel along the constraint surface to a minimum-weight design point, a "biased tangent" approach and the "method of feasible directions" (see References 9-4 and 9-5) were each employed separately, starting with the last design obtained by the flutter-velocity-gradient redesign method. Both procedures led to final designs having essentially the same weight as that achieved by the last energy-based optimality-criteria approach that aims for uniform flutter-velocity derivatives. However, although both procedures yielded good results, considerable difficulty was experienced in developing an efficient automated step-size determination procedure.

In summarizing the findings of these numerical-search studies, two major points should be noted. First, the requirement for a two-phase redesign operation, coupled with the problem of step-size determination, led to the conclusion that these procedures are computationally inefficient and not readily amenable to complete automation. Second, the biased-tangent and feasible-direction methods yield the same design as that achieved by the energy-based resizing method that aims for uniform flutter-velocity derivatives, thus giving added confidence in the superiority of this optimality criterion.

9.3 THE SELECTED FLUTTER RESIZING ALGORITHM

From the results of the studies described in the previous subsection, it was concluded that the finally selected flutter resizing algorithm should be a direct rather than a two-phase procedure that achieves a state of uniform flutter-velocity

derivatives for flutter-critical elements. Moreover, for the overall problem of determining a near-minimum-weight design that satisfies both strength requirements and a minimum flutter-speed constraint (for one critical flutter mechanism), the resizing procedure should aim toward a composite optimality criterion with the following characteristics:

- Flutter-critical elements have uniform flutter-velocity derivatives for the Mach number and altitude of the prescribed critical flutter condition,
- Strength-critical elements are fully stressed for at least one of the specified design loading conditions,
- Other elements are at a minimum or maximum manufacturing gage.

To achieve the uniform-flutter-velocity-derivative criterion, the following resizing formula is used in FASTOP:

$$m_{i_{new}} = m_{i_{old}} \sqrt{\frac{\left(\frac{\partial V_f}{\partial m_i}\right)_{old}}{\left(\frac{\partial V_f}{\partial m_i}\right)_{target}}} \quad , \qquad (9.2)$$

where

$m_{i_{old}}$, $m_{i_{new}}$ are the i^{th} design variable (structural element or mass balance) weights before and after a resizing step, respectively,

$(\partial V_f/\partial m_i)_{old}$ is the flutter-velocity derivative of the i^{th} design variable before a resizing step, and

$(\partial V_f/\partial m_i)_{target}$ is an approximation of the desired uniform positive value of the derivative after a resizing step, to be discussed in Subsection 9.4.1.

This formula resulted from a simplification of the equation that was used in the last of the energy-based optimality-criteria methods discussed earlier. It, however, does not suffer from the shortcoming of its predecessor, in that it is mathematically capable of dealing with mass-balance as well as structural design variables. When this resizing technique, hereafter referred to as the "velocity-derivative-ratio method," was applied to the same example wing structure used in the previous study efforts, it displayed excellent convergence characteristics, rapidly leading to a design requiring the same weight increase as those obtained by the best energy-based method and by the numerical-search procedures. When mass-balance design variables were introduced into the example problem, the ability of the method to cope with this type of variable, in combination with structural design variables, was also verified. The results of further demonstrations of the application of this method in optimizing realistic structural designs is presented in Section 12.

9.3.1 Calculation of Flutter Velocity Derivatives in FASTOP

As stated previously, in the latter part of Subsection 9.2.1, it became evident in studying the energy-based optimality-criteria methods, that it is possible to cast the analytic flutter-velocity derivatives of Reference 9-2 into a new form that is identifiable in terms of generalized energy quantities. The development proceeds as follows:

Consider the flutter-mode vector $\{U\}$ and its associated row vector $\{V\}^T$, in the structures mathematical model, to be normalized such that

$$\{V\}^T([M] + [A])\{U\} = 1. \tag{9.3}$$

Rudisill and Bhatia's final flutter-velocity derivatives (Reference 9-2) may then be expressed in the following form:

$$\frac{\partial V_f}{\partial m_i} = \frac{V_f}{\omega_f^2}\left[\tfrac{1}{2}\,\mathrm{Re}\,(\{V\}^T[\partial[K]/\partial m_i - \omega_f^2\,\partial[M]/\partial m_i]\{U\}) - \frac{\mathrm{Im}\,(\{V\}^T[\partial[K]/\partial m_i - \omega_f^2\partial[M]/\partial m_i]\{U\})}{\mathrm{Im}(\omega_f^2\{V\}^T(\partial[A]/\partial k)\{U\})} \times \left(\frac{\omega_f^2}{2}\,\mathrm{Re}\,(\{V\}^T(\partial[A]/\partial k)\{U\}) + \frac{\omega_f^2}{k}\right)\right], \tag{9.4}$$

where [K] and [M] are the stiffness and mass matrices of the structures mathematical model; ω_f is the angular flutter frequency; k is the reduced frequency, $b\omega_f/V_f$, in which b is the reference wing semichord; and [A] is the complex aerodynamic force matrix compatible with the structural degrees of freedom of the surface.

If the i^{th} element's stiffness and mass matrices, $[K_i]$ and $[M_i]$, vary linearly with its design variable, Equation (9.4) can be manipulated into a new "energy-density" form:

$$\frac{\partial V_f}{\partial m_i} = \left(\frac{V_f}{2\omega_f^2}\left[\frac{\{V_R\}^T[K_i]\{U_R\}}{m_i} - \frac{\{V_I\}^T[K_i]\{U_I\}}{m_i} - C\left(\frac{\{V_R\}^T[K_i]\{U_I\}}{m_i} + \frac{\{V_I\}^T[K_i]\{U_R\}}{m_i}\right)\right]\right) - \left(\frac{V_f}{2}\left[\frac{\{V_R\}^T[M_i]\{U_R\}}{m_i} - \frac{\{V_I\}^T[M_i]\{U_I\}}{m_i} - C\left(\frac{\{V_R\}^T[M_i]\{U_I\}}{m_i} + \frac{\{V_I\}^T[M_i]\{U_R\}}{m_i}\right)\right]\right) \qquad (9.5)$$

or

$$\frac{\partial V_f}{\partial m_i} = SED_i - KED_i , \qquad (9.6)$$

where the subscripts R and I indicate the real and imaginary components, respectively, of the flutter vector and its associated row vector, and where C is a real quantity defined by

$$C = \frac{Re\ (\{V\}^T(\partial[A]/\partial k)\{U\}) + 2/k}{Im\ (\{V\}^T(\partial[A]/\partial k)\{U\})} . \qquad (9.7)$$

In Equation (9.5), terms have been grouped into two categories. The first, SED_i, includes what may be interpreted as a linear combination of generalized strain-energy-density terms. The second category, KED_i, contains a similar set of generalized kinetic-energy-density terms. This grouping of terms is adopted in the formulation and programming of the flutter-velocity derivatives to enable the FASTOP user to readily compare the separate contributions of each element's stiffness and mass to its derivative. An example of

the usefulness of this feature occurs when identifying locations in the structure where mass-balance could be effective in increasing a surface's flutter speed (i.e., where large negative KED's exist). This concept is discussed further in Subsection 10.5.2.

In order to compute the derivatives defined by Equation (9.5), it is necessary to first transform the flutter vector and its associated row vector from the modal coordinates used in the flutter analysis module to absolute structural coordinates. The different transformation relations required for cantilevered structures and free-free structures are discussed below.

(a) Cantilevered Structures - In cantilever analyses, the transformation between modal and structural coordinates utilizes the normal mode shapes $[X]$ (see Equation (7.9)) of the dynamics model, and matrix $[B]^T$ which transforms displacements from dynamics coordinates to structures coordinates (see Equations (5.6) and (5.7)). If lower and upper case symbols are respectively used to denote vectors in modal coordinates and structures coordinates, the required transformations take the form

$$\{U\} = [Q]\{u\} \quad , \{v\}^T = \{v\}^T[Q]^T \tag{9.8}$$

where

$$[Q] = [B]^T [X] \tag{9.9}$$

(b) Free-Free Structures - It may be recalled that the basic vibration equation for free-free analyses (see Equation (7.20)) was cast in terms of relative dynamic displacements $\{\phi_{DR}\}$. Thus, $\{u\}$ and $\{v\}^T$ are transformed to <u>relative</u> structural coordinates by the relations

$$\left\{U_{rel}\right\} = \left[Q_R\right]\{u\} \quad , \quad \left\{V_{rel}\right\}^T = \{v\}^T \left[Q_R\right]^T \quad , \tag{9.10}$$

where

$$\left[Q_R\right] = \left[B\right]^T \left[\phi_{DR}\right] . \tag{9.11}$$

Now, rigid-body motion of structures points depends on both the plug motion $\{\phi_P\}$ (see Equation (7.19)), and matrix $[\lambda_S]$ which defines those displacements for unit plug motions (see Section 7.4). Accordingly, $\{u\}$ and $\{v\}^T$ are transformed to absolute structural coordinates by the relations

$$\{U_{abs}\} = [Q_A]\{u\} \ , \ \{V_{abs}\}^T = \{v\}^T[Q_A]^T \ , \tag{9.12}$$

where

$$[Q_A] = [Q_R] + [\lambda_S][\phi_P] \ . \tag{9.13}$$

The transformation to absolute coordinates given by Equations (9.12) and (9.13) is used in the computation of the kinetic-energy-density expression in Equation (9.5). Equations (9.12) and (9.13) can also be used in the computation of the strain-energy-density expression. However, as strain-energy-density is only a function of relative displacements, Equations (9.10) and (9.11) are used for that computation since better numerical accuracy is achieved.

9.3.1.1 A Theoretical Consideration. In the computation of the flutter-velocity derivatives, the normalization step defined in Equation (9.3) and the computation of the coefficient C defined by Equation (9.7) are actually carried out directly in modal coordinates using $[\bar{Q}]$, the generalized air force matrix (instead of $[A]$), and the generalized mass matrix (instead of the structures-model mass matrix). Moreover, the flutter vector and its associated row vector are also initially computed in modal coordinates before transforming to structural coordinates.

Now, in modal coordinates, the flutter equation takes the form

$$\left([K_m] - \omega_f^2\left([M_m] + [\bar{Q}]\right)\right)\{u\} = 0 \ , \tag{9.14}$$

where $[K_m]$, $[M_m]$ and $[\bar{Q}]$ are the generalized stiffness, mass and aerodynamic matrices, respectively. That is,

$$[K_m] = [Q]^T[K][Q] \ , \tag{9.15a}$$

$$[M_m] = [Q]^T[M][Q] \ , \tag{9.15b}$$

$$[\bar{Q}] = [Q]^T[A][Q] \ , \tag{9.15c}$$

where $[K]$, $[M]$ and $[A]$ are the structural stiffness, mass, and aerodynamic matrices, respectively, and $[Q]$ is the transformation matrix defined in Equation (9.9); for a free-free analysis, matrix $[Q_A]$ (defined in Equation (9.13)) replaces $[Q]$ in Equations (9.15). If Equation (9.14) is used as the starting point, the derivation of the flutter-velocity derivative expression results in an equation identical to Equation (9.4) except that all vectors and matrices are in modal rather than physical coordinates; thus terms of the form $\{v\}^T \frac{\partial [K_m]}{\partial m_i} \{u\}$ and $\{v\}^T \frac{\partial [M_m]}{\partial m_i} \{u\}$ arise. In order to evaluate these terms, Equations (9.15a) and (9.15b) must be used. Now, the columns of $[Q]$ are simply the vibration mode shapes expressed in structural coordinates. If these mode shapes are assumed to remain constant during a variation in m_i , it follows from Equations (9.15a) and (9.15b) that

$$\{v\}^T \frac{\partial [K_m]}{\partial m_i} \{u\} = \{v\}^T [Q]^T \frac{\partial [K]}{\partial m_i} [Q] \{u\},$$

$$\{v\}^T \frac{\partial [M_m]}{\partial m_i} \{u\} = \{v\}^T [Q]^T \frac{\partial [M]}{\partial m_i} [Q] \{u\}. \qquad (9.16)$$

It is noted that the terms on the right-hand side of equations (9.16) are precisely the terms obtained by substituting the transformations of Equations (9.8) or (9.12) into Equation (9.5), as described previously. Thus it follows that the computation of flutter-velocity derivatives within FASTOP assumes the $[Q]$ matrix to be constant, i.e., the vibration mode shapes, expressed in structural coordinates, are retained as the generalized displacement vectors during a variation in the design variables.

9.4 IMPLEMENTATION OF THE COMBINED STRENGTH AND FLUTTER RESIZING PROCEDURE

9.4.1 Determination of a Design Change for a Desired Flutter-Speed Increment

In applying the flutter resizing formula of Equation (9.2), an iterative procedure is used to determine the value of the target derivative, $(\partial V_f/\partial m_i)_{target}$. The procedure makes use of the assumption that for small design changes, the flutter-velocity derivatives may be used to predict a change in flutter speed, $\Delta V_{f_{pred}}$, as a linear combination of element weight changes, Δm_i; that is

$$\Delta V_{f_{pred}} = \sum_i \left(\frac{\partial V_f}{\partial m_i}\right) \Delta m_i . \qquad (9.17)$$

To start the iteration, a target derivative of 80% of the average of all positive derivatives is assumed. Equation (9.2) is then used to determine a new weight, $m_{i_{new}}$, for each variable. The new weights are then adjusted so that no design variable (a) falls below that required for strength, (b) violates minimum and maximum gage constraints, or (c) is reduced by more than the percentage specified by user-supplied "max.-cut" parameters. (These considerations are discussed more fully in Subsection 9.4.2). The resulting incremental weights, $\Delta m_i = m_{i_{new}} - m_{i_{old}}$, are then used in the linear relationship of Equation (9.17) to compute a predicted velocity increment, $\Delta V_{f_{pred}}$, which is then compared with the desired velocity increment, $\Delta V_{f_{des}}$. Two convergence criteria are used for this comparison: satisfactory convergence occurs when

$$\left| \Delta V_{f_{des}} - \Delta V_{f_{pred}} \right| < \Delta \qquad (9.18a)$$

or when

$$\left| \frac{\Delta V_{f_{des}} - \Delta V_{f_{pred}}}{\Delta V_{f_{des}}} \right| < \epsilon_2 , \qquad (9.18b)$$

where Δ and ϵ_2 are specified by the user. If neither criterion is satisfied, the target derivative is automatically adjusted within the program (see discussion below) and the entire procedure is repeated to obtain another trial redesign. This iterative process continues until either a) at least one criterion is satisfied, or b) it is established that neither criterion can ever be met. For the latter case, wherein the design does not change from one trial resizing to the next, the last trial design is accepted; this situation may arise, for example, due to the presence of maximum gage constraints.

The automatic adjustment of the target derivative from one trial redesign to the next proceeds in the following manner. Suppose that the first trial redesign indicates that the predicted velocity increment is larger than the desired increment.

So long as this condition holds true ($\Delta V_{f_{pred}} > \Delta V_{f_{des}}$), the target derivative is repeatedly increased by 10% of its previous value in each of the ensuing trial resizings. Eventually, when the predicted increment becomes smaller than the desired increment ($\Delta V_{f_{pred}} < \Delta V_{f_{des}}$), the target derivative is repeatedly decreased by 1% of its previous value; when $\Delta V_{f_{pred}}$ again becomes larger than $\Delta V_{f_{des}}$, the target derivative is successively increased by 0.1% of its previous value. That is, each time $\Delta V_{f_{pred}}$ "crosses" $\Delta V_{f_{des}}$ the program changes both the sense and magnitude of the target derivative adjustments (+10%, -1%, +0.1%, etc.). As mentioned above, the process terminates when Equation (9.18a) or Equation (9.18b) is satisfied, or when the design does not change from one trial resizing to the next. Clearly, the initial supposition ($\Delta V_{f_{pred}} > \Delta V_{f_{des}}$) in the first trial redesign is immaterial; if the opposite were true, the starting target derivative would be decreased, not increased, by 10%.

9.4.2 Definition of "Max.-Cut" Parameters and Representation of Strength and Manufacturing Constraints when Resizing for Flutter

When using the flutter resizing equation, Equation (9.2), the question of how to resize elements with very small, or even negative, derivatives must be addressed. In such cases, it might appear desirable to reduce the element's size to its value dictated by strength or minimum-gage requirements. However, in some cases it has been found that the stability of the resizing procedure is improved if the reduction in a structural element's size, in a single redesign step, is constrained to a specified precentage of its previous value. Since it has not been found necessary to apply the same restriction to mass-balance design variables, the user may specify a seperate reduction factor for mass balance (normally zero, i.e., no restriction). These reduction factors, referred to as the "max.-cut" parameters, are discussed further in Subsection 10.5.4.

In addition to these "max.-cut" constraints, strength requirements and minimum and maximum manufacturing gage limitations must be considered when resizing for flutter. The interaction of a flutter-speed constraint with strength requirements is accounted for by successively optimizing for strength and flutter, with the strength-designed members from the fully-stressed-design procedure (ASOP), (see Section 4) being considered as minimum gages in the next flutter optimization, and vice versa.

An element's minimum and maximum manufacturing gages, t_{min} and t_{max}, are supplied by the user during the initial pass through the strength analysis and redesign module of FASTOP. The output of that module includes element gage size, t, and stress ratio, s (actual stress/allowable stress), which, along with t_{min} and t_{max}, are transferred to the flutter resizing module. The stress ratio will be very close to unity for a stress-critical element, but it will be less than unity for a flutter-critical element, i.e., for an element that has been resized for flutter (without encountering strength or minimum manufacturing constraints) in a previous pass through the flutter-resizing module. The minimum strength-adequate gage size for any element is therefore the product of its stress ratio and associated gage size, i.e., $t_s = s \times t$. Thus, when resizing for flutter, an element is not permitted to be sized below t_{min} or t_s, whichever is larger. Also, the element cannot be sized to a value greater than t_{max}.

9.4.3 Multiple Flutter-Redesign Steps

FASTOP allows the user the option to perform successive flutter-redesign steps without computing new normal modes of vibration after each step. In this "coupled-mode" approach, the last set of computed normal mode shapes are retained as assumed modes and the changes in the modal stiffness and mass matrices, $[\Delta K_m]$ and $[\Delta M_m]$, are given by the following expressions.

Case (a). Cantilevered Structure

$$[\Delta K_m] = [Q]^T [\Delta K_s][Q] , \quad [\Delta M_m] = [Q]^T [\Delta M_s][Q] . \tag{9.19}$$

Case (b). Free-Free Structure

$$[\Delta K_m] = [Q_R]^T [\Delta K_s][Q_R] , \quad [\Delta M_m] = [Q_A]^T [\Delta M_s][Q_A] \tag{9.20}$$

Here, $[\Delta K_s]$ and $[\Delta M_s]$ are the cumulative incremental changes in the structures-model stiffness and mass matrices since the last normal-mode computation, and $[Q]$, $[Q_R]$ and $[Q_A]$ are the transformations defined in Equations (9.9), (9.11) and (9.13). The adjusted generalized stiffness and mass matrices, $[K_m]_{new}$ and $[M_m]_{new}$, are then obtained by adding the above incremental matrices to the orthogonal ones corresponding to the last set of normal modes; that is

$$[K_m]_{new} = [K_m] + [\Delta K_m] \tag{9.21}$$

and

$$[M_m]_{new} = [M_m] + [\Delta M_m] . \tag{9.22}$$

Note that these new matrices are no longer diagonal (i.e., the original normal-mode coordinates become "coupled").

The following section describes this interactive resizing process from the user's point of view.

Section 10

USE OF FASTOP FOR INTEGRATED ANALYSIS AND DESIGN

10.1 SUMMARY

FASTOP is an analysis and redesign tool that can be used to generate near-minimum-weight designs for aircraft structures subject to combined strength and flutter-speed requirements. Two basic programs are involved; one is primarily concerned with the static strength problem, and the other addresses the flutter condition. In the typical redesign process, each of the programs is executed several times. Communication between the programs ensures that the design requirements for one type of constraint are not intentionally violated by the other. The material contained in this section is intended to guide a user through the entire redesign procedure. Numerous suggestions are put forward based upon the experience gained in the solution of the demonstration problems to be discussed in Section 12.

10.2 ORGANIZATION OF FASTOP

The Flutter And STrength Optimization Package, FASTOP, is comprised of a Strength Optimization Program, SOP, and a Flutter Optimization Program, FOP. As shown in Figure 10.1, each of these major programs is organized on a modular basis. The modules are defined as follows:

SOP Modules

ALAM - Automated Load Analysis Module

ATAM - Automated Transformation Analysis Module

ASAM - Automated Strength Analysis Module

ASOM - Automated Strength Optimization Module

FOP Modules

AVAM - Automated Vibration Analysis Module

AFAM - Automated Flutter Analysis Module

AFOM - Automated Flutter Optimization Module

These acronyms will be used to facilitate the discussion throughout this section.

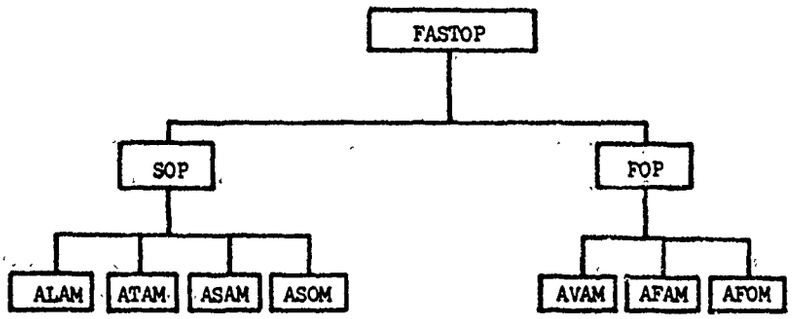

Figure 10.1 Modular Organization of FASTOP

10.3 SEQUENTIAL USE OF THE STRENGTH AND FLUTTER OPTIMIZATION PROGRAMS

SOP and FOP may be executed individually or, if desired, they may be run back-to-back as a multiple step job. Theoretically, there is no restriction on the number of SOP and FOP steps that may be executed in a given job. However, practical considerations such as running time and the normal desire of the user to examine the output of one program before executing the next will limit the number of steps. It is recommended, therefore, that generally no more than two steps (either SOP-FOP or FOP-SOP) be executed in a multiple-step job.

Figure 10.2 illustrates the first four steps in a typical redesign procedure. Notice that SOP must be the first program executed in the entire procedure and that the two programs alternate thereafter. As shown in the figure,

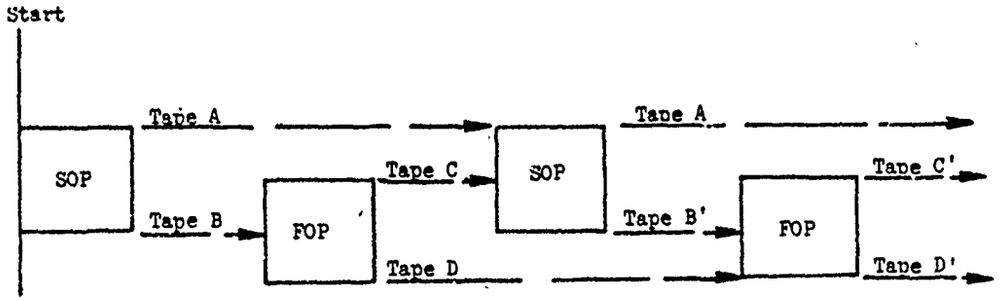

Figure 10.2 Basic I/O Tapes in FASTOP

data is transferred between programs by means of magnetic tapes. Each program generates two basic output tapes; one is intended for the next SOP step and the other is intended for the next FOP step. The general contents of these tapes are briefly discussed below.

Tape A - This tape, referred to as the "SOTOSO" tape, is generated by SOP for use in the subsequent SOP step. Essential data such as structures model geometry, boundary conditions, applied loads, etc. are passed via this tape.

Tape B - This "SOTOFO" tape is generated by SOP and passed to the next FOP step. Latest member sizes and the associated flexibility (or stiffness) matrix are among the data contained here.

Tape C - FOP accepts member sizes from the above "SOTOFO" tape, adjusts them by the flutter-resizing algorithm and passes the updated member data to the next SOP step via this "FOTOSO" tape.

Tape D - Data peculiar to FOP, such as mass data, mass balance locations, etc., are passed from one FOP step to the next by means of this "FOTOFO" tape.

10.4 USE OF THE STRENGTH OPTIMIZATION PROGRAM (SOP)

At any stage of the redesign procedure, SOP can be used in one of three possible modes:

(a) to simply compute the dynamics model flexibility matrix $[A]$, or the structural stiffness matrix $[K_s]$

(b) to stress analyze the structure and then compute $[A]$ or $[K_s]$

(c) to perform one or more FSD (fully stressed design) cycles and then compute $[A]$ or $[K_s]$

Use of one of these modes in any SOP step does not preclude the use of a different mode in a later step.

10.4.1 Conventional Use of SOP

The suggested procedure is to use mode (c) for the initial SOP step and then, depending on the degree of strength/flutter interaction encountered, to use either mode (a), (b) or (c) in subsequent SOP steps. Whenever mode (c) is employed, the user must specify the number of FSD cycles to be performed. For the initial SOP step, experience has indicated that four redesign cycles are normally adequate to transform a preliminary design (e.g., one having uniform gages) into a converged

fully stressed design. However, a single cycle should be sufficient in later SOP steps. In fact, the results of the demonstration cases described in Section 12 indicate that strength redesign could have been bypassed in all intermediate redesign cycles (mode (a)) with a final strength resizing near the end of the flutter redesign process. The user must also specify, in the initial SOP step, which, if any, of the total set of elements are to be permanently excluded from the strength resizing process. This elimination becomes necessary, for example, when some elements are adequately modeled to simulate the stiffness of a structure but are inadequately modeled for stress analysis and redesign - as when honeycomb core is modeled with rib and spar webs. Actual exclusion of an element is effected by simply setting its minimum and maximum allowable gages equal to its initial (desired) gage. Note that since these same allowable gages are transmitted to FOP, these elements are in fact withdrawn from the entire redesign procedure.

When mode (b) is used, strength resizing does not take place, but the element stress ratios (actual stress/allowable stress) are updated to define revised strength gage requirements of flutter design variables for use in the subsequent FOP step. This enables FOP to avoid violating strength requirements when resizing for flutter.

10.4.2 Use of SOP with Strength-Governed Designs not Generated by SOP

One other important use of FASTOP occurs when SOP is not intended to be used for stress analysis or redesign. This condition arises when a strength-adequate design, generated using criteria other than those embodied in SOP, is found to be flutter deficient. Under these circumstances, mode (a) should be used in all SOP steps and, in the first SOP step, the minimum allowable gage of each element should be set equal to its initial gage. This will ensure that any subsequent flutter redesign in the FOP steps will lead to a flutter adequate design in which member gages are nowhere less than those of the initial design.

10.4.3 Initial Design

Although resizing may have occurred in the first SOP step, the resulting design of this step - not the input preliminary design - is referred to as the initial design. It is this initial strength-adequate design which may be flutter deficient and require subsequent flutter/strength resizing to achieve an adequate design. If so, all changes in design parameters, such as flutter speed and total weight are defined with respect to the initial design.

10.5 USE OF THE FLUTTER OPTIMIZATION PROGRAM (FOP)

There are five possible modes in which FOP can be used:

(a) to perform a vibration analysis

(b) to perform a flutter analysis

(c) to perform both vibration and flutter analyses

(d) to perform vibration and flutter analyses and also compute flutter velocity derivatives

(e) to perform vibration and flutter analyses, compute flutter velocity derivatives and then perform one or more cycles of flutter redesign (each redesign cycle is followed by a "coupled mode" flutter analysis and computation of flutter velocity derivatives)

It is not unlikely that each of these modes will be exercised at some point in the entire redesign procedure.

10.5.1 Determination of Critical Flight Condition

After the first SOP step, the user must determine if the initial design is flutter adequate. The first requirement is to obtain a realistic dynamic mass matrix for the initial design. This task is normally the responsibility of a weights engineer who must account for the weight of detailed structural items (rivets, fittings, etc.), and other items (e.g., engines, fuel, actuators, external stores), as well as the idealized structural weight. FOP, however, does have the additional capability of automatically generating a dynamic mass matrix by using the idealized structural weights in conjunction with nonoptimum factors (see Section 10.5.3) and additional-mass data supplied by the user. The next step is to perform a series of vibration and flutter analyses for various flight conditions in order to determine the critical condition from the standpoint of flutter. The vibration analysis need only be done once for each weight condition, either independently (mode(a)), or in conjunction with the first flutter analysis for that weight condition (mode (c)). In any event, the vibration data is saved on tape and used in subsequent flutter analyses (mode (b)).

10.5.2 Initial Mass Balance Data

If a design is flutter deficient and the user intends to include mass balance in a redesign study, the location and an initial value of each mass balance must be specified. Experience has shown that the choice of this initial data can have a significant effect on the subsequent redesign behavior. For example, a case was encountered in which the effectiveness of a mass balance depended strongly upon its initial value; small initial values were not useful (negative flutter-velocity derivatives) and were subsequently eliminated from the design, while larger values were found to be very effective. Accordingly, it may be profitable to do a small separate mass-balance study (mode(d)), varying the initial values and locations. The resulting flutter-speed increments and mass-balance velocity derivatives should guide the urer in the selection of good initial mass-balance data. Note that the velocity derivatives of the structural elements also contain useful information. Specifically, the distribution of the kinetic-energy-density (KED) components of these derivatives is a direct measure of how flutter speed will be affected by small mass increments throughout the structure; mass increments are most beneficial in regions of large negative KED components. It is also suggested that the initial mass-balance data include a number of selected "dummy" locations where zero values of mass balance are specified. By means of this contrivance, the user essentially "reserves the right" to introduce real values of mass balance at these locations in any subsequent FOP step; that is, after the initial FOP step, the user will have the option of changing the mass balance value at any location specified in the initial data.

Finally, one last point must be made regarding mass-balance locations. Consider an initial mass balance, m_j. Unless the automatic mass generator option is being employed, the user must insert m_j directly into the initial dynamic mass matrix at the translational degrees of freedom associated with its dynamic model node point, "d". However, since all redesign, structural as well as mass balance, is accomplished in the structures model, any incremental mass balance Δm_j is first assigned to structural node point "s" (specified by the user) and then transformed to the dynamics model by means of the transformation defined in Equation (5.10). It is essential that the transformation of Δm_j from node s be made directly to node d and to no other dynamic node. The user should keep this requirement in mind when creating the force beaming table that prescribes the beaming of unit loads from dynamic nodes to structural nodes. This problem does not arise

when the automatic mass generator option is employed because both the initial and incremental mass balance are then specified in the structures model and transformed to the dynamics model.

10.5.3 Flutter Redesign Elements/Nonoptimum Factors

After the initial mass-balance data has been specified, the user should indicate which, if any, of the total set of structural elements are to be permanently excluded from the flutter resizing process. As a minimum, those elements which were previously eliminated from resizing in SOP should likewise be excluded in FOP. The user may now also introduce nonoptimum factors for use in the SOP/FOP redesign process - unless, of course, these factors were already introduced in conjunction with the automatic mass-generator option. Nonoptimum factors are intended to account for the fact that there is incremental weight, other than that of the primary structure, associated with the redesign of each element; for example, when redesigning an element with a nonoptimum factor of 1.2, the true incremental weight would be taken to be twenty percent larger than the computed incremental structural weight of the finite element.

10.5.4 Basic Parameters for Automated Flutter Redesign

Whenever mode (e) is exercised in a FOP application, the user must specify input data to control the number of redesigns to be accomplished in the step, the desired flutter speed step sizes, etc. Some important parameters are discussed below.

10.5.4.1 Flutter Band. Let V_f and $\overline{V}_{fdes}$ denote the current flutter speed and the desired final flutter speed, respectively. Whereas speeds much larger than $\overline{V}_{fdes}$ are undesirable because of the weight penalty associated with the extra speed, values nominally in excess of $\overline{V}_{fdes}$ are considered to be acceptable. Thus, the user must specify both $\overline{V}_{fdes}$ and an additional parameter ϵ_1, in order to define a "band" of acceptable flutter speeds; it is suggested that this bandwidth not exceed one percent of $\overline{V}_{fdes}$, in which case the band will extend from $\overline{V}_{fdes}$ to 1.01 $\overline{V}_{fdes}$.

10.5.4.2 Step Size/Normal vs. Coupled Modes. A step size parameter, NBAR, and a parameter defining the maximum permissible number of automatic redesign steps, NFIX, are also required by FOP. The program first undertakes to raise (or lower) the flutter speed from V to a value in the center of the flutter band, V^*, in NBAR approximately equal speed increments; thereafter, each successive redesign

attempts to get to V^* directly. Execution continues in this manner until the design converges, or until NFIX redesigns have been effected. The first flutter analysis in the foregoing procedure utilizes normal modes of vibration, but all subsequent analyses for modified designs are based on a coupled mode approach utilizing the original normal modes together with modified generalized mass and stiffness matrices including off-diagonal terms. Experience has indicated that coupled mode results are somewhat unreliable, and it is therefore recommended that generally only one redesign step be performed in each FOP application, i.e., the user is advised to set NFIX = 1. This restriction is not very severe because studies have shown that good results can be obtained with fairly large step sizes and consequently a small number of redesign cycles, when the flutter analyses and velocity derivative computations are based on revised normal modes. For example, the flutter speed of the Intermediate-Complexity Wing (see Section 12) was increased by thirty percent to a nearly converged optimum design in just four single-redesign FOP steps.

10.5.4.3 "Max.-Cut" Parameter. In preliminary studies of the aforementioned Intermediate-Complexity Wing, it was found that a few elements were undergoing severe fluctuations in gage size from one flutter redesign to the next. The phenomenon was attributed to the fact that, due to the coarseness of the model, the load paths were very sensitive to design changes. This stability problem was resolved by simply not allowing any gage size to be reduced by more than twenty-five percent in any single redesign, i.e., the "max-cut" parameter, D, was set equal to 0.75. Difficulties of this sort did not occur in the redesign study of the all-movable stabilizer - for which a very detailed model existed. Indeed, the entire resizing procedure progressed very smoothly and no restriction had to be imposed on gage size reduction (D = 0.0). Accordingly, the user is advised to begin the redesign procedure with D = 0.0; then, if gage-size instabilities appear, the "max-cut" parameter can be adjusted. Note that the user must specify a separate "max-cut" parameter, DBAL, for mass balance variables.

10.5.5 Termination of Redesign Process

It has already been pointed out that an efficient design (close to the optimum) can usually be achieved with fairly large step sizes provided the single-step, normal-mode approach is employed. Once a flutter adequate design has been obtained, the user should avoid excessive iterations within the flutter band while striving to effect a condition of uniform flutter-velocity derivatives.

Experience has shown that such an approach can expend large amounts of computing time for small improvements in design efficiency. It is recommended, therefore, that the redesign process be terminated when weight reductions from two or three successive iterations are no longer significant from an engineering point of view.

Section 11

EXAMPLES OF ANALYSIS RESULTS

11.1 SUMMARY

Calculations to demonstrate the capability and versatility of the FASTOP analysis package have been performed for three typical designs - a preliminary structures model of a simple cantilevered wing and detailed models of an all-movable stabilizer and a wing with a pylon-mounted external store.

The structures of all three surfaces were represented by finite-element idealizations and the degrees of freedom of the structures models were reduced to a lesser number of degrees of freedom required for the dynamics models by a force bearing transformation procedure. The types of calculations performed include subsonic and supersonic aerodynamic load predictions, inertial load predictions, load beaming to structural node points, determination of internal member loads and stress ratios, formation of dynamics model flexibility matrices, vibration mode analyses, and subsonic and supersonic flutter analyses using both the k and p-k solution procedures. Typical results obtained for the three demonstration problems are presented and discussed.

11.2 DESCRIPTION OF DEMONSTRATION PROBLEMS

11.2.1 Structures Model of the Intermediate Complexity Wing

The structural idealization for the so-called "intermediate complexity wing" is the simplest of the three demonstration cases selected and is representative of a typical preliminary design configuration. The all-aluminum two-cell wing box, illustrated in Figure 11.1, is modeled using 100 finite elements. Membrane elements are used to represent the wing covers, shear panels represent the spar and rib webs, and bar elements are introduced between upper and lower cover node points. The wing root is built-in by fully constraining all structural nodes on the root boundary. The structure has a total of 150 degrees of freedom comprising 3 translational degrees of freedom at each structural node point.

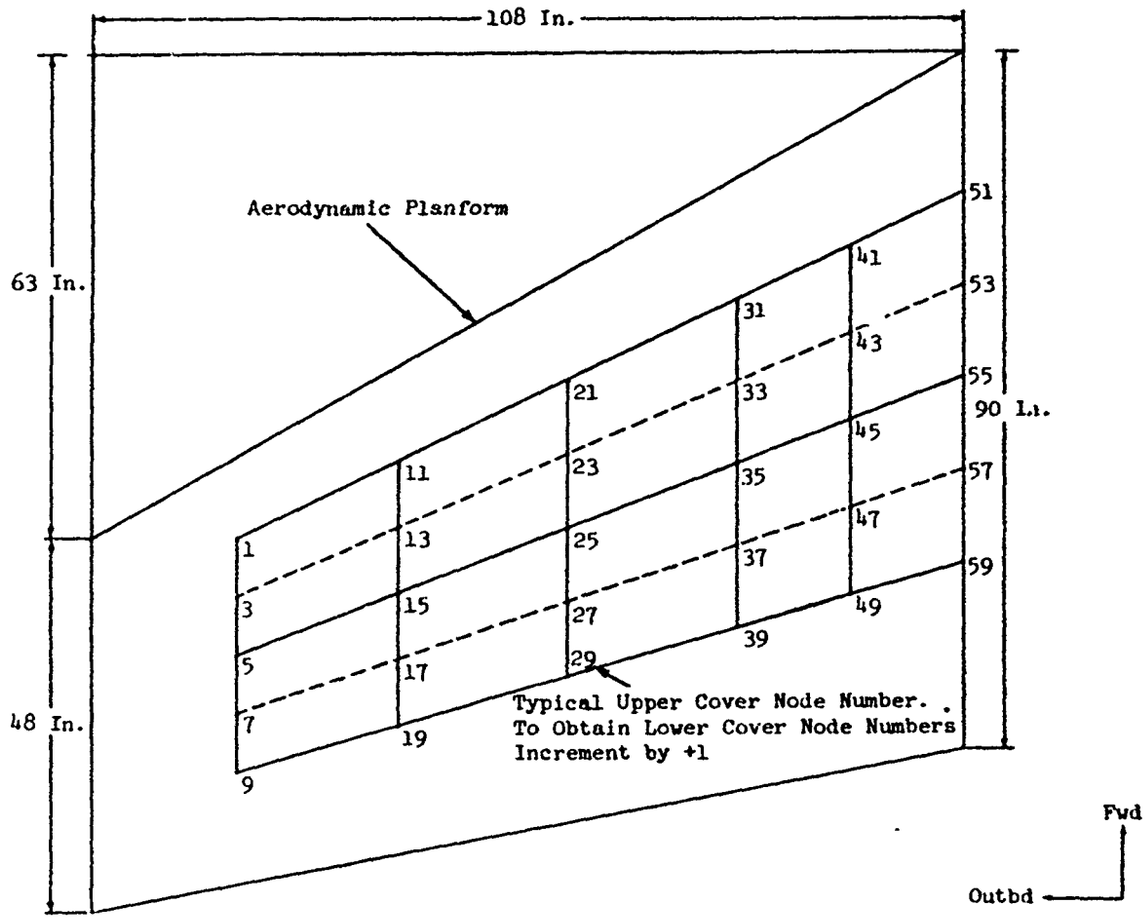

Figure 11.1 Intermediate Complexity Wing Structures Model

11.2.2 Dynamics Model of the Intermediate Complexity Wing

The 150 degrees of freedom of the structures model are transformed to 39 dynamic degrees of freedom using the force beaming procedures described in Section 5. The selected dynamic degrees of freedom, indicated in Figure 11.2, include out-of-plane (z direction) displacements at all dynamic nodes, these nodes being located between adjacent upper and lower cover structural nodes in the mid-plane of the wing. The overhanging panels, representing the mass and moment of inertia of structure external to the wing box are also included in the dynamics model. Their inertia effects are included by introducing rotational degrees of freedom of each panel about an axis parallel to its attaching structure i.e., front beam, rear beam, or tip rib. The local axis system for each panel is indicated in Figure 11.2.

11.2.3 Structures Model of the All-Movable Stabilizer

The all-movable stabilizer model, shown in Figure 11.3, is representative of a complex detailed design configuration. A total of 891 finite elements are used to model the stabilizer surface including its pivot and actuator restraints. (The details of the pivot restraints and the actuator are omitted from the figure to preserve clarity of presentation). It should be noted that the inner and outer stabilizer-to-pivot support points are modeled in the mid-plane of the surface, enclosed by structural nodes 481, 483, 463, 461 and structural nodes 379, 381, 349, 347 respectively. The stabilizer construction consists of titanium covers, modeled as membrane elements, with an aluminum honeycomb core. The honeycomb core is modeled as spanwise and chordwise shear panel elements with stiffness properties representative of the actual honeycomb structure. The model has a total of 1172 degrees of freedom.

11.2.4 Dynamics Model of the All-Movable Stabilizer

The force beaming procedure, described in Section 5, is used to transform the 1172 structural degrees of freedom of the stabilizer to 92 dynamic degrees of freedom. Vertical (out-of-plane) degrees of freedom are specified at the 73 dynamic node points shown in Figure 11.4, and additional rotational degrees of freedom are specified at overhanging panel points, designated as points 1 through 17 and 65 through 72.

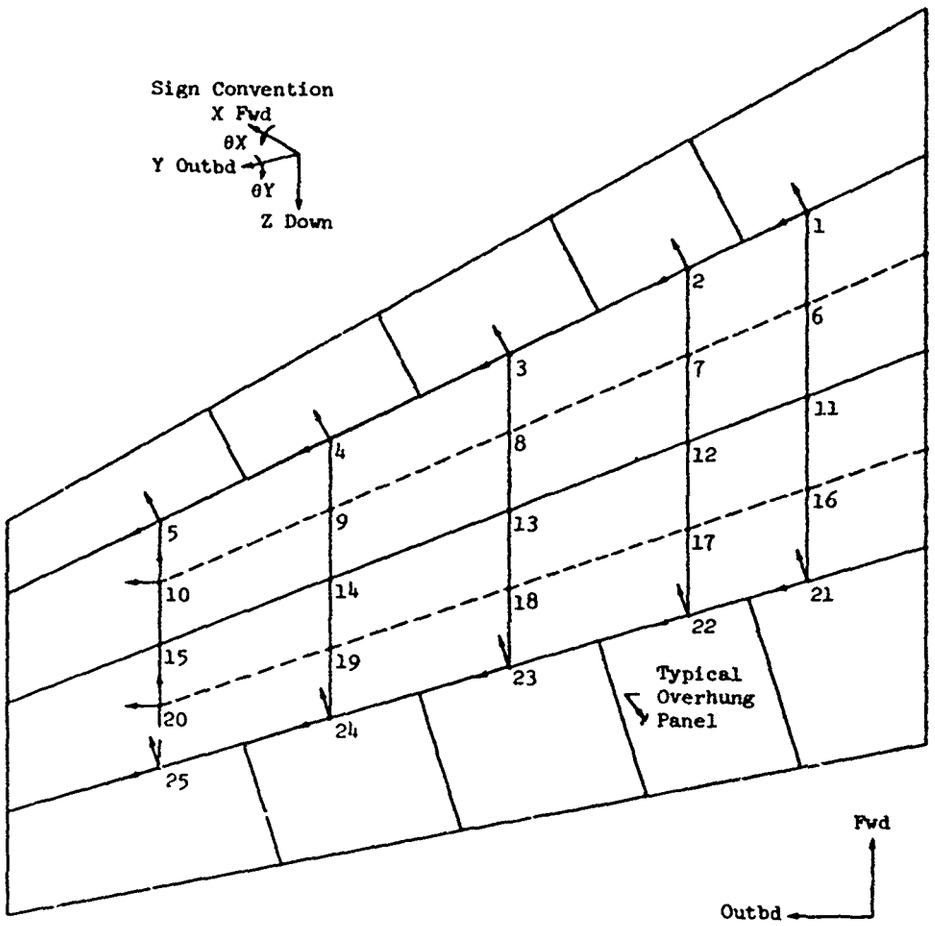

Dynamic Node	Dynamic Degrees of Freedom		
	Z	θX	θY
1	1		2
2	3		4
3	5		6
4	7		8
5	9		10
6	11		
7	12		
8	13		
9	14		
10	15	16	17
11	18		
12	19		
13	20		
14	21		
15	22		
16	23		
17	24		
18	25		
19	26		
20	27	28	29
21	30		31
22	32		33
23	34		35
24	36		37
25	38		39

Figure 11.2 Intermediate Complexity Wing Dynamics Model

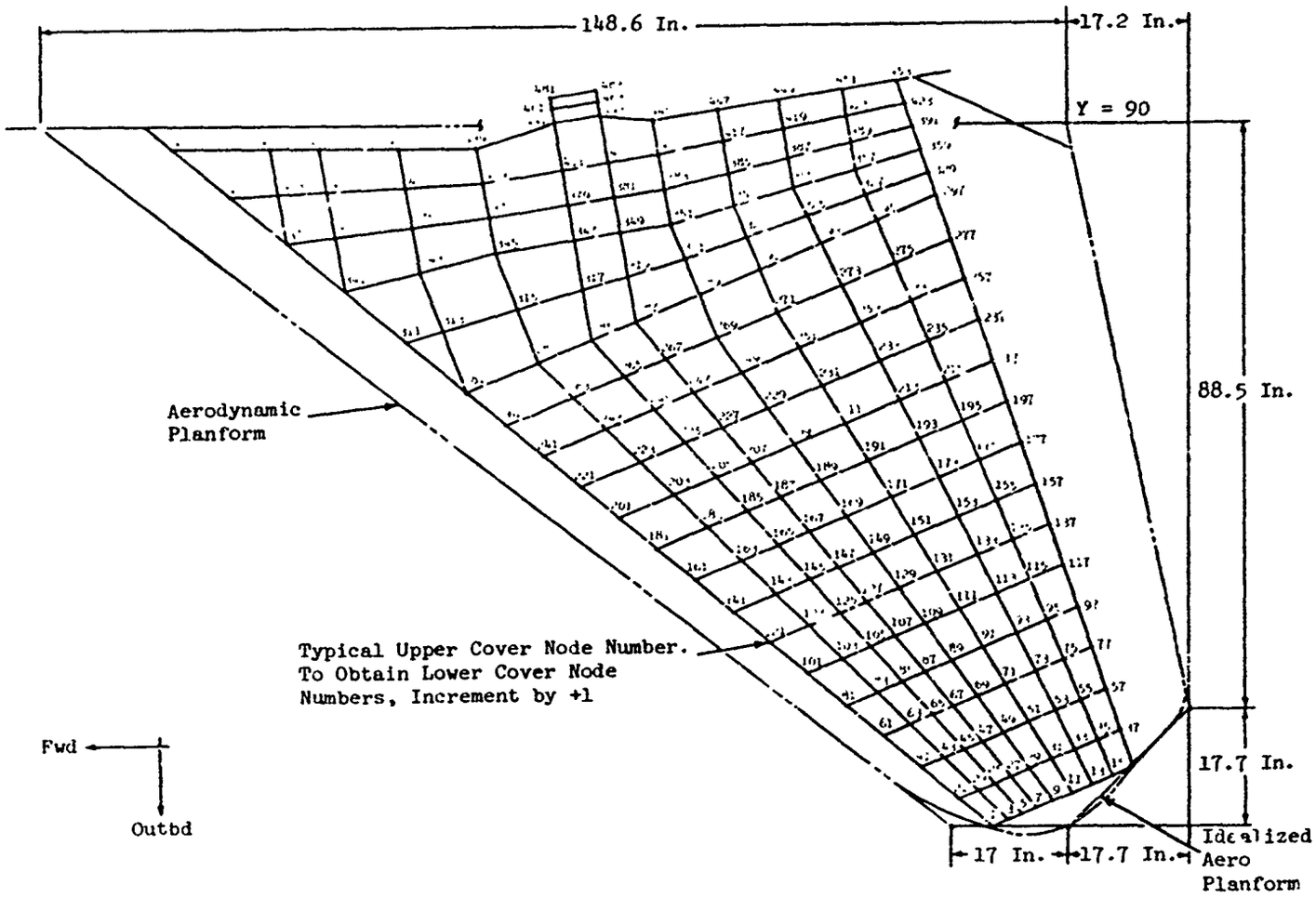

Figure 11.3 All-Movable Stabilizer Structures Model

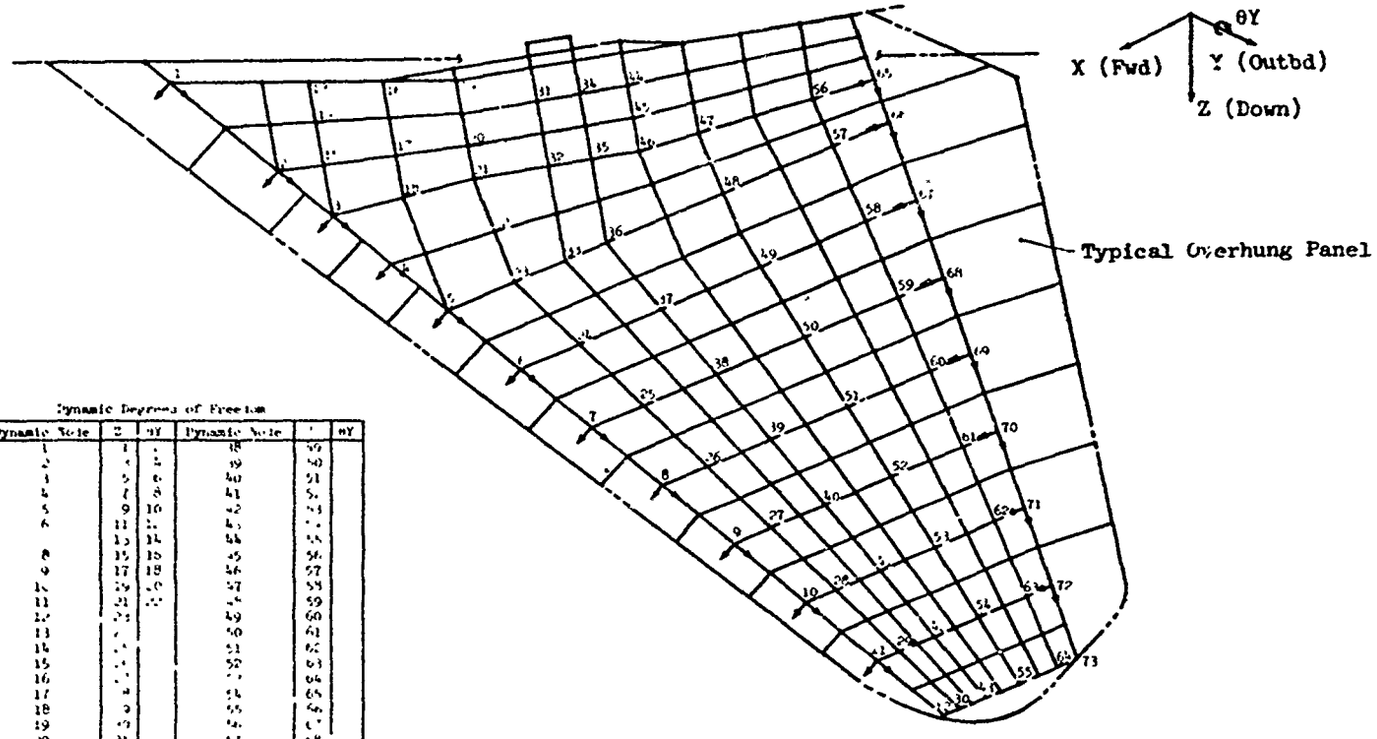

Dynamic Degrees of Freedom

Dynamic Node	Z	θY	Dynamic Node	Z	θY
1	1	2	37	73	74
2	3	4	38	75	76
3	5	6	39	77	78
4	7	8	40	79	80
5	9	10	41	81	82
6	11	12	42	83	84
7	13	14	43	85	86
8	15	16	44	87	88
9	17	18	45	89	90
10	19	20	46	91	92
11	21	22	47	93	94
12	23	24	48	95	96
13	25	26	49	97	98
14	27	28	50	99	100
15	29	30	51	101	102
16	31	32	52	103	104
17	33	34	53	105	106
18	35	36	54	107	108
19	37	38	55	109	110
20	39	40	56	111	112
21	41	42	57	113	114
22	43	44	58	115	116
23	45	46	59	117	118
24	47	48	60	119	120
25	49	50	61	121	122
26	51	52	62	123	124
27	53	54	63	125	126
28	55	56	64	127	128
29	57	58	65	129	130
30	59	60	66	131	132
31	61	62	67	133	134
32	63	64	68	135	136
33	65	66	69	137	138
34	67	68	70	139	140
35	69	70	71	141	142
36	71	72	72	143	144

Figure 11.4 All-Movable Stabilizer Dynamics Model

11.2.5 Structures Model of the Wing-with-Store

A second, but significantly different detailed design configuration is the wing with external-store shown in Figure 11.5. The structural idealization of the multi-spar aluminum wing box uses warped quadrilateral membrane elements to represent the wing covers and quadrilateral shear panels for rib and spar webs. The semi-wing is modeled from the tip to the airplane centerline and symmetric structural boundary conditions are specified for all nodes in the plane of symmetry. The wing-to-fuselage connection is accomplished with vertical shear attachments at nodes 37 and 47 and a drag attachment at node 47. A wing-store pylon, modeled with beam elements, is attached to the wing at nodes 175, 176, and 181, 182. The structural model has a total of 602 elements and 885 degrees of freedom.

11.2.6 Dynamics Model of the Wing-with-Store

The dynamics model, illustrated in Figure 11.6, is schematically similar to the two previous models. However, for the wing-with-store there is an additional requirement to include fore-and-aft degrees of freedom at every node to account for dynamic coupling between wing pitch and store translation. The store is allowed 5 degrees of freedom and the dynamics model contains a total of 136 degrees of freedom.

11.3 DISCUSSION OF ANALYSIS RESULTS OBTAINED WITH FASTOP

11.3.1 Loads Analysis

Data pertaining to the basic aerodynamic characteristics of each surface, plus a summary of flight conditions for which aerodynamic load distributions were computed using FASTOP, are presented in Table 11.1. Two examples of pressure distributions are presented for the intermediate-complexity-wing demonstration case. The first example (Figure 11.7) shows the subsonic pressure distribution for the Mach 0.9 flight condition noted in Table 11.1. The pressures were computed by the vortex-lattice aerodynamics routine described in Section 3. The pressure distribution for the Mach 2.0 flight condition, computed by the supersonic source distribution aerodynamics routine, is presented in Figure 11.8. In the supersonic case, the pressure is almost

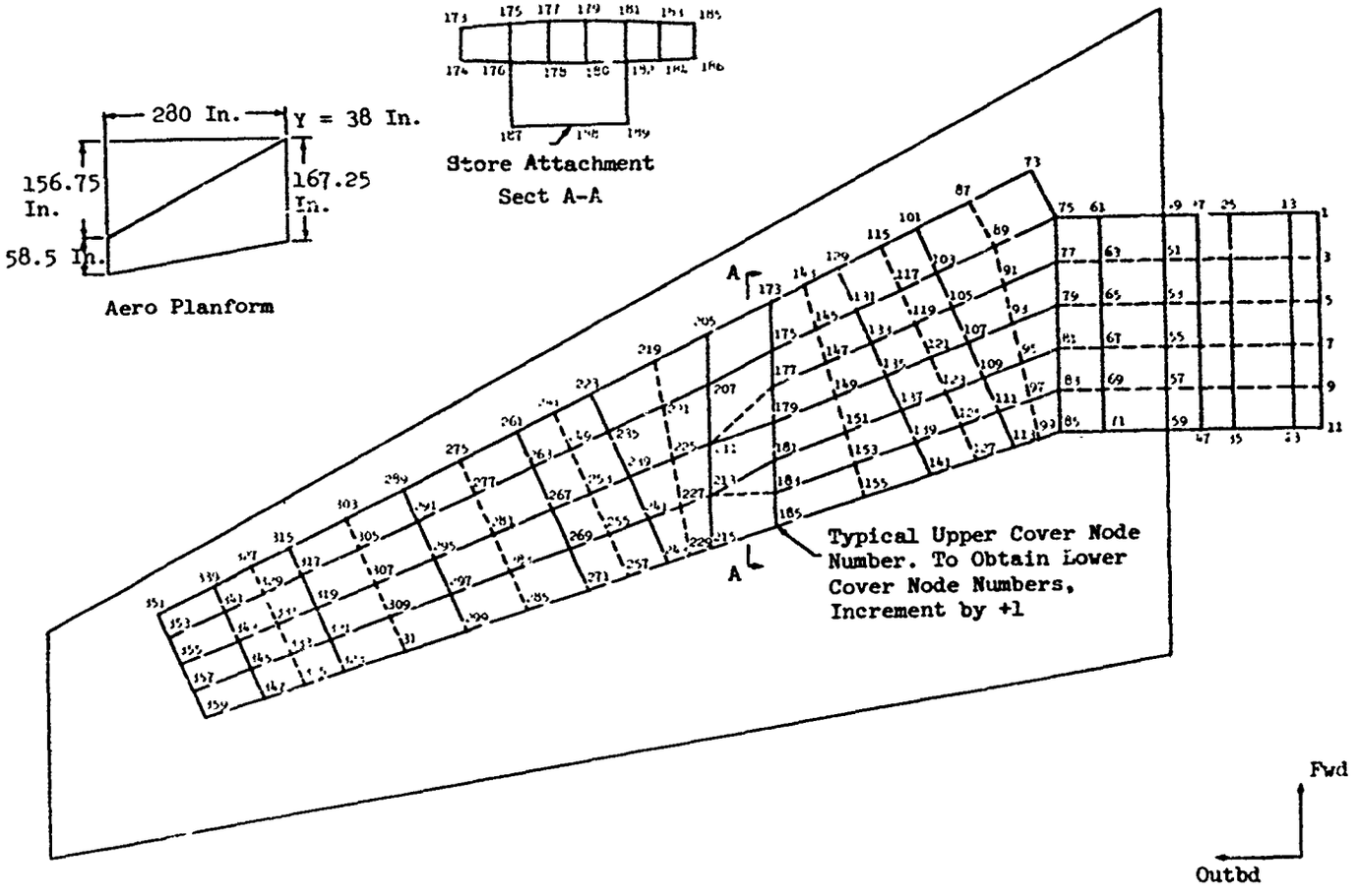

Figure 11.5 Wing-with-Store Structures Model

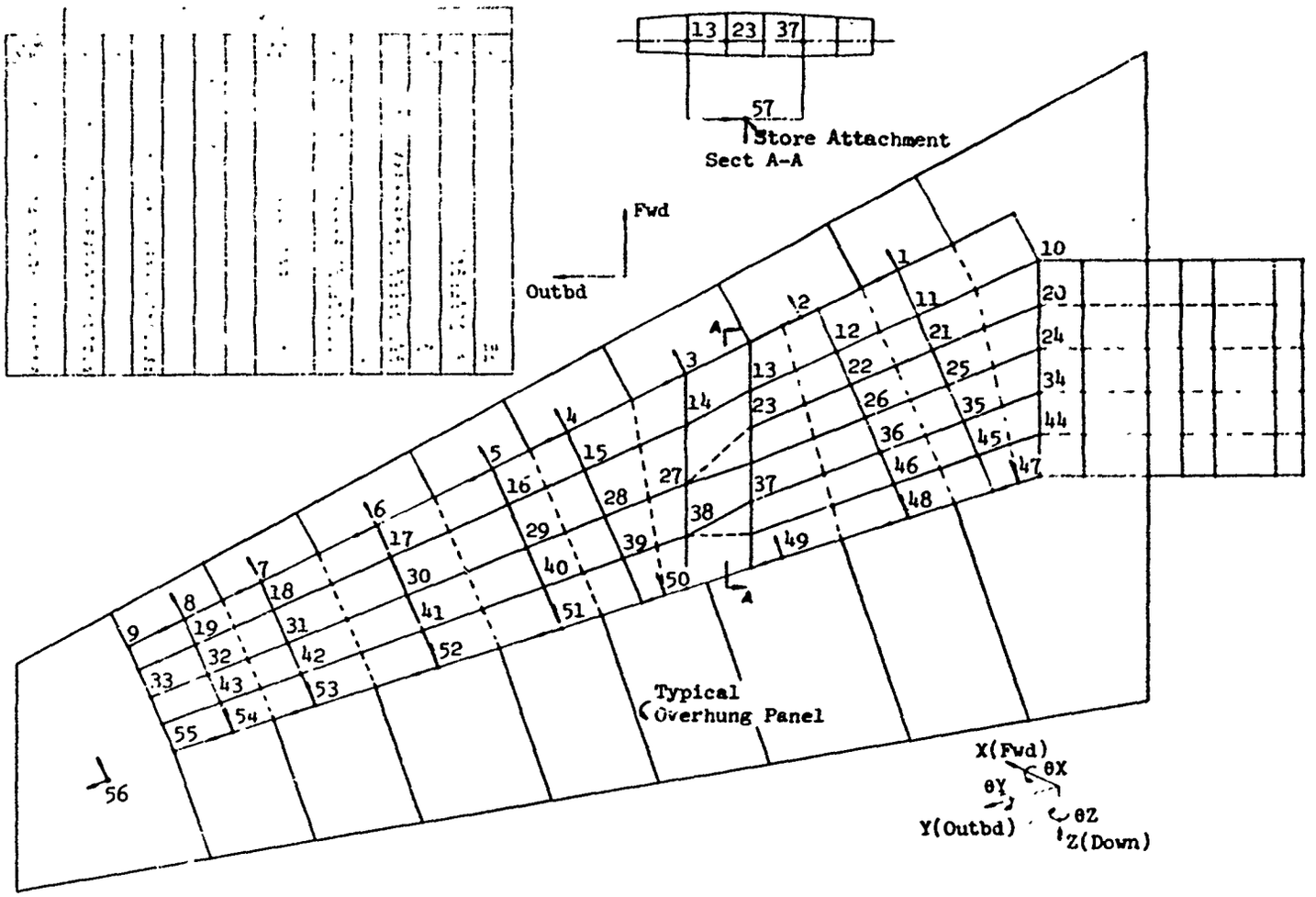

Figure 11.6 Wing-with-Store Dynamics Model

TABLE 11.1 BASIC WING DATA AND SUMMARY OF FLIGHT CONDITIONS FOR COMPUTED AERODYNAMIC LOADS

Model	Aspect ratio	Leading edge sweep angle	Number of aerodynamic panels used to represent wing	Flight Conditions		
				Mach No.	Alt. ($ft.x10^{-3}$)	Angle of Attack
Intermediate Complexity Wing	3.13	31°	36	0.5	30	3°
				0.9	30	2°
				2.0	30	2°
All-Movable Stabilizer	2.52	51°	100	0.8	0	16.5°
				1.3	10	9.0°
Wing-with-Store	4.96	29°	84	0.85	0	9.2°

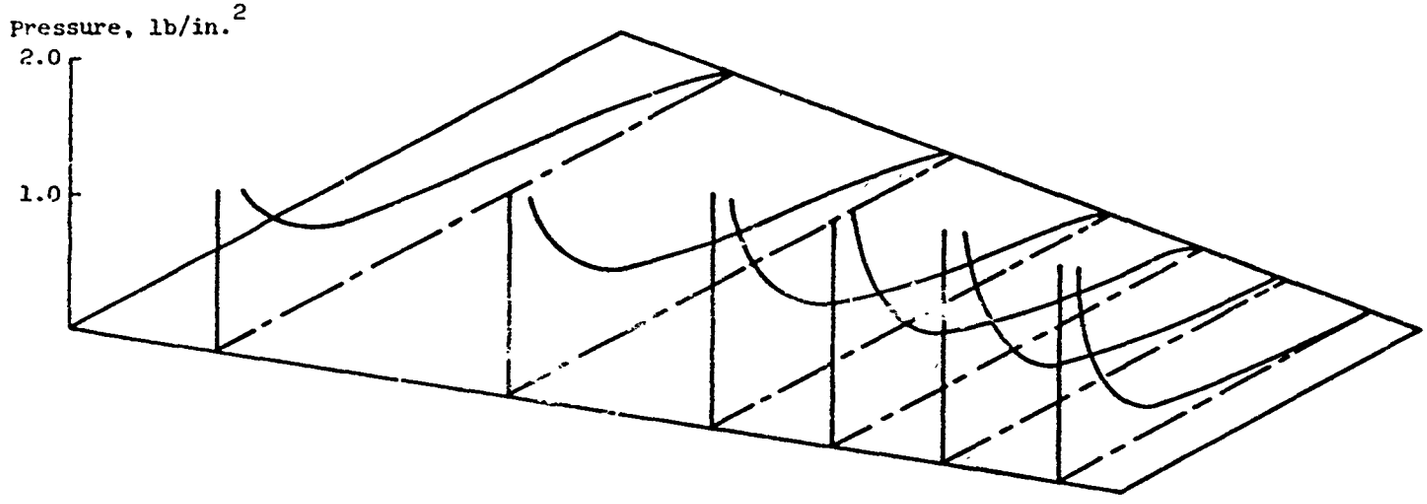

Figure 11.7 Subsonic Pressure Distribution, Intermediate Complexity Wing (Mach 0.9, 30,000 ft, $\alpha = 2°$)

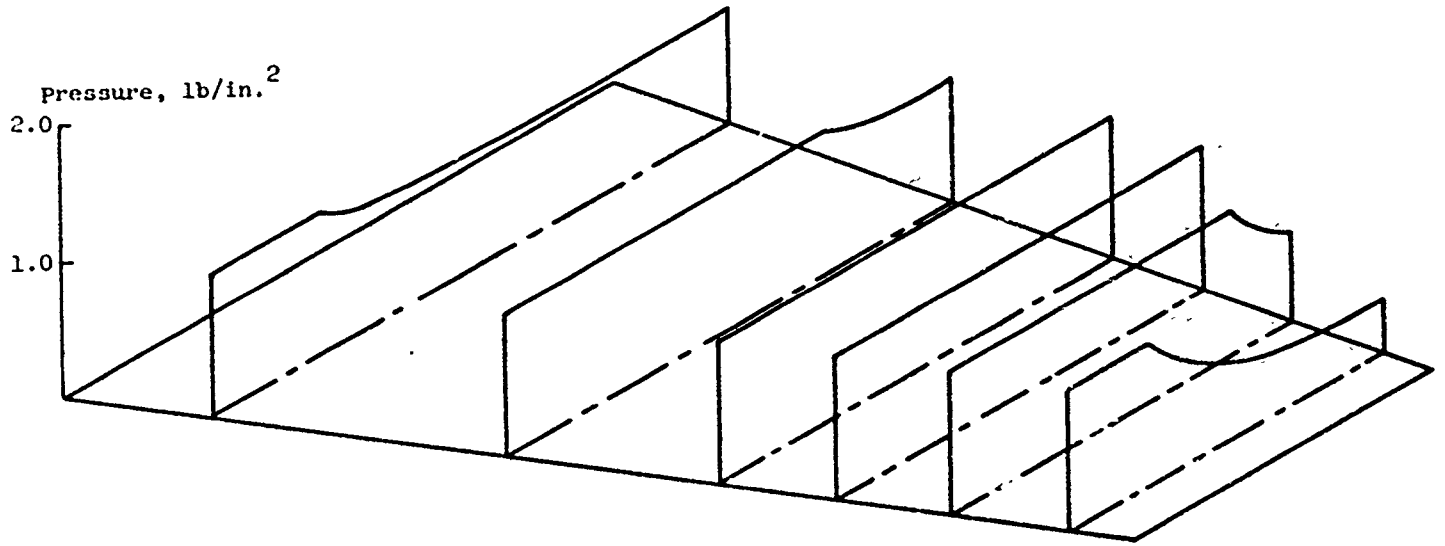

Figure 11.8 Supersonic Pressure Distribution, Intermediate Complexity Wing (Mach 2.0, 30,000 ft, $\alpha = 2^\circ$)

uniform in the mid-span region due to the almost two-dimensional flow characteristics at high Mach number. The abrupt pressure reductions in the inboard and tip regions of the wing occur at locations where the root and tip Mach lines intersect the chords along which pressures have been computed. Symmetric boundary conditions have been specified for both cases, although loads may be optionally calculated for antisymmetric or asymmetric conditions.

FASTOP was also used to compute inertial load distributions for the intermediate complexity wing for translational and angular accelerations which could correspond to the aerodynamic flight conditions of Table 11.1. The weights model used for this purpose closely resembled the dynamics model presented in Figure 11.2, except that overhanging panel mass and inertia properties were specified at panel c.g.'s in an unswept axis system. The results of the inertial load analysis are in the form of inertial forces and moments in the weights grid.

11.3.2 Structural Analysis

The structural analysis module was used for each example structure to determine its level of strength adequacy and to establish its flexibility characteristics for subsequent vibration analysis. Finite element sizes in each structural idealization were selected to be reasonable but are regarded as only preliminary.

The previously computed aerodynamic and inertial applied loads were transformed to the structures models by using the procedures of Section 5, and ratios of maximum working stress to allowable stress (stress ratios) were computed for every finite element in each model. Since these stress ratios are based on initial element sizes (for a non-fully-stressed design), they are of little significance except to demonstrate the proper working of the program.

In the same analysis module, the structural stiffness matrices were assembled. These were subsequently transformed into dynamics model flexibility matrices by again utilizing the transformation procedures of Section 5.

11.3.3 Vibration Analysis

Vibration analysis mode shape plots for the three demonstration structures are presented in Figures 11.9-11.11. These plots were generated using the CALCOMP plotter and associated software routines which are part of the FASTOP system. In each case the plotted data consists of modal displacements of the surface dynamic node points. A summary of the modal characteristics of each demonstration structure appears in Table 11.2. Some particular features of the vibration analysis results follow.

The intermediate-complexity-wing mode shapes are typical for a simple cantilevered structure. Wing torsion (Figure 11.9b), which is the second mode, has a node line running spanwise, in close proximity to the trailing edge. Chordwise bending is evident in modes 2-4.

The stabilizer mode shapes (Figures 11.10a-d) indicate the presence of root rotational motion due to the pivot and actuator support flexibilities. Because of this flexibility, the stabilizer has both a pitch mode, in which the stabilizer rotates about its pivot (Figure 11.10b), and a torsion mode, in which the surface twists with virtually no pivot rotation (Figure 11.10d).

The mode shape plots for the wing-with-store example are presented in Figures 11.11a-f. The fore-aft deflections for the wing leading edge are included on a separate reference line located in the lower portion of each figure. The hand plotted store motions, both translational and rotational, are shown with respect to the undisplaced store position. The initial requirement to make the wing flutter-critical was accomplished by defining relatively high store mass and inertia properties. The resulting high store pitch inertia causes significant wing torsion in the store pitch mode, shown in Figure 11.11c.

TABLE 11.2. SUMMARY OF DEMONSTRATION PROBLEM
VIBRATION MODE CHARACTERISTICS

Model	Mode number	Mode frequency (Hz.)	Mode description	Figure number
Intermediate	1	20.58	First bending	11.9a
Complexity	2	49.66	First torsion	11.9b
Wing	3	71.83	Second bending	11.9c
	4	93.90	Second torsion	11.9d
All	1	14.8	First bending	11.10a
Movable	2	30.1	Pitch	11.10b
Stabilizer	3	42.3	Second bending	11.10c
	4	52.2	Torsion	11.10d
Wing-with-	1	4.63	Store yaw	11.11a
Store	2	5.04	Wing bending	11.11b
	3	6.11	Store pitch & wing torsion	11.11c
	4	7.04	Store lateral	11.11d
	5	11.39	Wing second bending	11.11e
	6	12.49	Wing fore-aft	11.11f

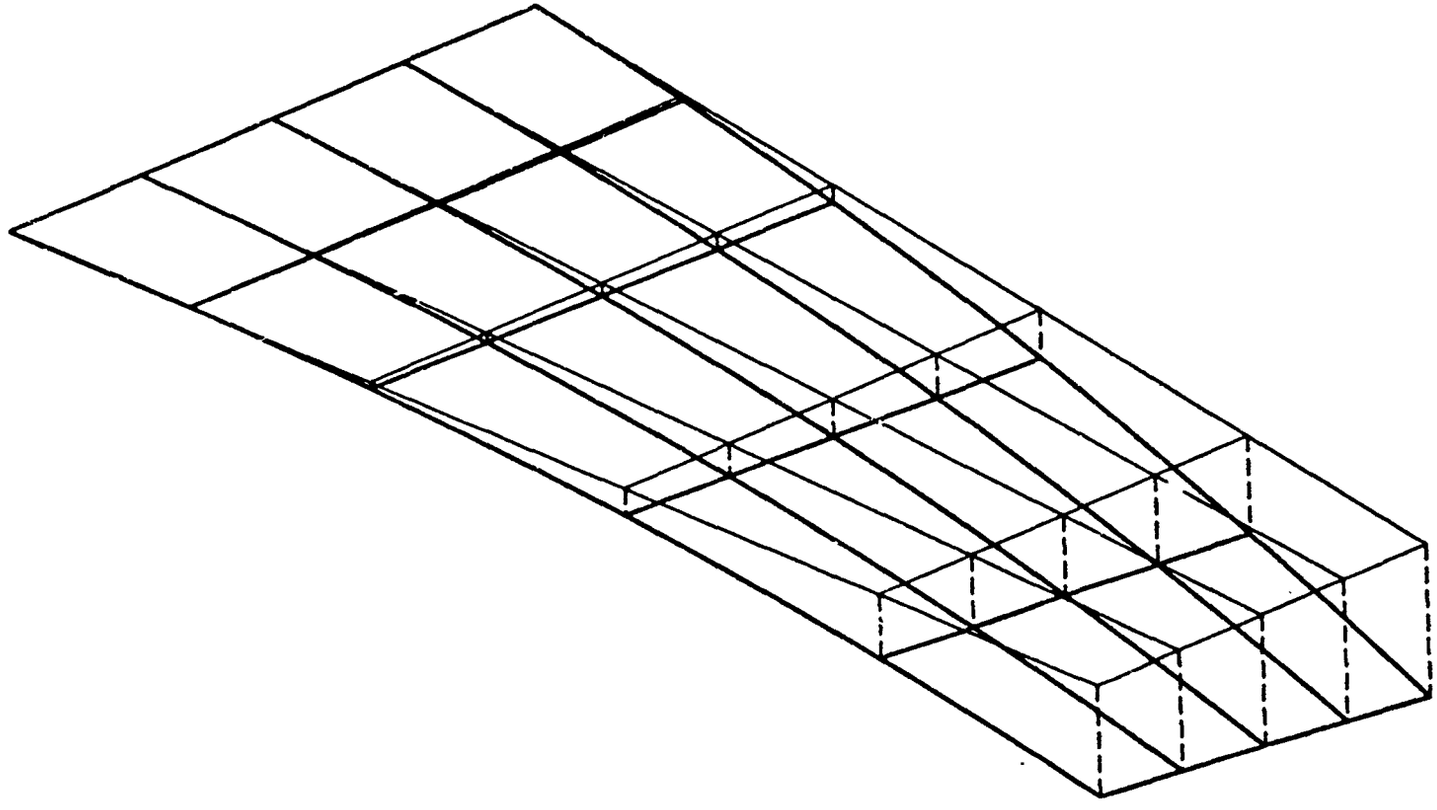

a. Mode No. 1, Frequency = 20.58 Hz

Figure 11.9 Intermediate Complexity Wing Vibration Mode, Sheet 1 of 4

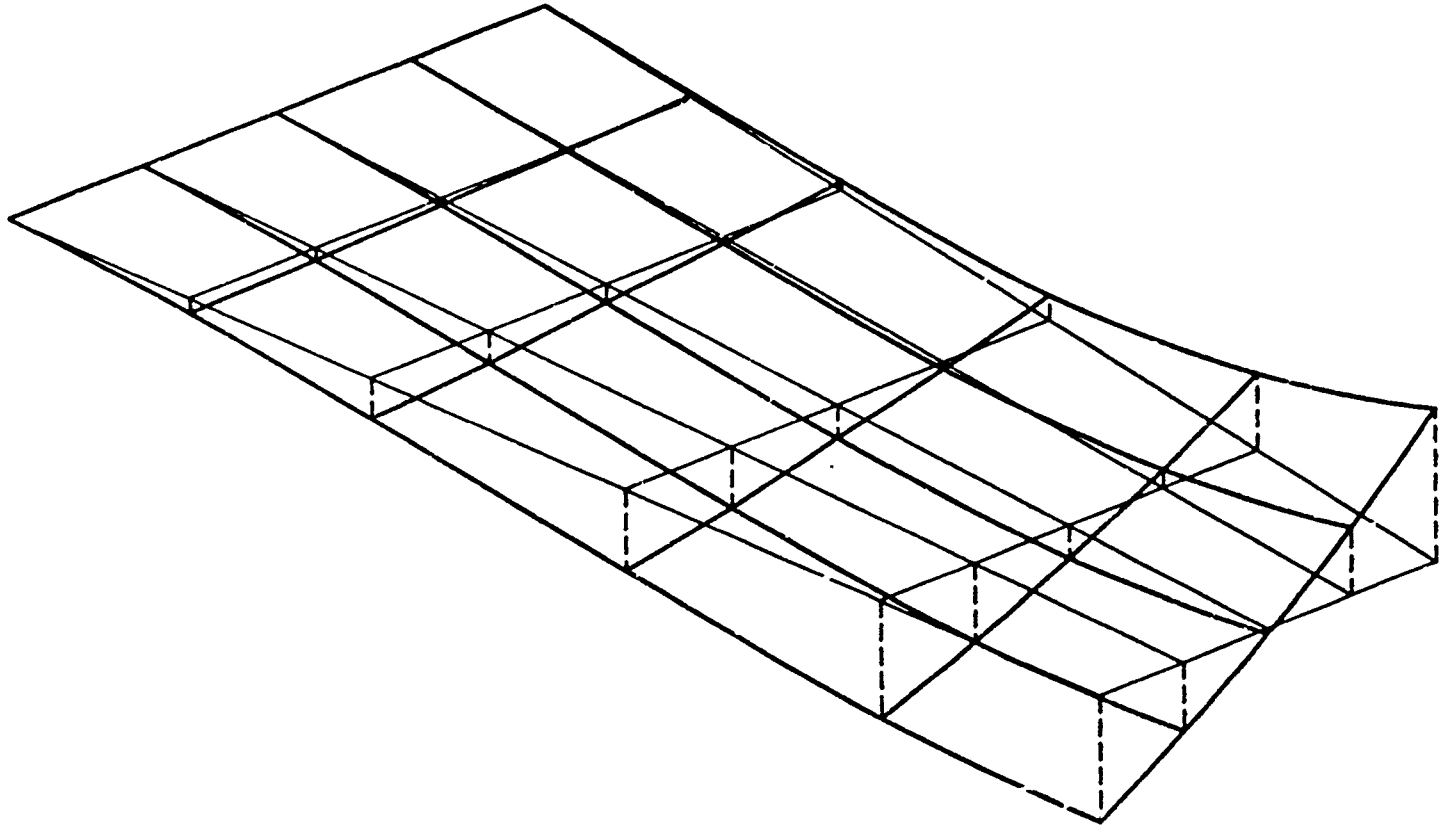

b. Mode No. 2, Frequency = 49.66 Hz

Figure 11.9 Intermediate Complexity Wing Vibration Mode, Sheet 2 of 4

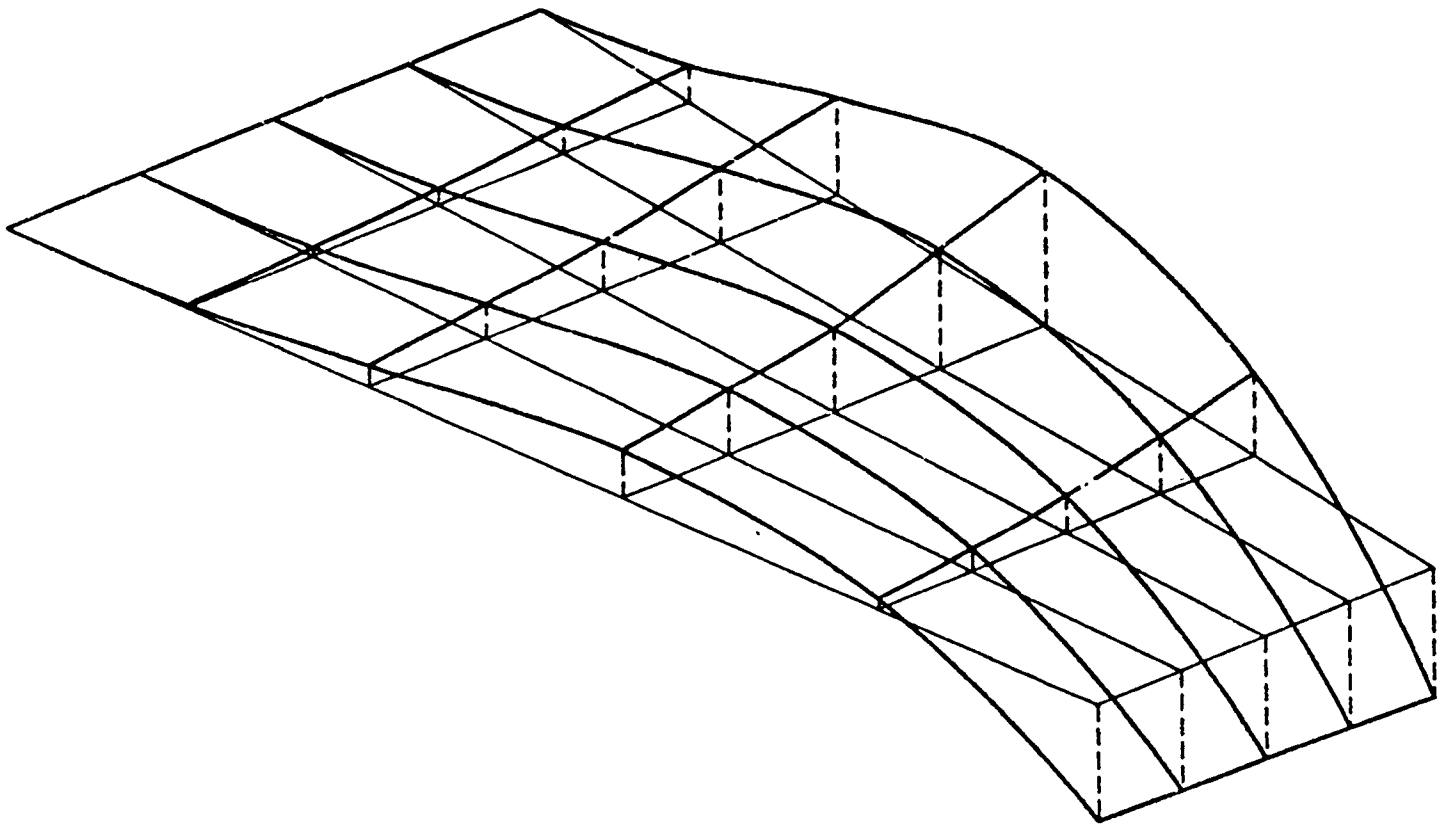

c. Mode No. 3, Frequency = 71.83 Hz

Figure 11.9 Intermediate Complexity Wing Vibration Mode, Sheet 3 of 4

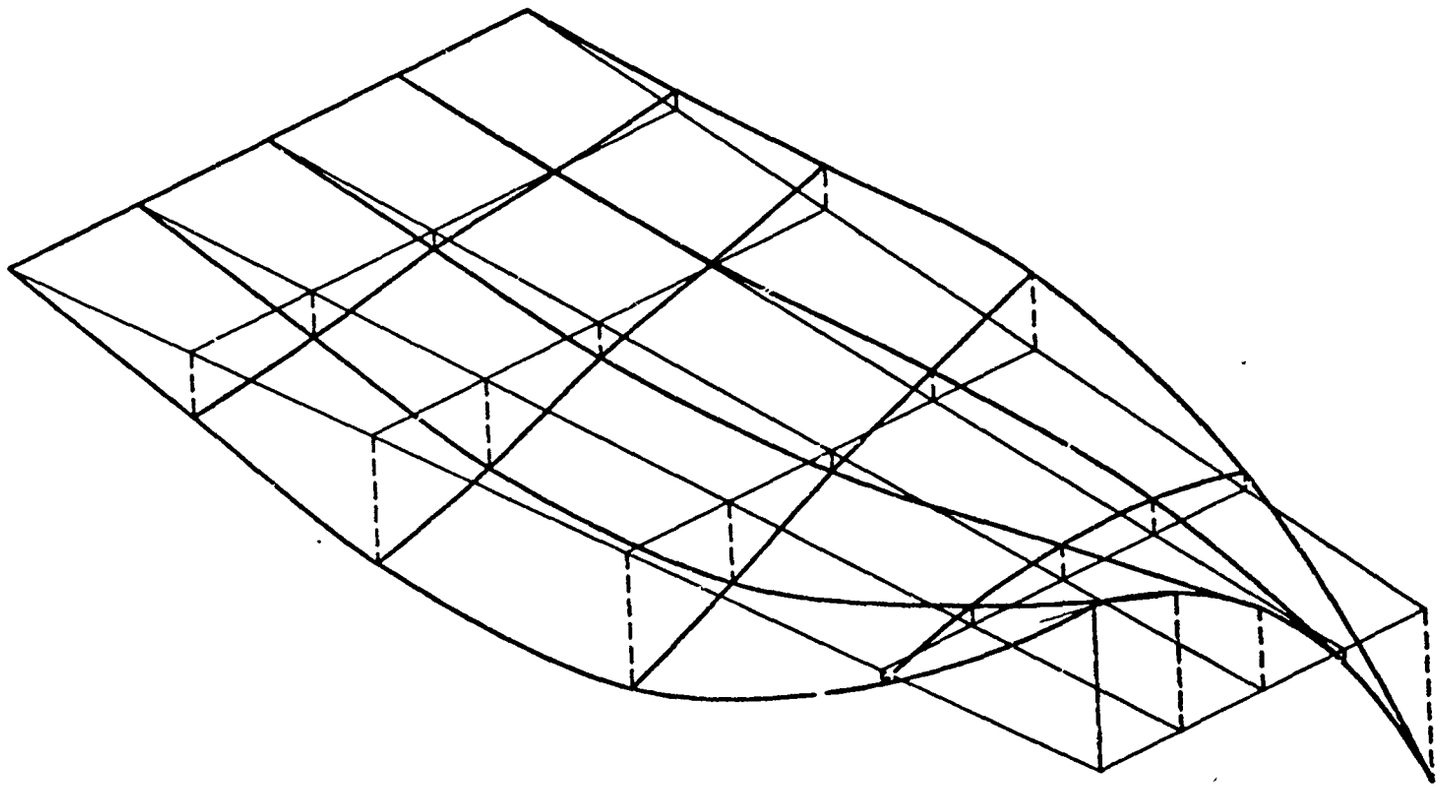

d. Mode No. 4, Frequency = 93.90 Hz

Figure 11.9 Intermediate Complexity Wing Vibration Mode, Sheet 4 of 4

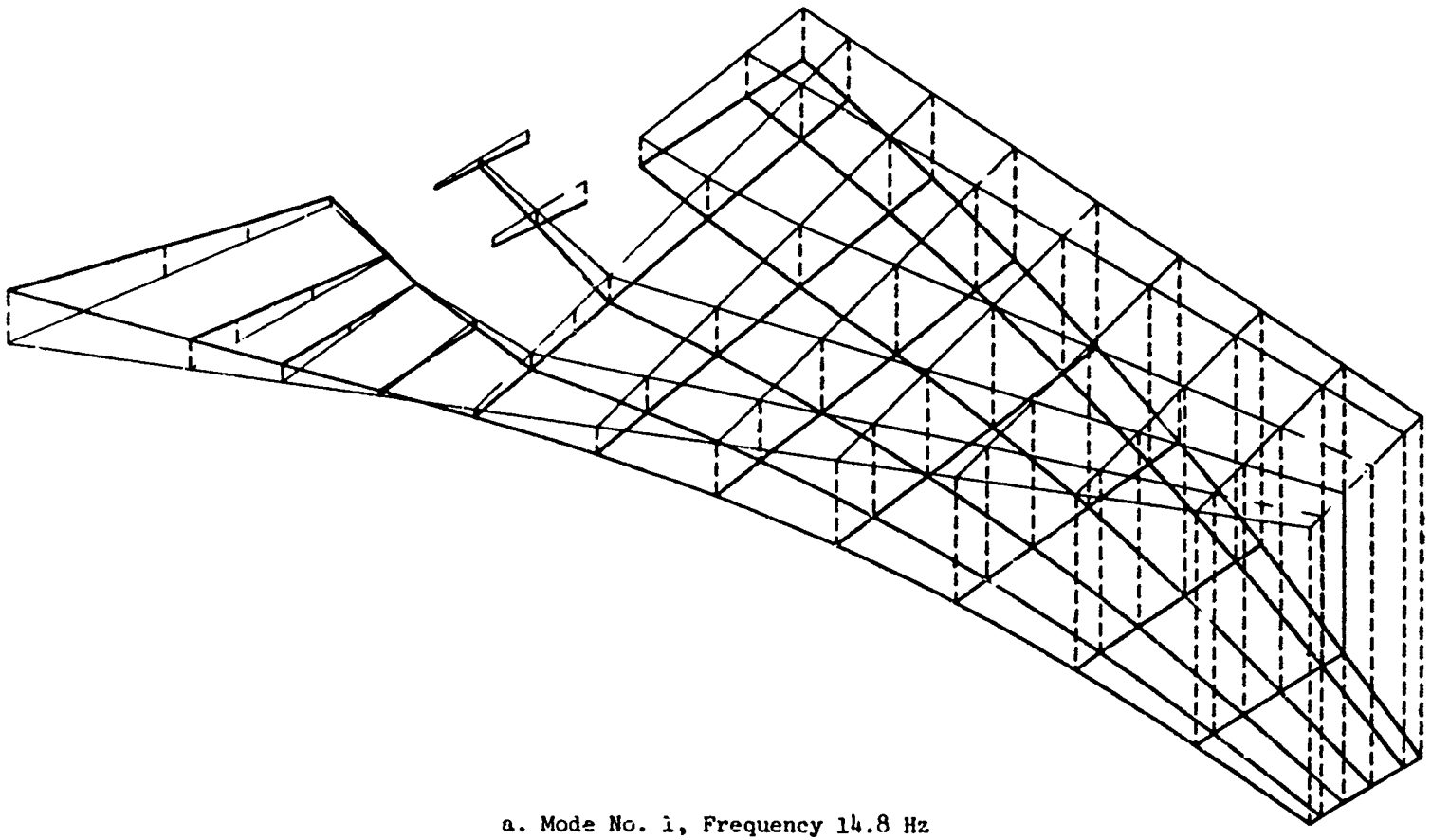

a. Mode No. 1, Frequency 14.8 Hz

Figure 11.10 All-Movable Stabilizer Vibration Mode, Sheet 1 of 4

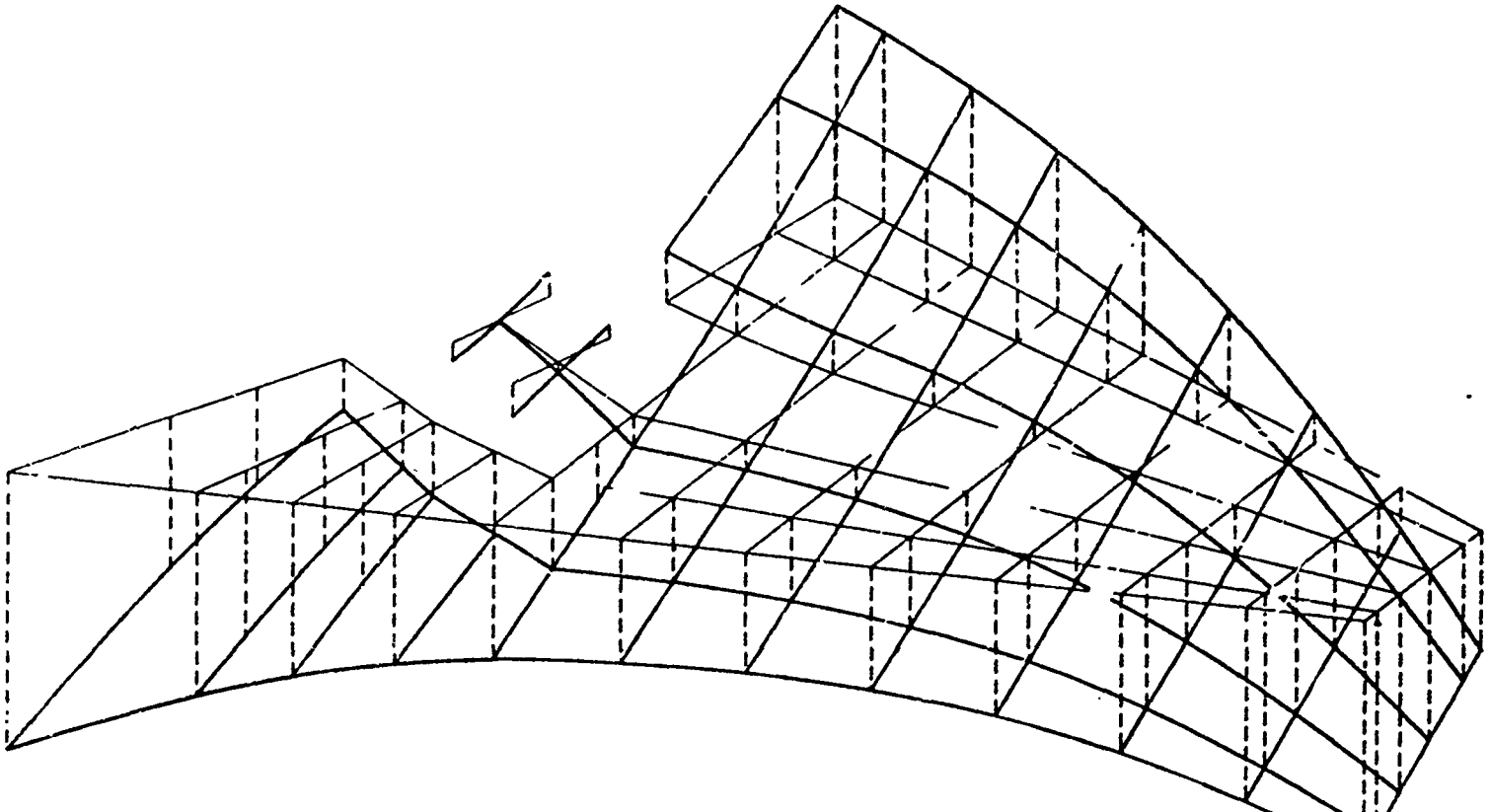

b. Mode No. 2, Frequency = 30.1 Hz

Figure 11.10 All-Movable Stabilizer Vibration Mode, Sheet 2 of 4

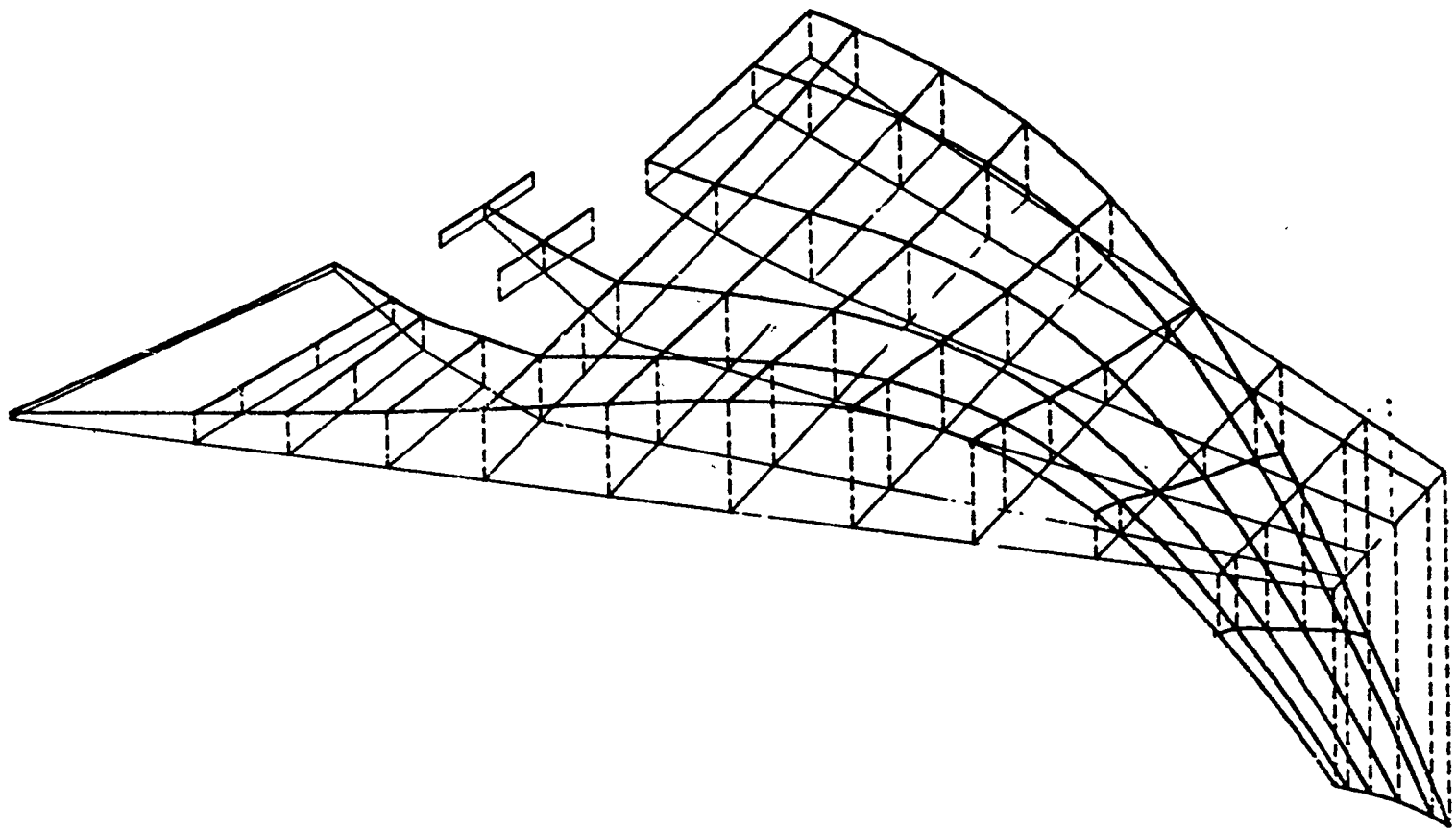

c. Mode No. 3, Frequency = 42.3 Hz

Figure 11.10 All-Movable Stabilizer Vibration Mode, Sheet 3 of 4

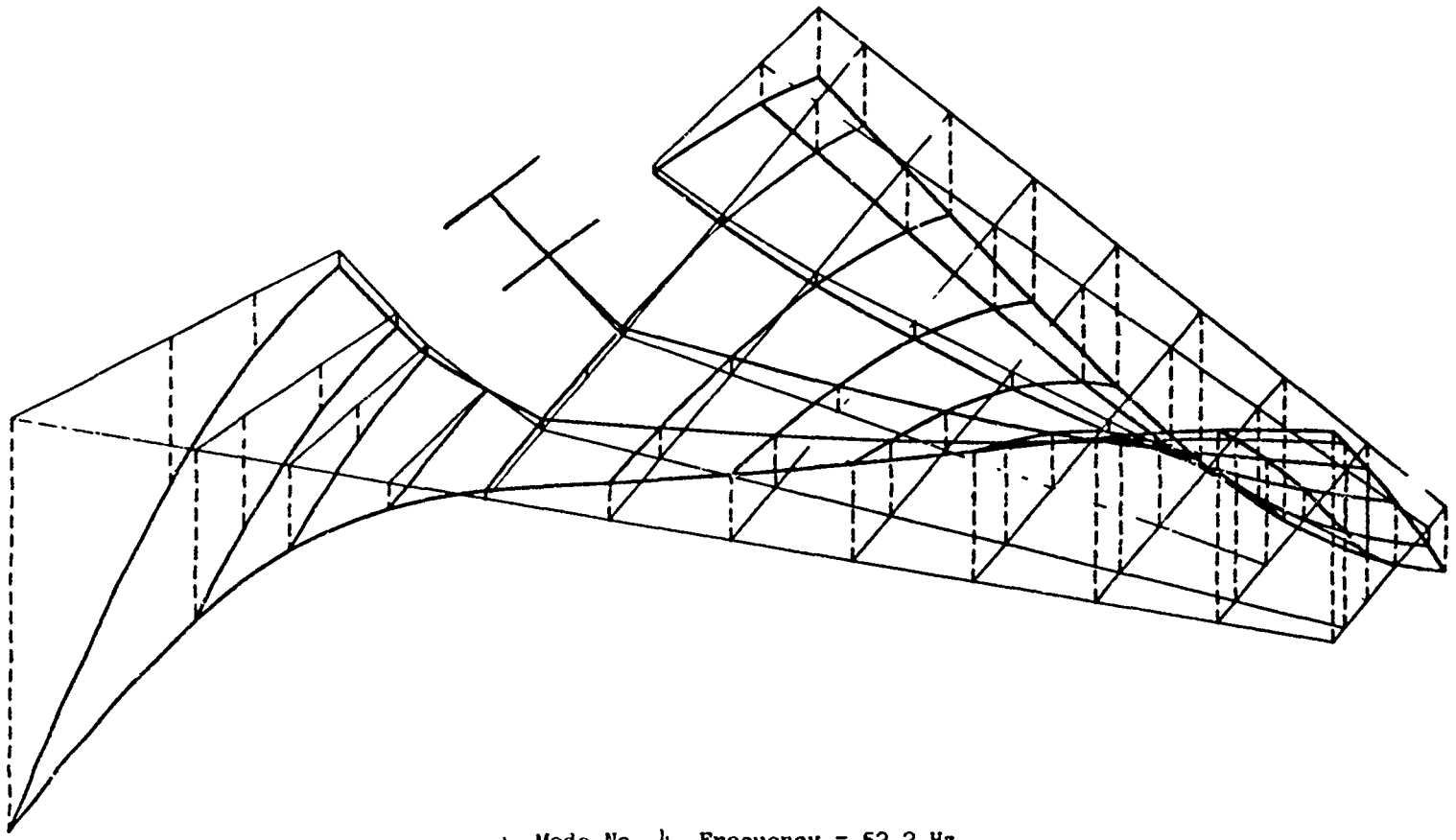

d. Mode No. 4, Frequency = 52.2 Hz

Figure 11.10 All-Movable Stabilizer Vibration Mode, Sheet 4 of 4

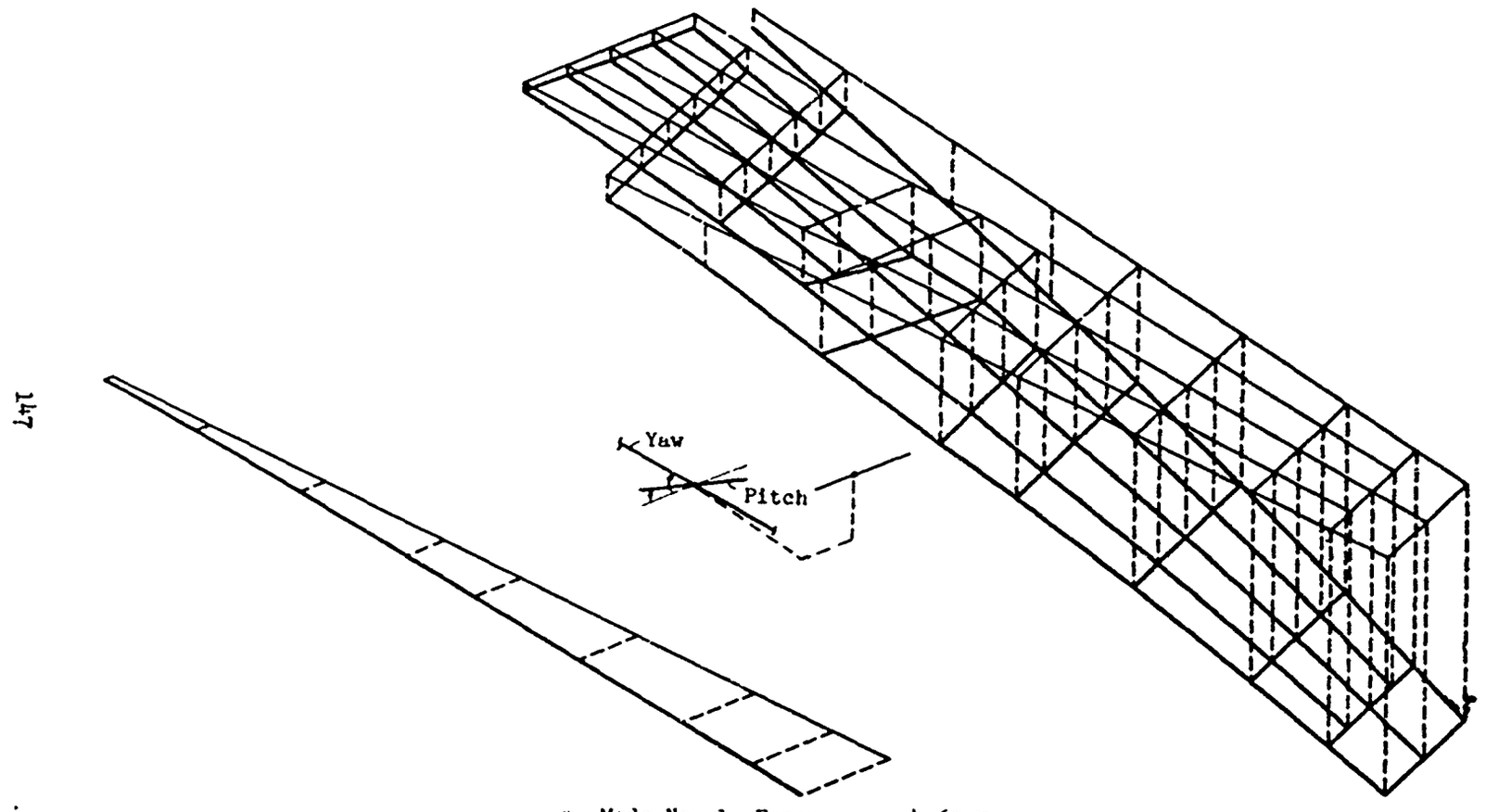

a. Mode No. 1, Frequency = 4.63 Hz

Figure 11.11 Wing-with-Store Vibration Mode, Sheet 1 of 6

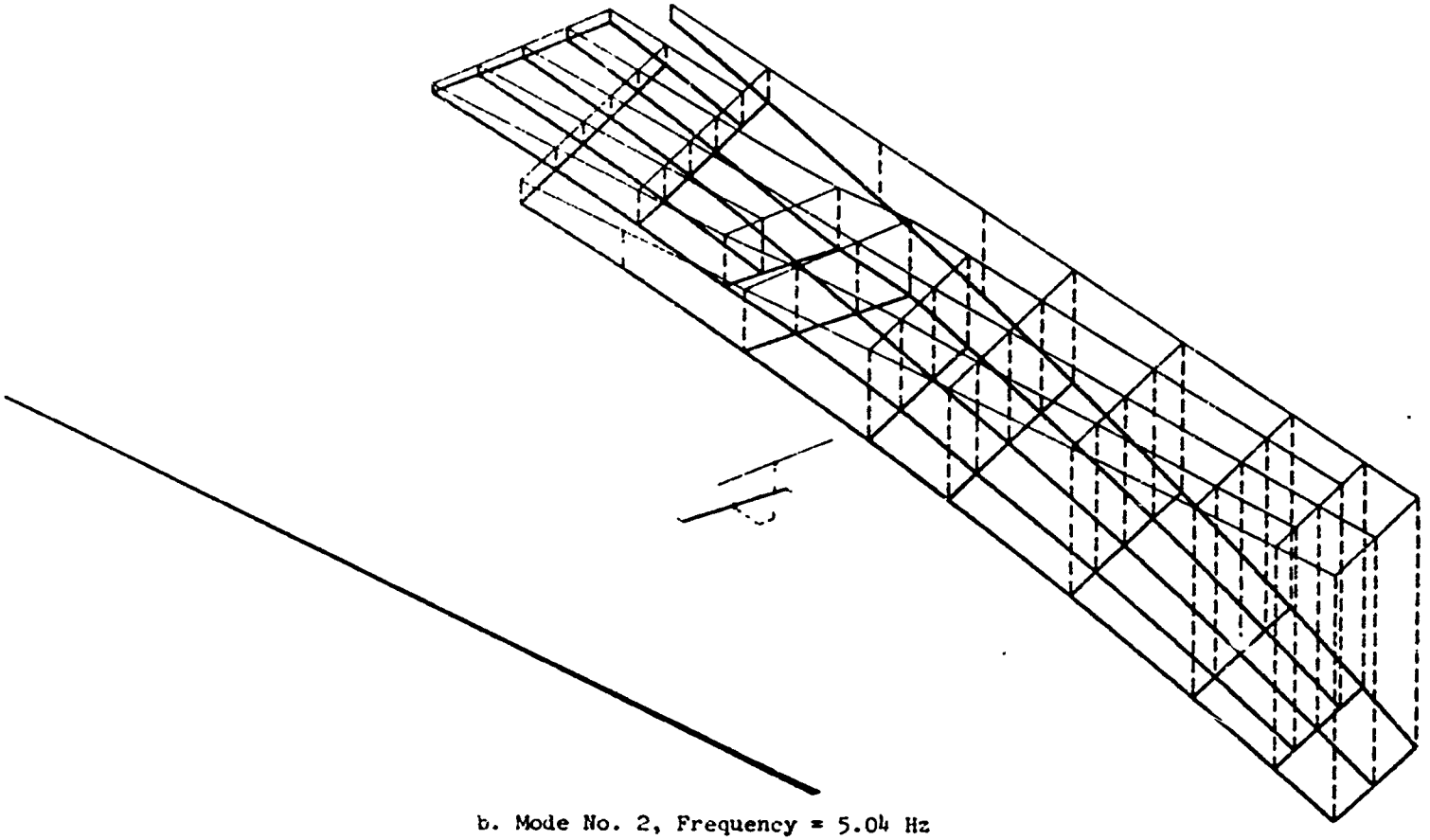

b. Mode No. 2, Frequency = 5.04 Hz

Figure 11.11 Wing-with-Store Vibration Mode, Sheet 2 of 6

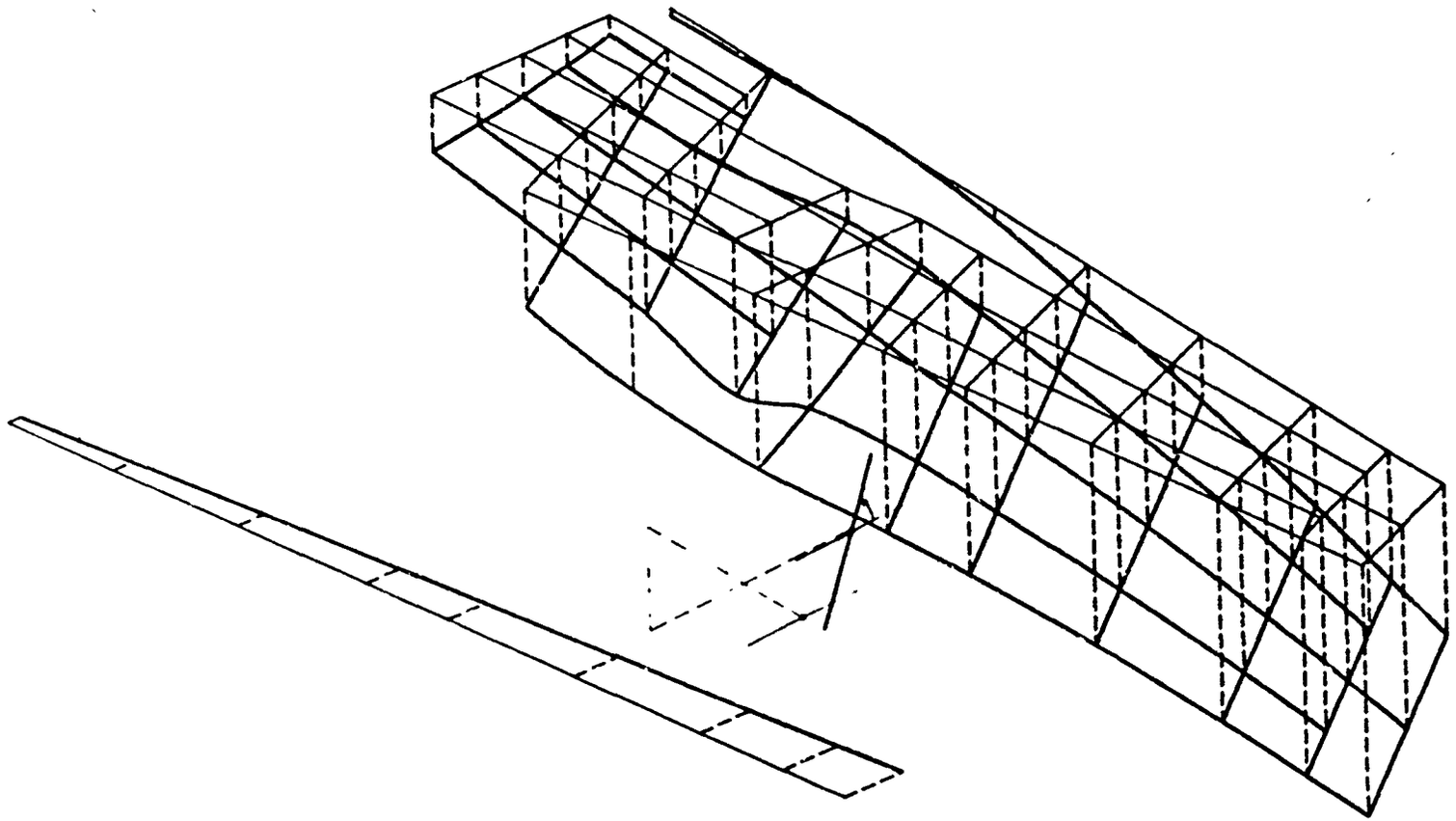

c. Mode No. 3, Frequency = 6.13 Hz

Figure 11.11 Wing-with-Store Vibration Mode, Sheet 3 of 6

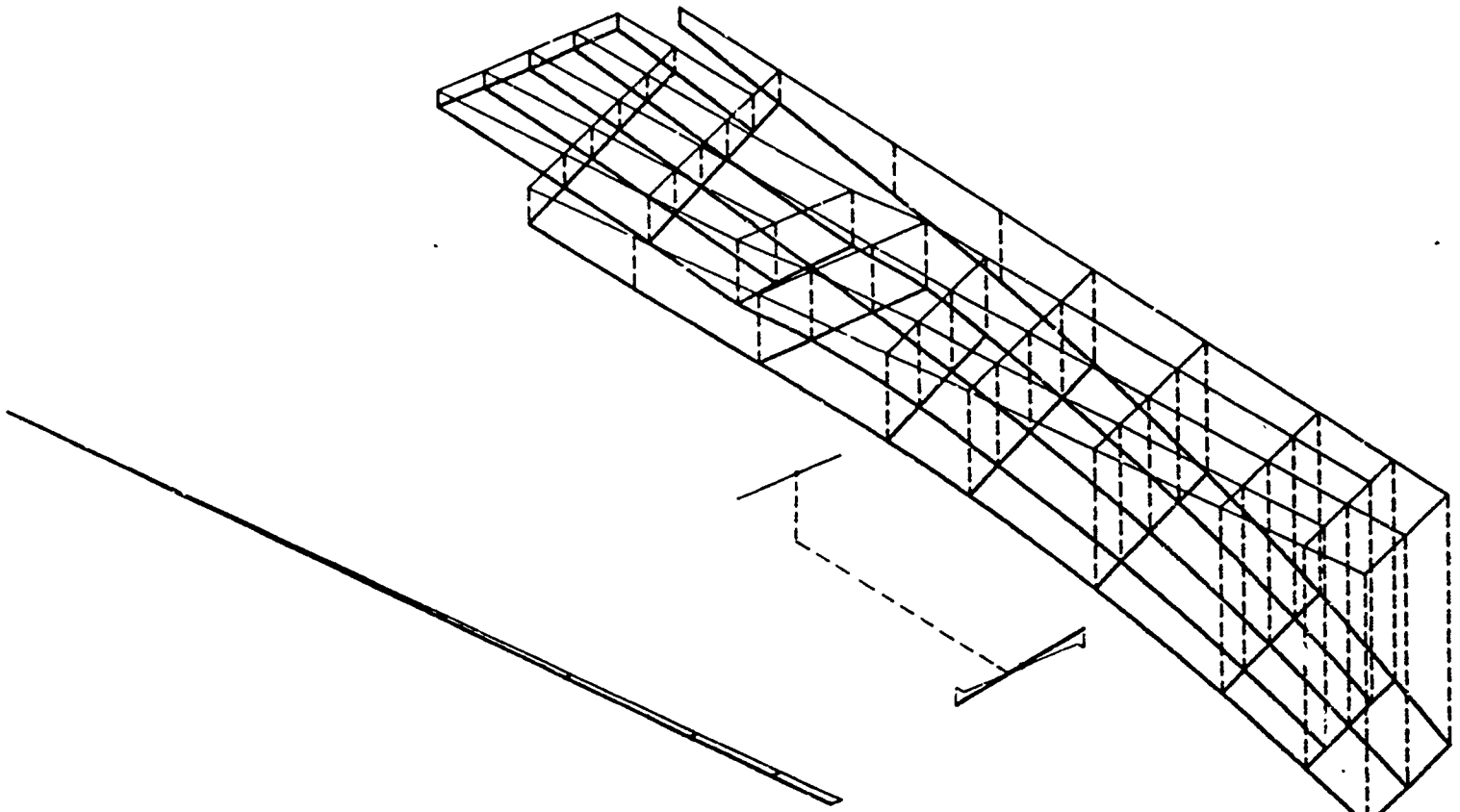

d. Mode No. 4, Frequency = 7.04 Hz

Figure 11.11 Wing-with-Store Vibration Mode, Sheet 4 of 6

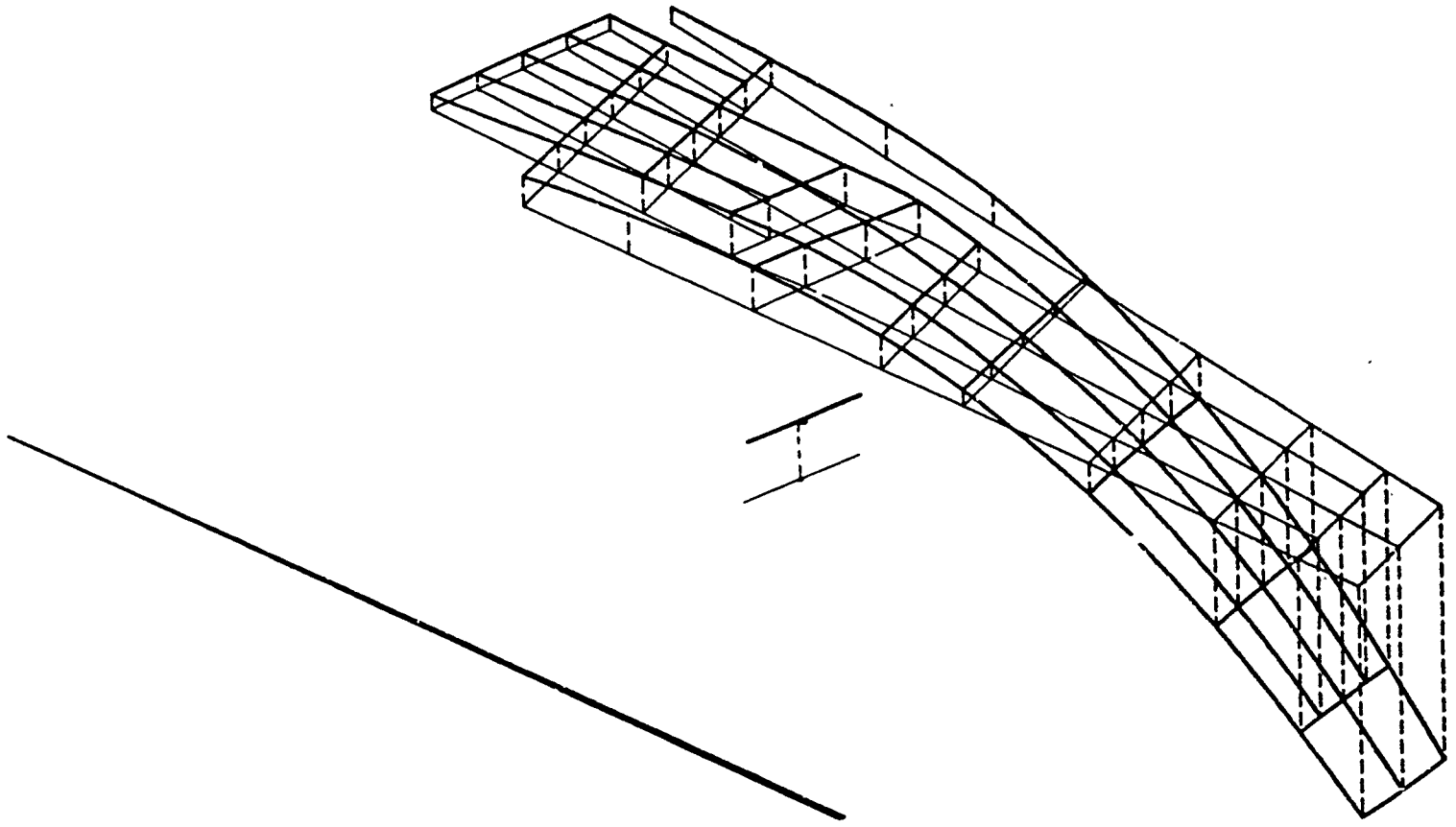

e. Mode No. 5, Frequency = 11.39 Hz

Figure 11.11 Wing-with-Store Vibration Mode, Sheet 5 of 6

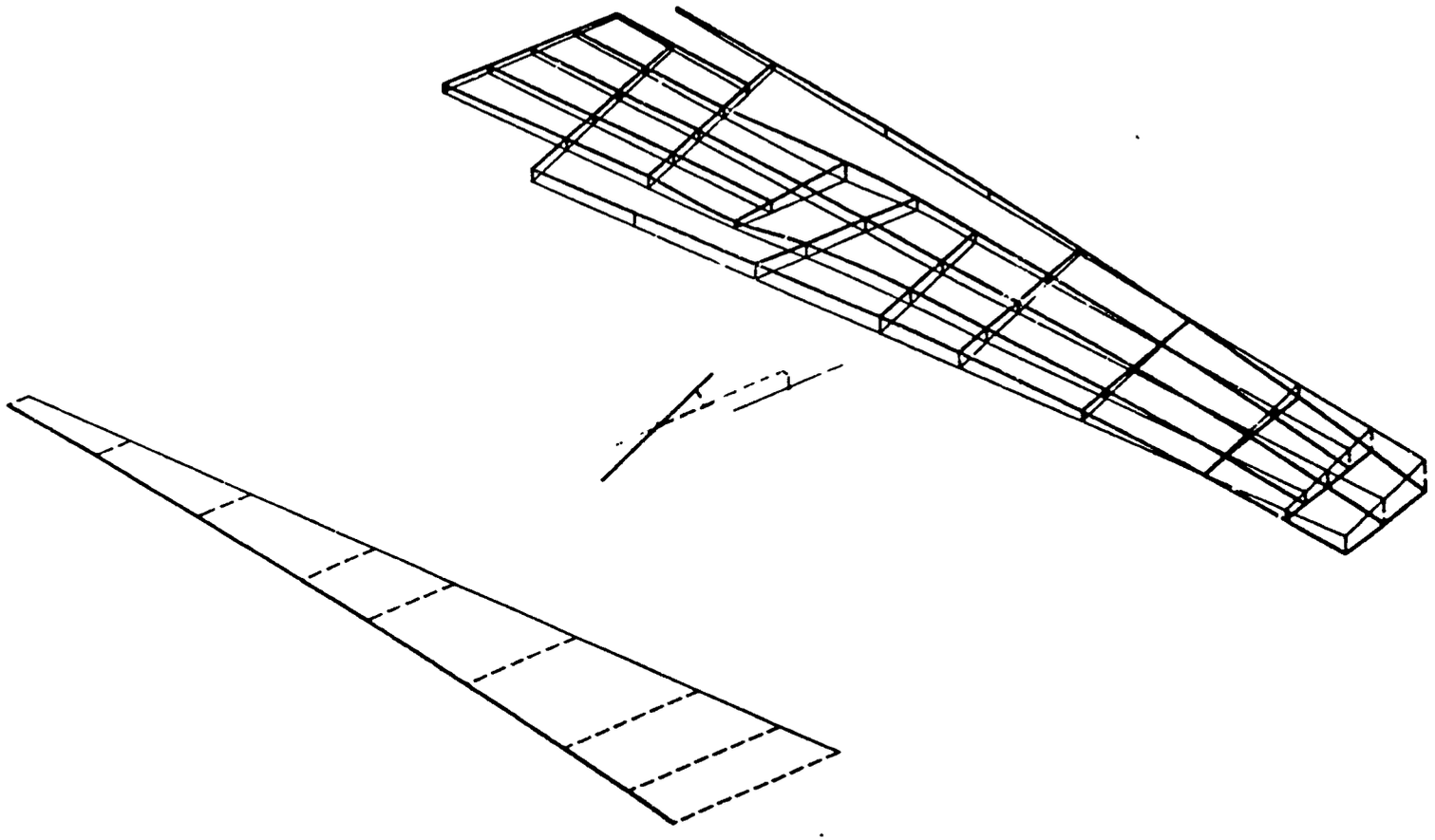

f. Mode No. 6, Frequency = 12.49 Hz

Figure 11.11 Wing-with-Store Vibration Mode, Sheet 6 of 6

11.3.4 Flutter Analysis

All of the flutter plots presented in this section were obtained using a CALCOMP plotting routine, which is an integral part of FASTOP. It should be mentioned that this routine plots the data points using symbol identification, while the curve fairing is a hand process.

The intermediate-complexity-wing flutter analysis for Mach 0.8, sea level, was performed using both the doublet-lattice and assumed-pressure-function procedures. The planform was idealized by 72 aerodynamic panels in the doublet-lattice approach and the chordwise and spanwise polynomials assumed for the pressure-function method were 3rd and 6th degree, respectively. Flutter results for both aerodynamic representations using the k-method of solution are presented in Figures 11.12 and 11.13. An additional analysis that uses the doublet-lattice approach and the p-k method of solution is presented in Figure 11.14. All three analyses yield almost identical flutter speeds. However, the subcritical frequency and damping trends differ. In particular, the frequency coalescence of the bending and torsion modes, which causes the flutter instability, is more evident in the results from the p-k method of solution.

The flutter analysis of the all-movable stabilizer was performed using the Mach-box method for a Mach number of 1.6 and an altitude of 30,000 feet. The aerodynamic surface was represented by 334 rectangular boxes and the free-stream diaphragm region, defined by the aft Mach line from the outboard tip of the leading edge and the forward Mach line from the outboard tip of the trailing edge, was represented by two diaphragm boxes. The small number of required diaphragm boxes concentrated in the tip region is explained by the fact that both the leading and trailing edges of the stabilizer are supersonic at Mach 1.6. The flutter analysis results, presented in Figures 11.15a,b show that the flutter mechanism is caused by a coupling between the stabilizer bending and pitch modes.

Flutter analyses of the wing-with-store, using the doublet-lattice method, are presented in Figures 11.16 a, b. The results, computed for

Mach 0.8, sea level, clearly show a number of store modes with very low aerodynamic damping. The lowest flutter instability occurs at 330 knots equivalent airspeed and is caused by coupling between the first wing bending mode and the store pitch mode. The damping trend of the critical root is characteristic of the "grazing" instabilities encountered in store flutter problems.

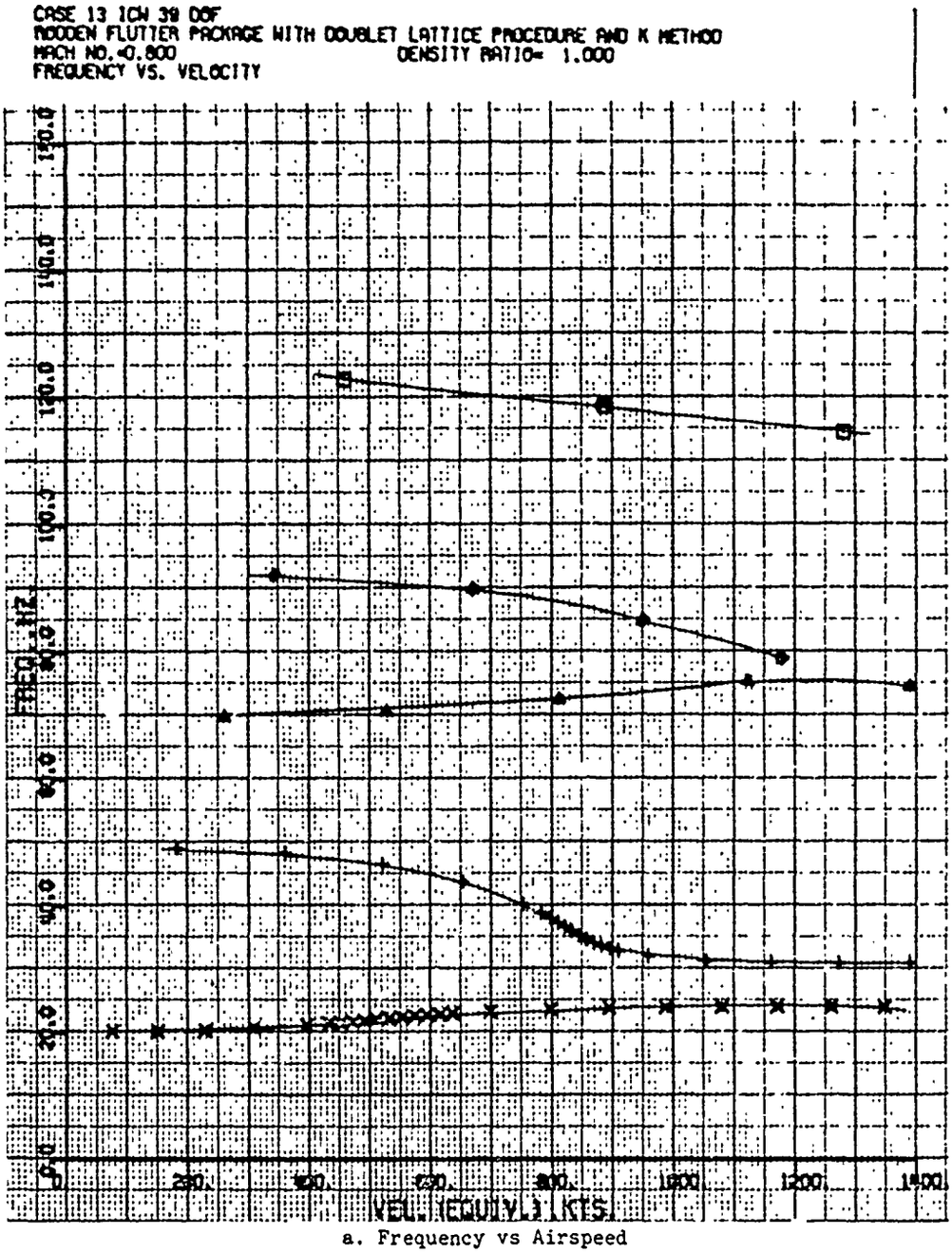

a. Frequency vs Airspeed

Figure 11.12 Intermediate Complexity Wing Flutter Analysis (Doublet Lattice Aerodynamics, k Solution), Sheet 1 of 2

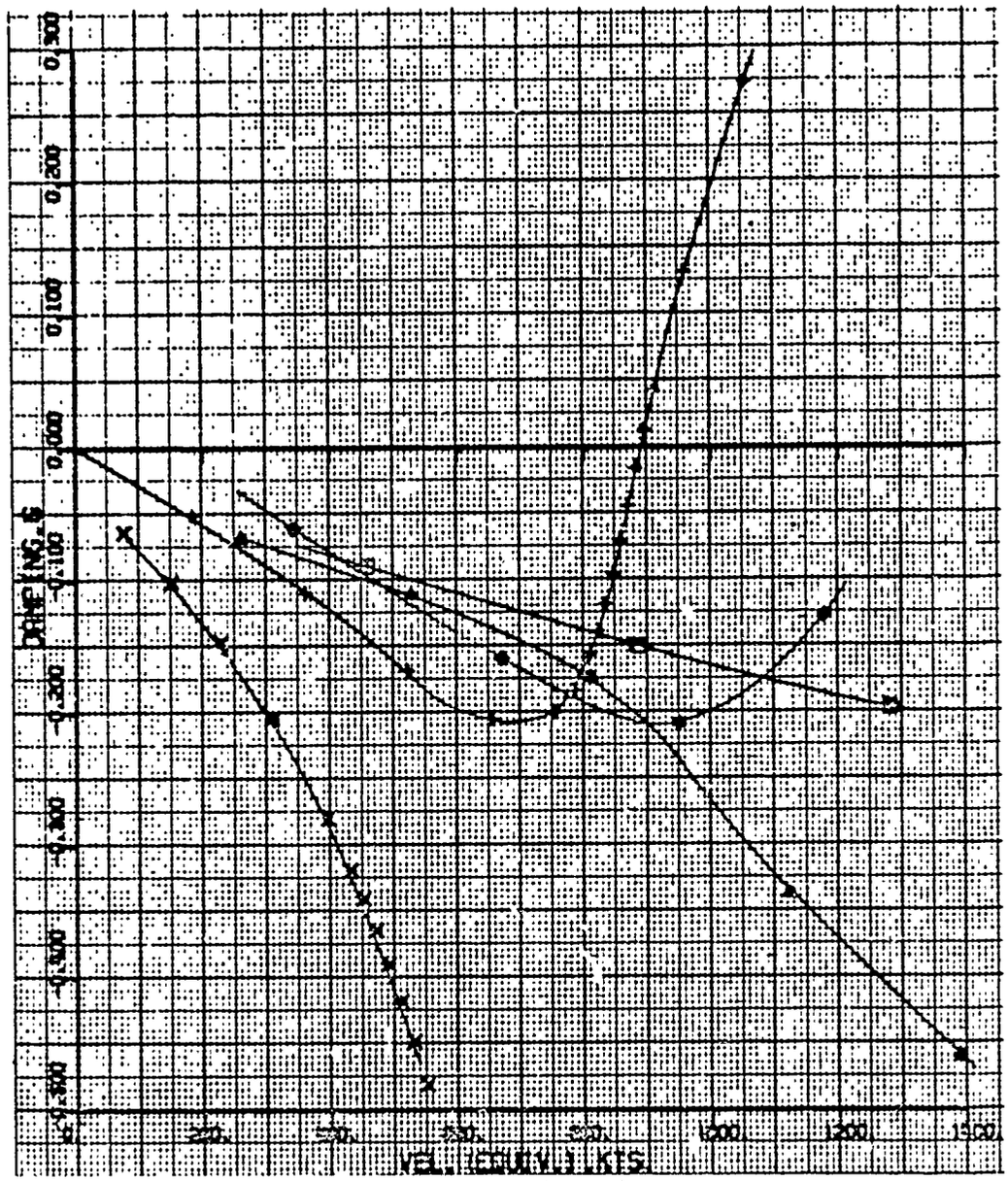

b. Damping vs Airspeed

Figure 11.12 Intermediate Complexity Wing Flutter Analysis (Doublet Lattice Aerodynamics, k Solution), Sheet 2 of 2

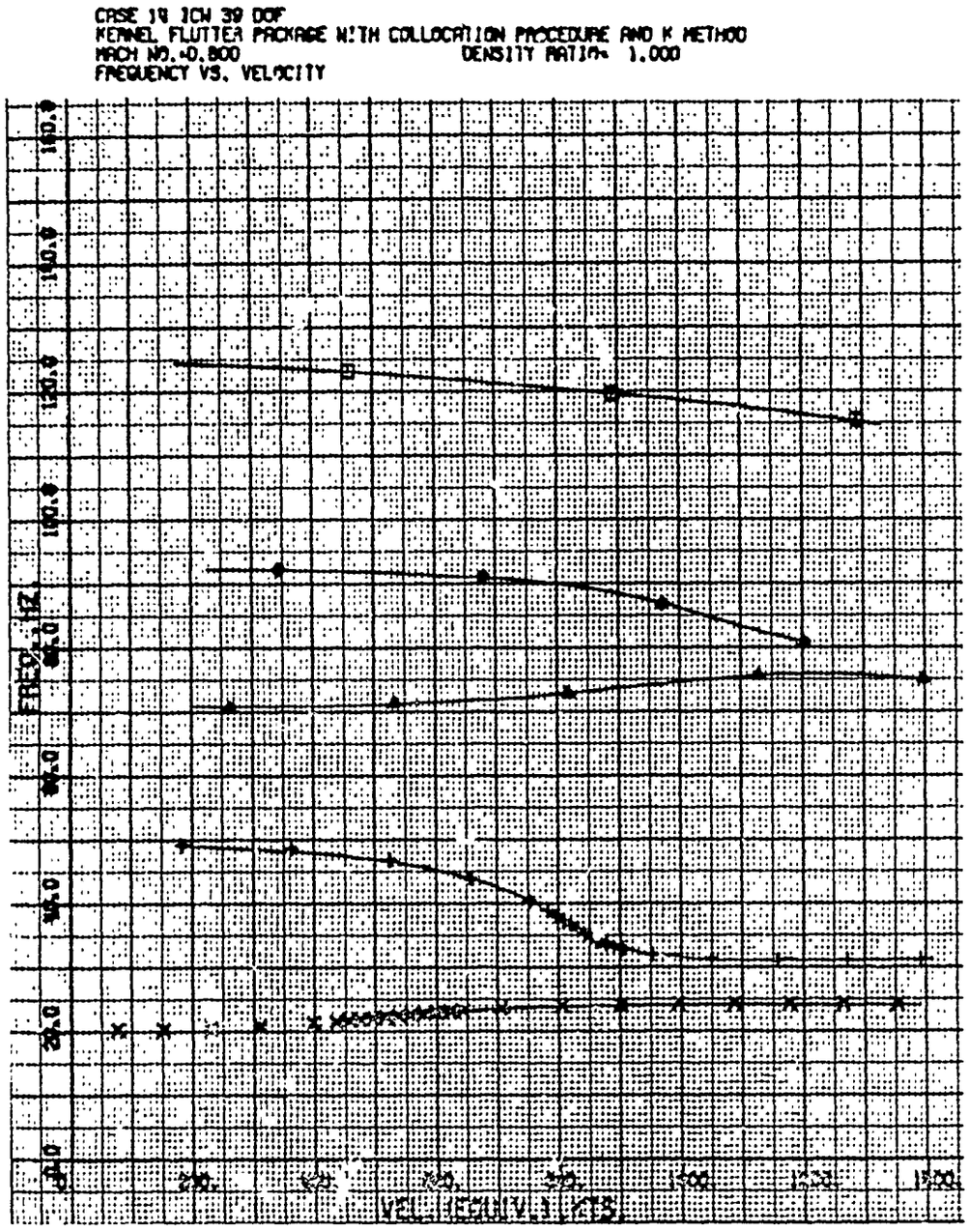

a. Frequency vs Airspeed

Figure 11.13 Intermediate Complexity Wing Flutter Analysis (Assumed Pressure Function Aerodynamics, k Solution), Sheet 1 of 2

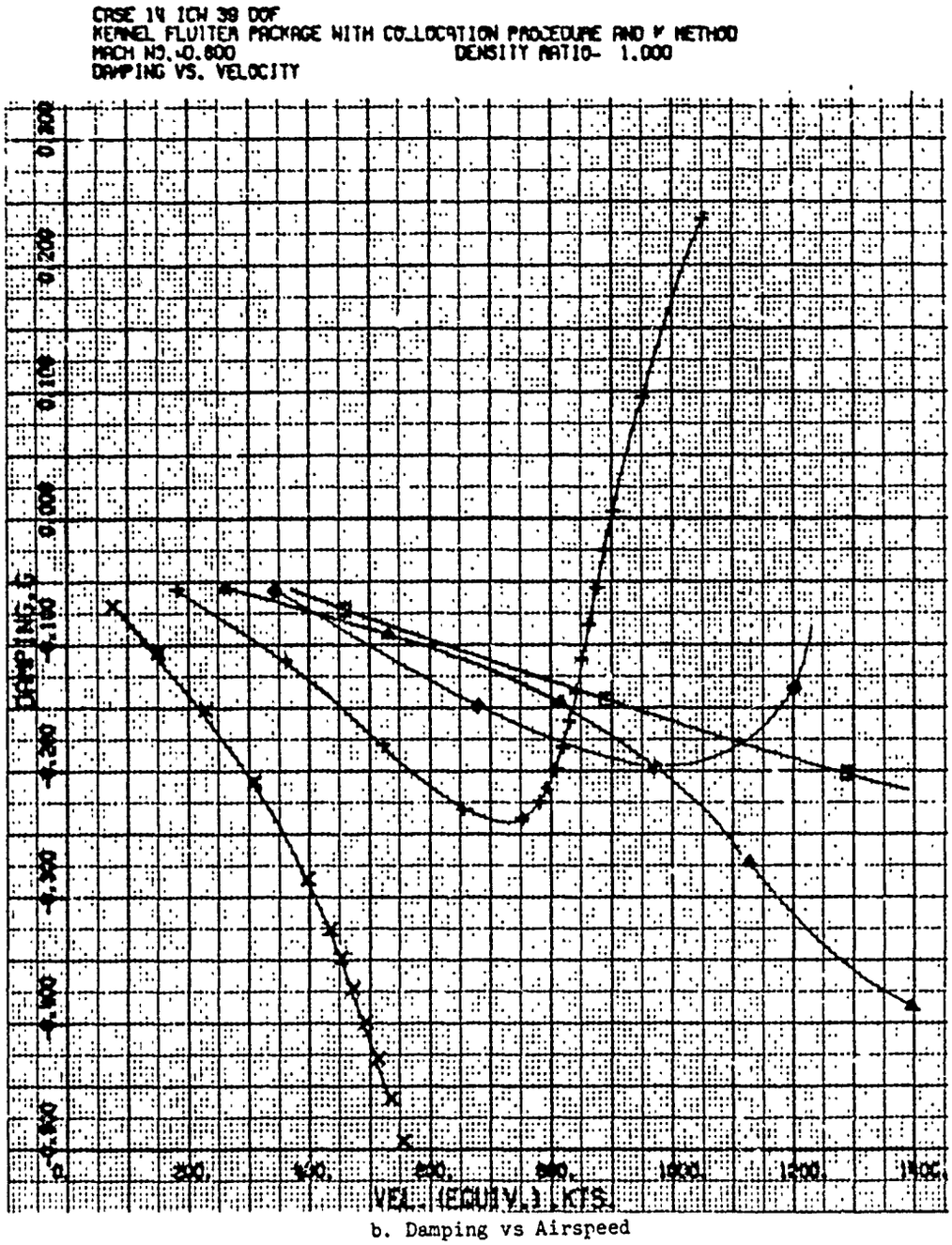

b. Damping vs Airspeed

Figure 11.13 Intermediate Complexity Wing Flutter Analysis (Assumed Pressure Function Aerodynamics, k Solution), Sheet 2 of 2

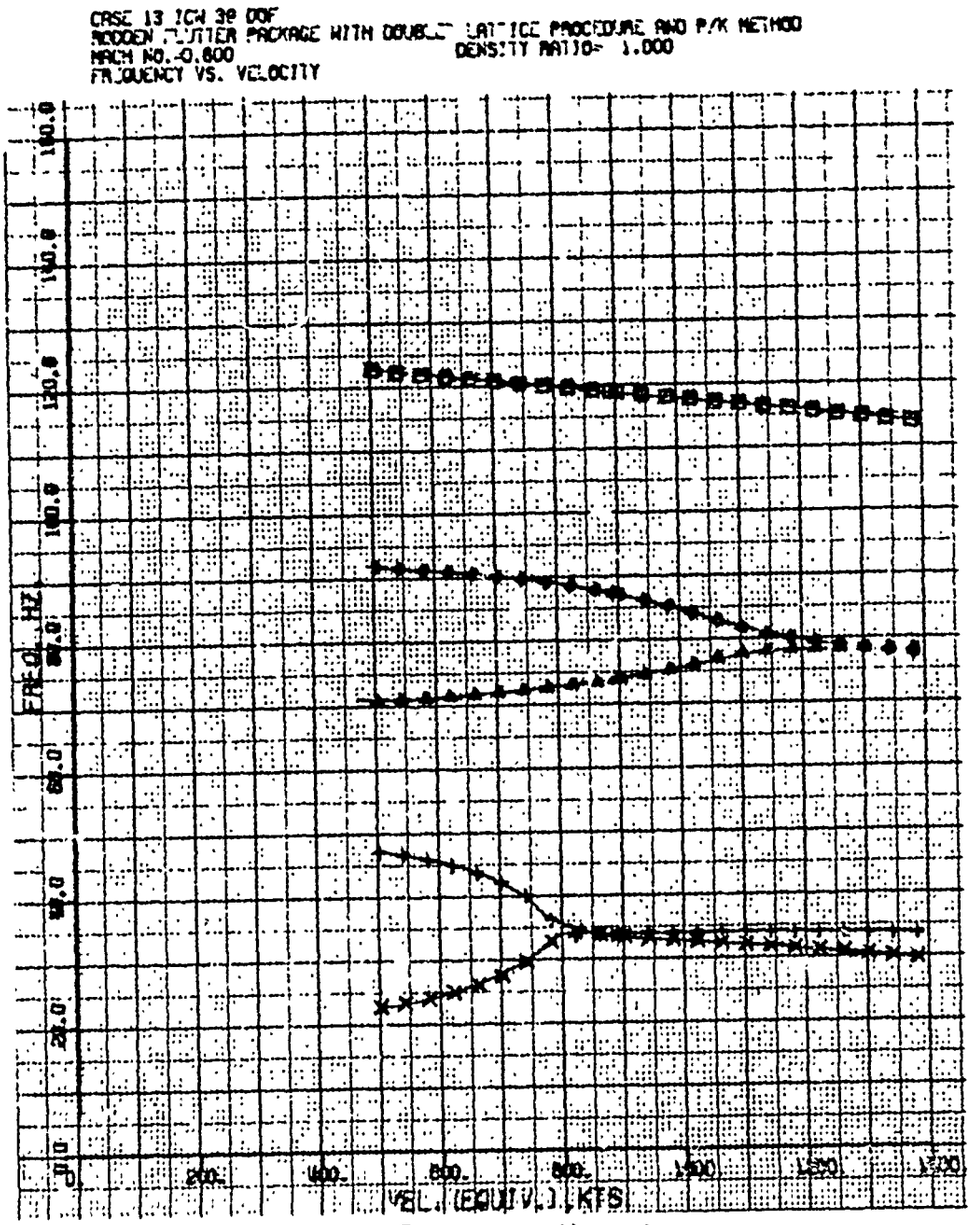

a. Frequency vs Airspeed

Figure 11.14 Intermediate Complexity Wing Flutter Analysis (Doublet Lattice Aerodynamics, p-k Solution), Sheet 1 of 2

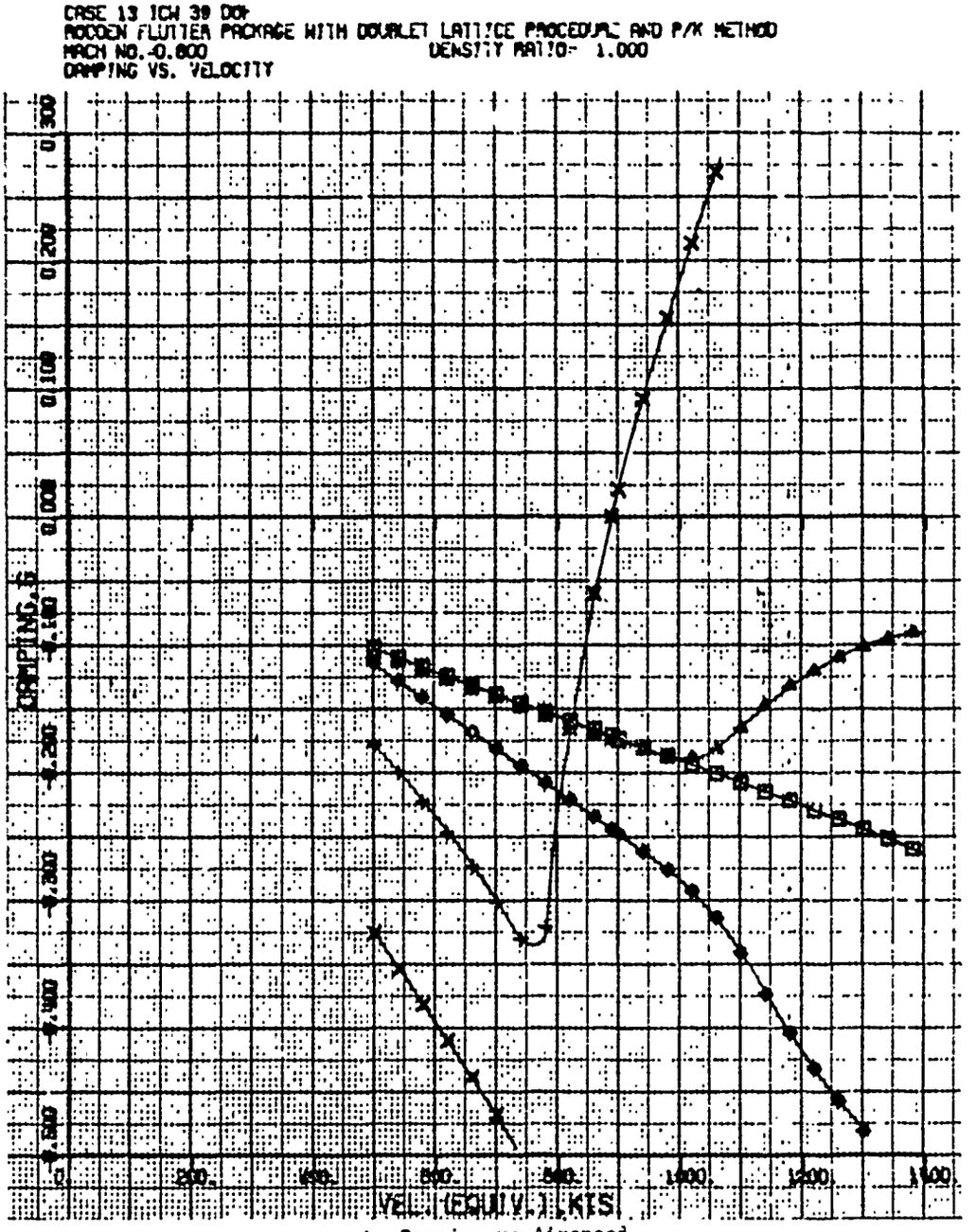

b. Damping vs Airspeed

Figure 11.14 Intermediate Complexity Wing Flutter Analysis (Doublet Lattice Aerodynamics, p-k Solution), Sheet 2 of 2

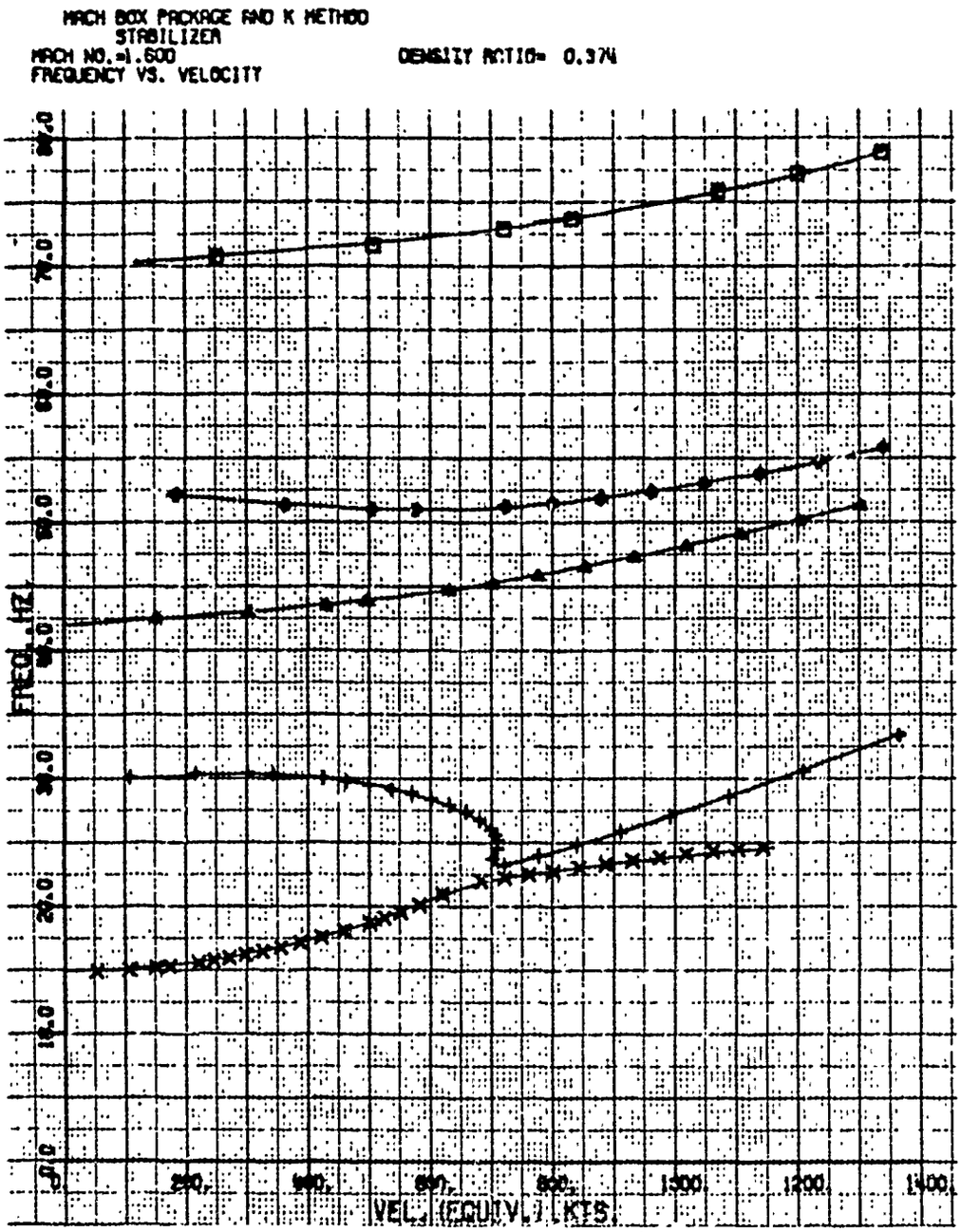

a. Frequency vs Airspeed

Figure 11.15 All-Movable Stabilizer Flutter Analysis (Mach Box Aerodynamics, k Solution), Sheet 1 of 2

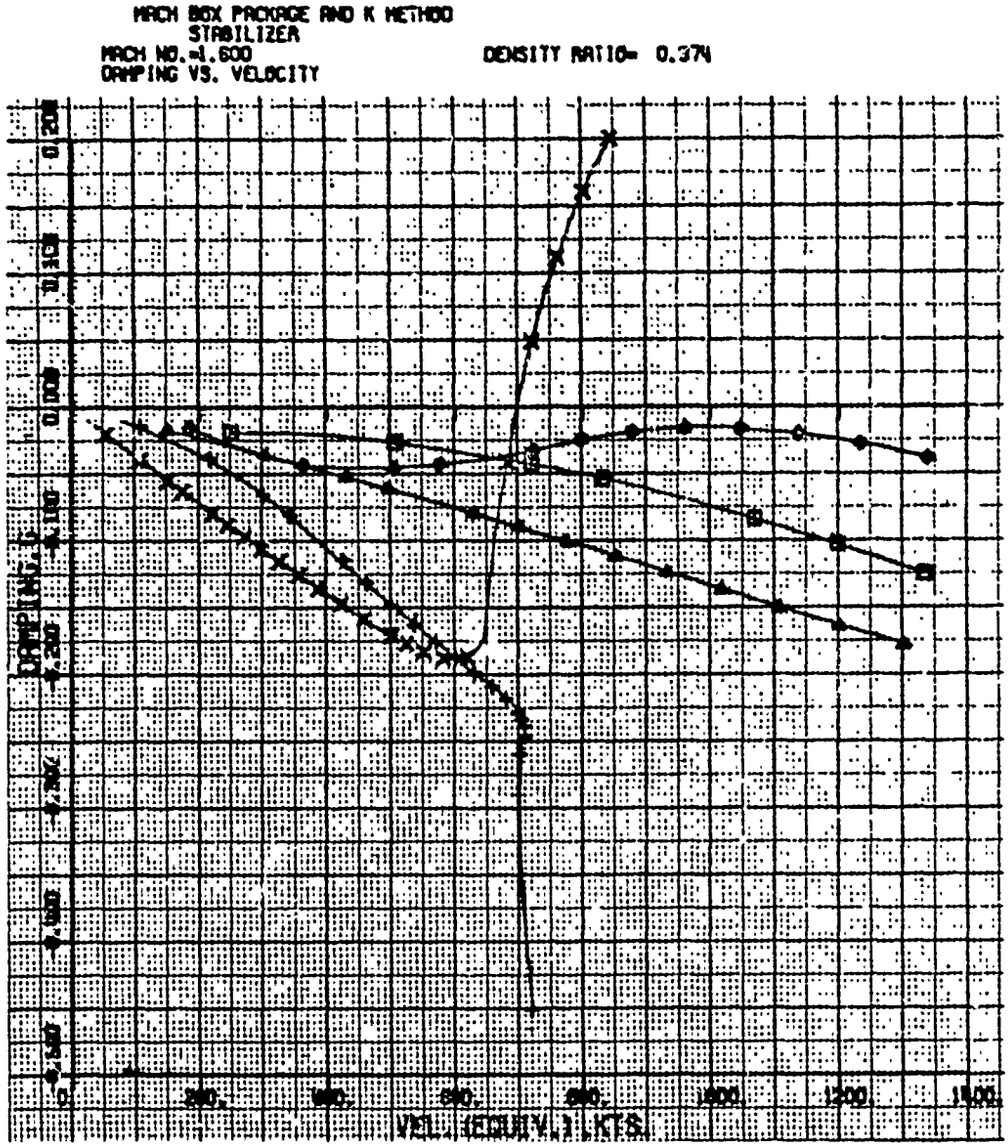

b. Damping vs Airspeed

Figure 11.15 All-Movable Stabilizer Flutter Analysis (Mach Box Aerodynamics, k Solution), Sheet 2 of 2

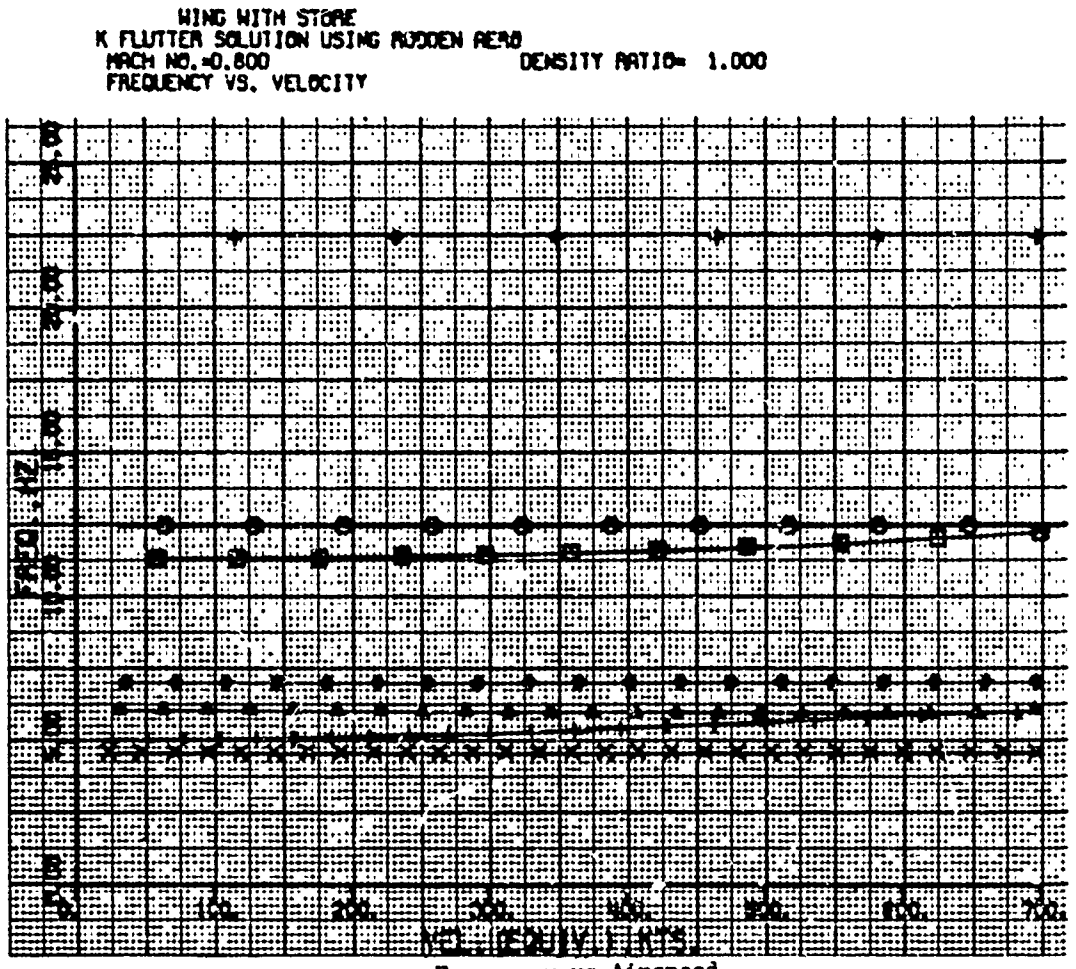

a. Frequency vs Airspeed

Figure 11.16 Wing-with-Store Flutter Analysis (Doublet Lattice Aerodynamics, k Solution), Sheet 1 of 2

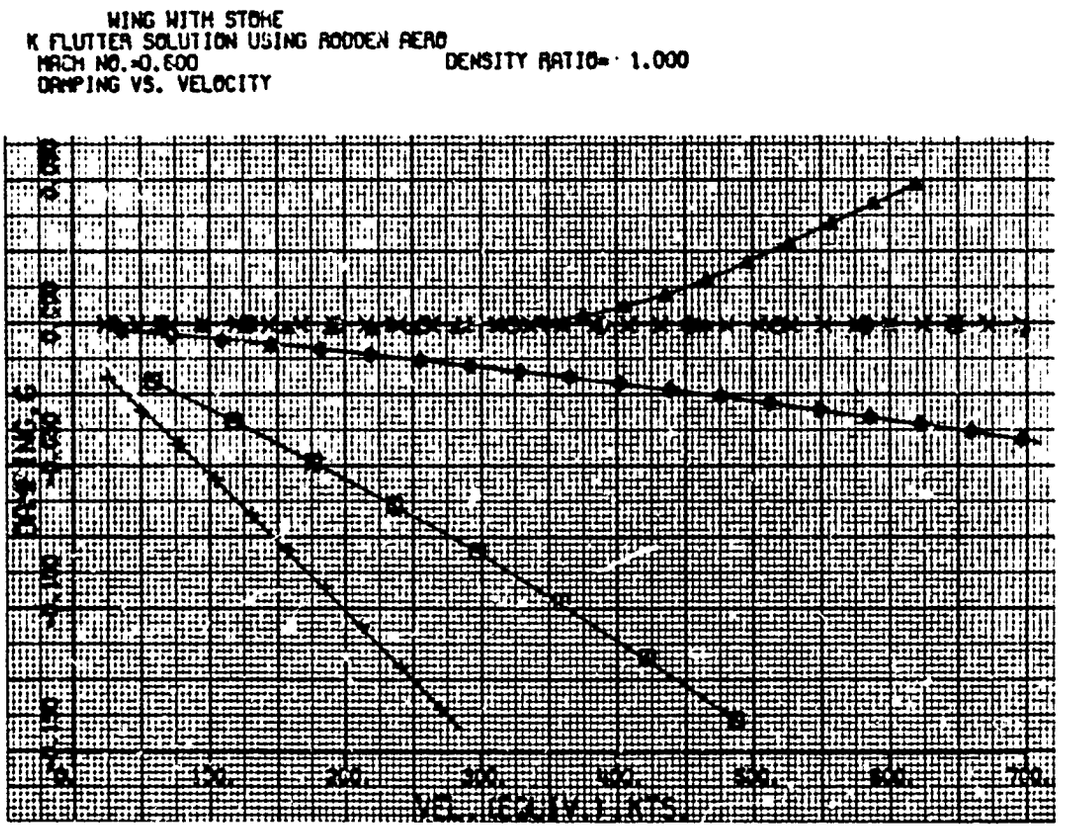

b. Damping vs Airspeed

Figure 11.16 Wing-with-Store Flutter Analysis (Doublet Lattice Aerodynamics, k Solution), Sheet 2 of 2

Section 12

EXAMPLES OF OPTIMIZATION RESULTS

12.1 SUMMARY

Calculations to demonstrate the redesign capability of FASTOP have been performed using the intermediate complexity wing, all-movable stabilizer, and wing-with-store models. The characteristics of these models are described in Section 11. The cantilever-structure dynamics model of the wing-with-store, described in Section 11, was converted to a free-free model for flutter redesign. This was done to fully demonstrate FASTOP's redesign capabilities for a configuration where dynamic interaction between the wing and fuselage might be important. The details of the changes that were made to the dynamics model are included in the discussion of wing-with-store redesign results.

Initially, the strength optimization portion of FASTOP was used to obtain a fully stressed design (FSD) for each demonstration structure. In order to accomplish this calculation, it was necessary to specify flight design load conditions for the loads analysis module, initial member sizes in the strength optimization module, and force beaming data required for the transformation analysis module. The latter group of data was needed to create transformation matrices from the aerodynamics and dynamics mathematical models to the structures mathematical model. Thus in the initial FASTOP application the design loads were computed, these were then beamed to the structures model and the structure was resized for strength. The analysis terminated with computation of a flexibility matrix for the dynamics model. The subsequent redesign to achieve a specified flutter speed improvement was achieved through multiple sequential submissions of the two major programs of FASTOP - the structural optimization program and the flutter optimization program. Except when otherwise noted, strength redesign was accomplished after each flutter redesign cycle to account for interaction between flutter and strength requirements.

Results of redesign studies using the two cantilever - structure models and the free-free model are presented and discussed below.

12.2 DISCUSSION OF REDESIGN RESULTS

12.2.1 Intermediate Complexity Wing

Two aerodynamic design load conditions were specified for the intermediate - complexity wing, namely, M = 0.5, sea level, $\alpha = 38^{\circ}$, and M = 0.9, sea level, $\alpha = 9.3^{\circ}$. Uniform initial gages (0.16 in.) were selected for all 100 elements of the structures model, and a minimum manufacturing gage of 0.02 in. was specified for all cover, rib web, and spar web elements. The structure was resized for strength in five FSD cycles resulting in a weight reduction of the idealized structure from 143.0 lb. to 61.1 lb. Adequate convergence to a fully stressed design was indicated by the weight change in the fifth redesign cycle, which was only 0.1% of the total final weight. The final gage sizes of the fully stressed structure are presented in Figure 12.1.

This initial application of the strength optimization program terminated with the computation of a flexibility matrix for the dynamics model. Dynamics-model mass data corresponding to the selected degrees of freedom were then calculated by applying realistic nonoptimum factors to the weight of the fully stressed wing-box structure and also by separately accounting for the weight of the overhanging structure not included in the finite element model (see figure 11.2). The resulting total wing weight was 187.3 lbs. compared with 61.1 lbs. for the idealized primary structure.

Flutter resizing was performed using all 100 elements of the structures model as flutter redesign variables. Flutter analyses performed in the flutter optimization program utilized the doublet-lattice unsteady aerodynamics routine and the p-k solution procedure. The flutter-critical flight condition was designated as Mach 0.8, sea level.

The required flutter speed increment from the fully-stressed design point was specified to be 30% with an acceptable flutter speed band of 30-31%. It was decided to achieve the desired flutter speed in four combined strength/flutter redesign cycles (user input). In all subsequent redesign cycles the mid-band flutter speed (30.5%) was automatically selected as the target value. The design steps, indicated in Figure 12.2, show convergence to the design optimum in eight cycles, although a design very close to the optimum point was achieved after only four cycles.

Note: Gage sizes in inches.

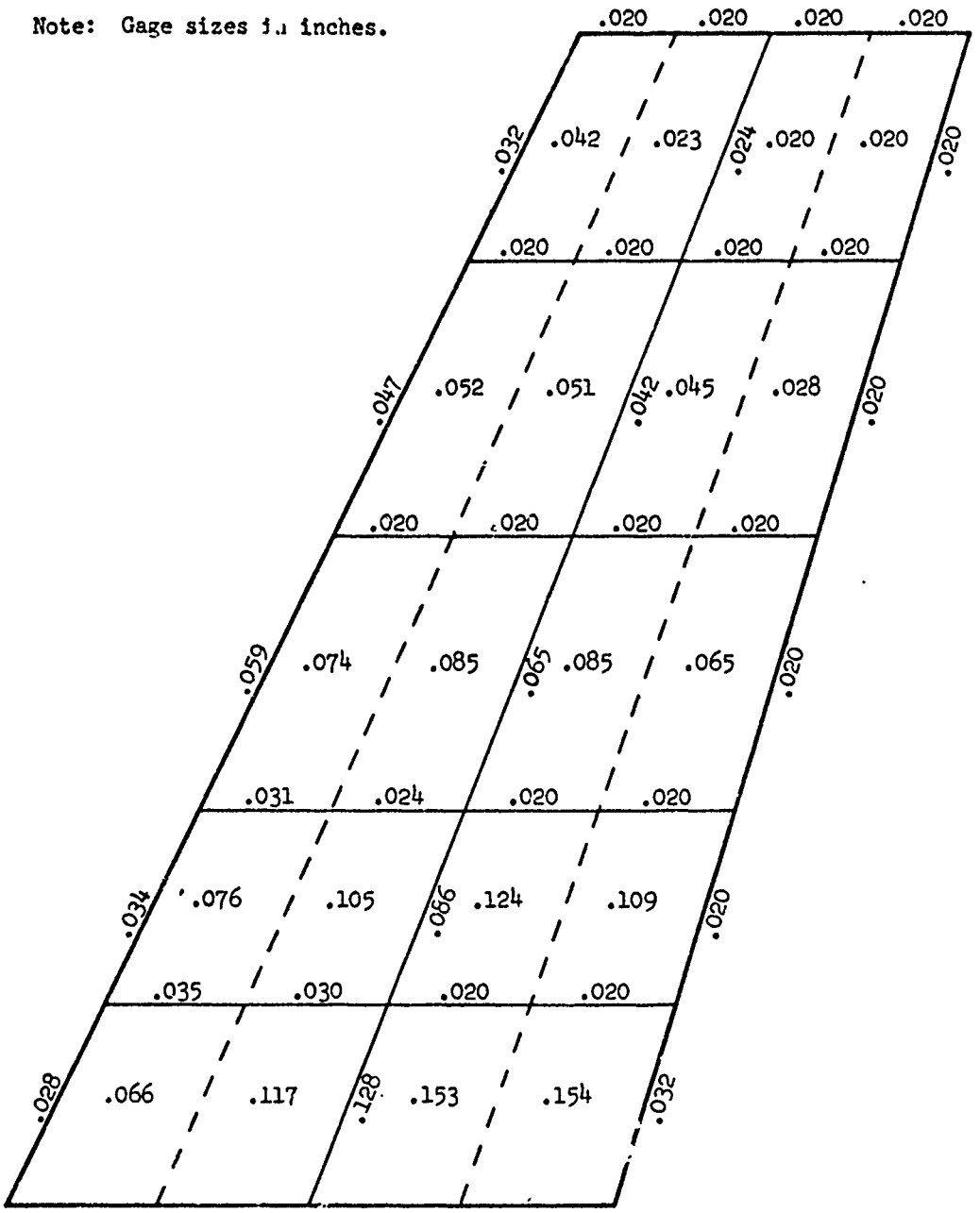

Figure 12.1 Gage Sizes for Fully-Stressed Design Intermediate-Complexity Wing.

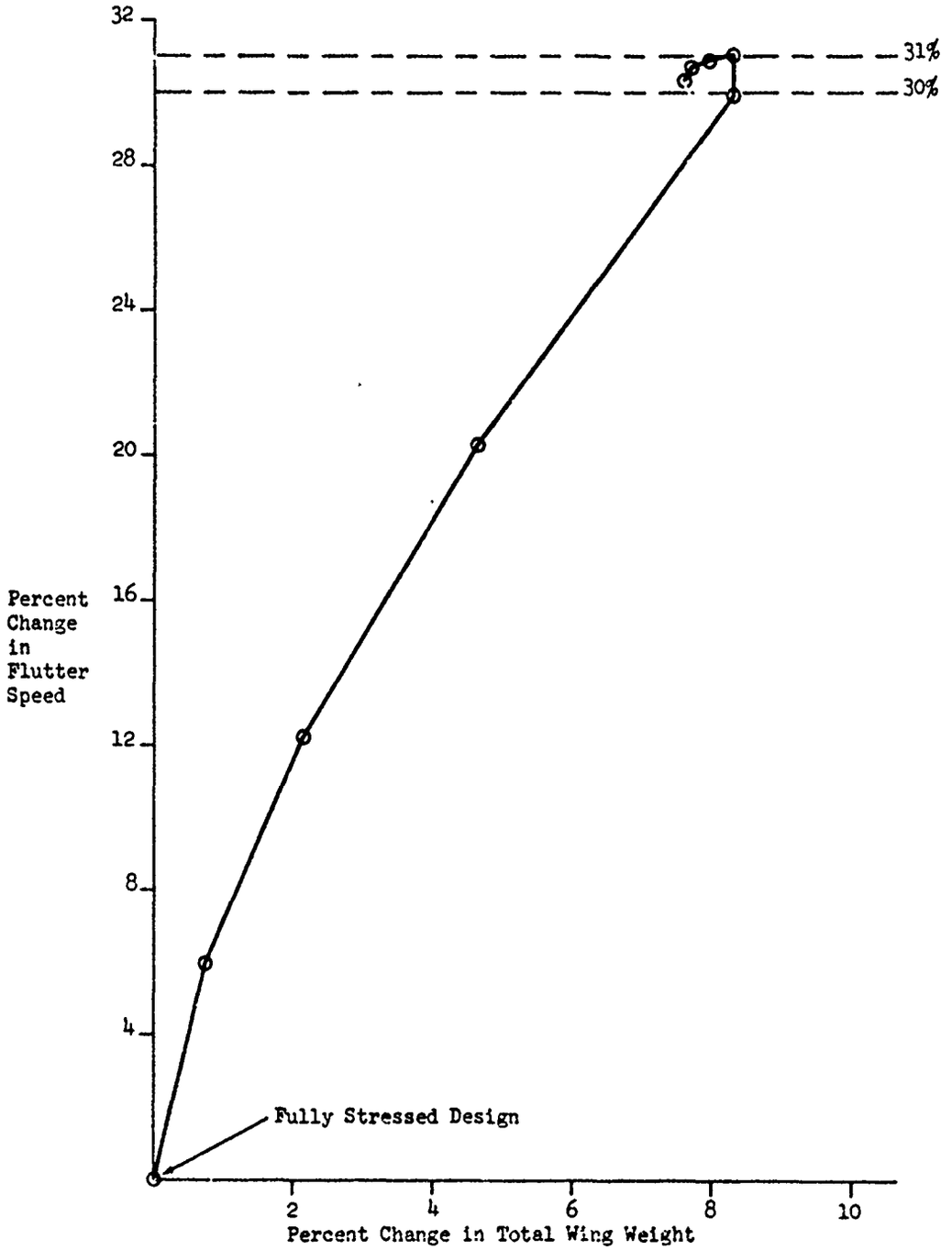

Figure 12.2 Results of Intermediate-Complexity-Wing Redesign Study

Figure 12.3 shows the distribution of the total weight added to flutter-critical elements in the final design. Also shown are the final gages of the flutter-critical elements. It is interesting to note that the weight added to the second bay inboard from the tip accounts for approximately half of the total weight increment.

The level of uniformity of the final flutter-velocity derivatives of the critical members may be observed in Figure 12.4, which also shows the original values of these derivatives for the fully stressed design. The tabular summary of final design data (Table 12.1) indicates that only 0.6 lbs. of structural weight was eliminated from the strength-critical structure in the course of redesign. Thus the resizing required for flutter had only a secondary effect on the structure's internal load distribution.

It should be noted that strength resizing may be optionally by-passed in any resizing cycle when it is apparent that strength-flutter interaction is insignificant. In this particular calculation, strength resizing was accomplished in each cycle simply to demonstrate the total program capability.

12.2.2 All-Movable Stabilizer

All-movable stabilizer design load distributions were computed for two flight conditions: M = 0.8, sea level, $\alpha = 16.5^{\circ}$, and M = 1.3, 10,000 ft., $\alpha = 9.0^{\circ}$, and the preliminary gages of the structures-model were resized for strength in five FSD cycles. Since the chordwise and spanwise shear panel elements in the stabilizer structures model simulated the stiffness properties of an aluminum honeycomb core, they could not be logically resized for either strength or flutter requirements. Consequently they were eliminated from the redesign process by setting their maximum and minimum manufacturing gages equal to their initial gages. The weight of the idealized structure was reduced by 15% (39.5 lbs.) in strength redesign. The initial strength-optimization program analysis terminated with the computation of a flexibility matrix for the 92 degrees of freedom selected for the dynamics model (see Figure 11.4).

The dynamics model mass matrix was then calculated by applying non-optimum factors to the weights of all the finite elements in the structures model and then distributing these weights to the selected dynamic points. This hand calculation was performed by a weights engineer.

Note: Percentages shown for cover-skin elements are for one cover only.

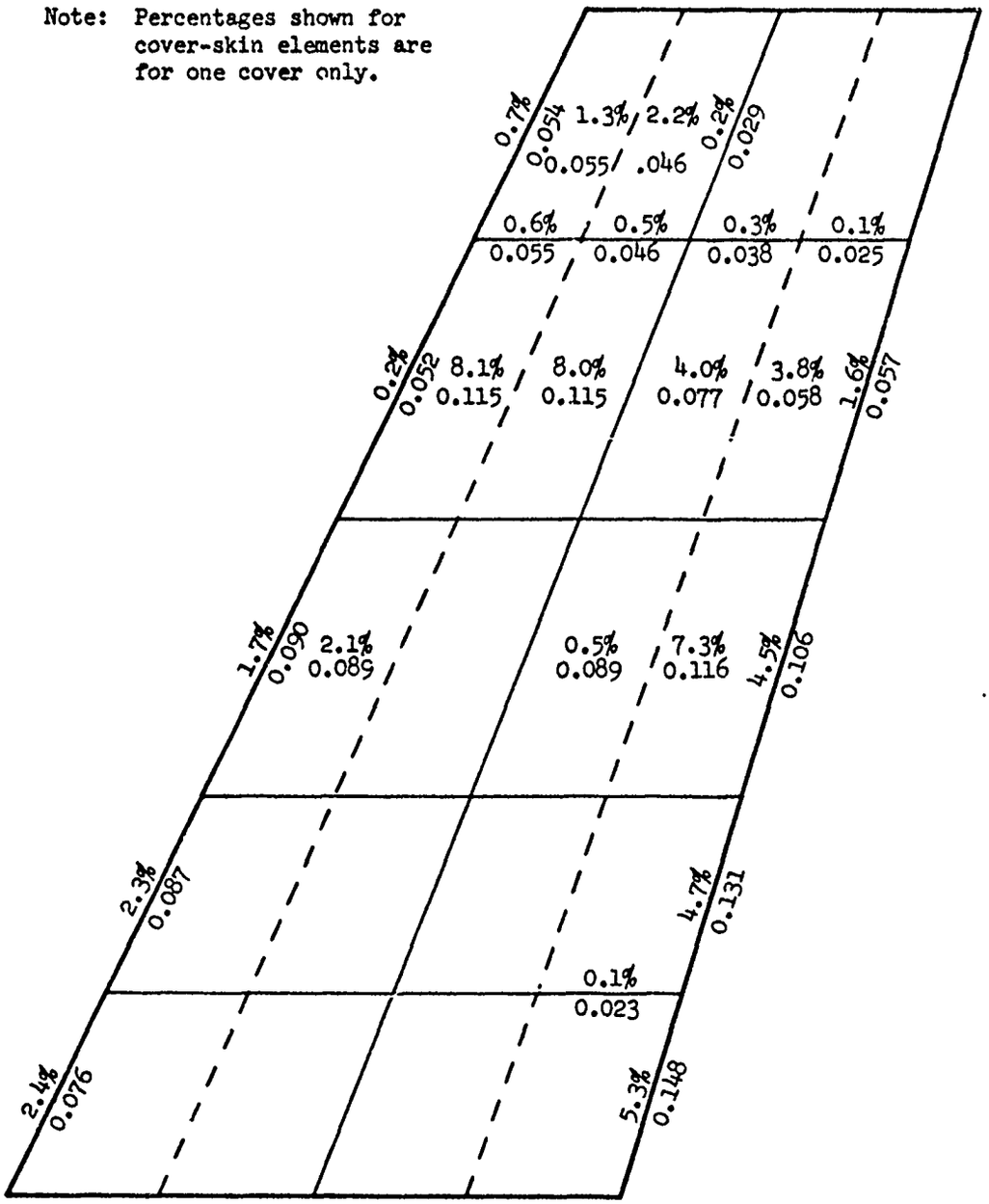

Figure 12.3 Distribution of Total Weight Increase for 30% Flutter-Speed Improvement and Final Gages - After Redesign for Intermediate Complexity Wing

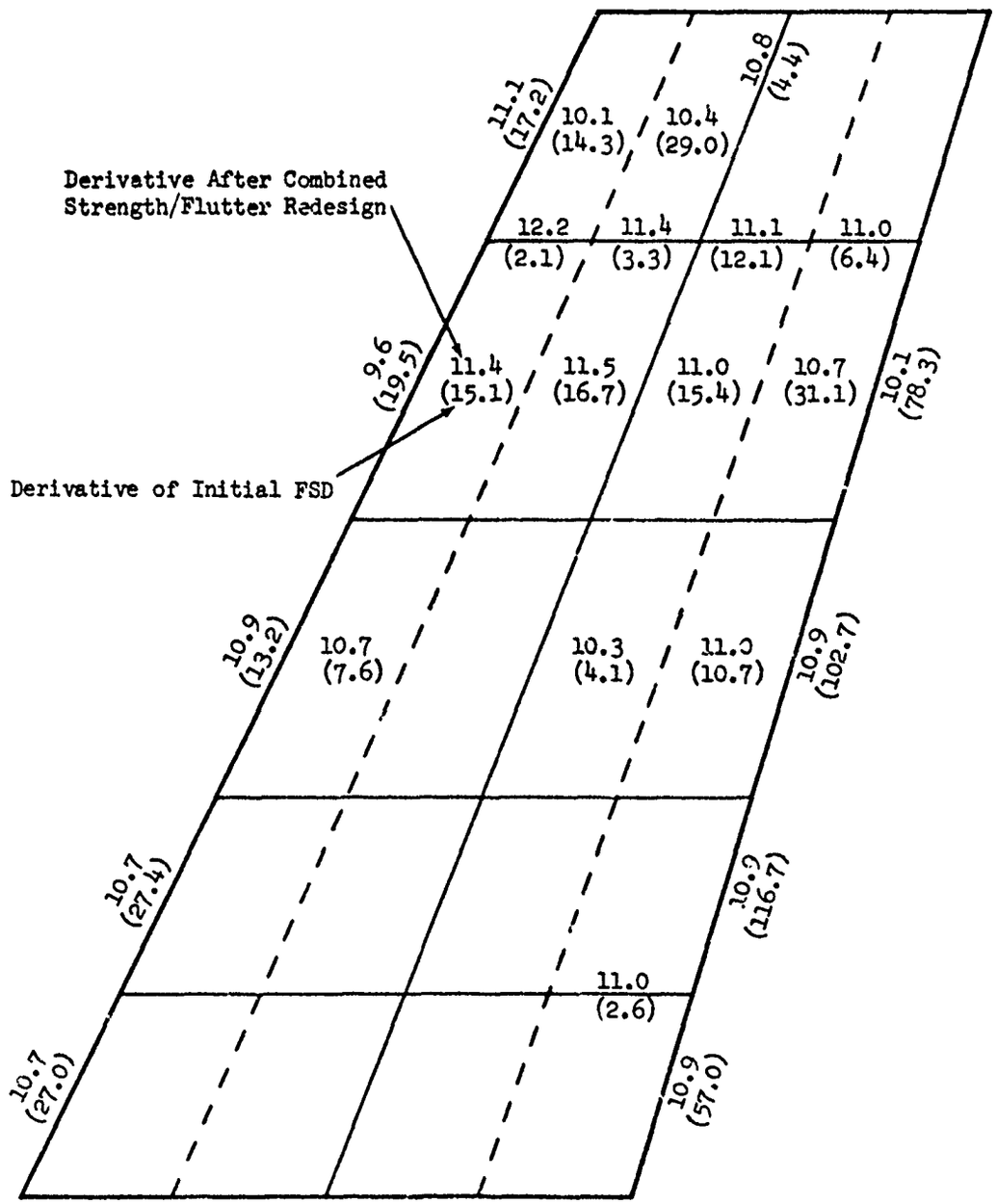

Figure 12.4 Comparison of Flutter-Velocity Derivatives (Knots/Lb) of Flutter-Critical Elements for Intermediate Complexity Wing - Before and After Redesign

TABLE 12.1 - FINAL DESIGN DATA FOR THE INTERMEDIATE-COMPLEXITY WING AND ALL-MOVABLE STABILIZER DEMONSTRATION PROBLEMS

WEIGHT IN POUNDS

	INTERMEDIATE-COMPLEXITY WING	ALL-MOVABLE STABILIZER
Weight of finite element model - preliminary sizing of members	143.0	259.7
- - - after FSD	61.1	220.2
Total weight of FSD structure including non-optimum factors	187.3	414.5
Total weight increment of flutter-critical elements from FSD (final design)	14.76	Structure = 3.71 Mass balance = 6.78
Total weight change of strength-critical elements from FSD	-0.60	-0.24
Total weight increment from FSD	14.16	10.25

A supersonic flutter-critical flight condition, Mach 1.6, 30,000 ft, was selected for flutter redesign with the design goal being a 25% increase in flutter speed. Two separate studies were then performed, one using both structural and mass balance design variables and the other using only structural design variables. In the former case, 3 lbs. of initial mass balance was arbitrarily added at each of three selected mass balance locations (see Figure 12.5). Reasonably large values of mass were selected to avoid the possibility, observed in previous studies, of mass balance being ineffective for low initial values even though it becomes effective for larger values.

The results of the combined strength/flutter redesign study, including mass balance variables, showed that the mass balance at point B was increased beyond its initial value whereas the masses at points A and C were progressively eliminated. It was obvious, after the third flutter redesign cycle that the mass balance at points A and C would be zero in the final design; it was decided therefore to override the existing program values and set them equal to zero at this design point. This had the effect of accelerating convergence to the design optimum point.

It is seen in Figure 12.6 that a near optimum design with combined structural and mass-balance variables was achieved after only five flutter redesign cycles. The net weight increase to achieve a 25% increase in flutter speed was only 10.7 lbs or 2.58%. A further three redesign cycles beyond this point eliminated an additional 0.5 lbs., a relatively insignificant amount. The distribution of mass balance and structural weight in the final design is presented in Figure 12.7. The standard deviation of flutter-velocity derivatives for the nine flutter critical elements in the final design was 0.33 knots/lb with a mean value of 17.7 knots/lb. A summary of final design data is presented in Table 12.1 wherein it is noted that resizing for strength (a single cycle of FSD in each combined resizing cycle) resulted in a very small reduction in the weight of the strength-critical structure.

The second all-movable stabilizer study, which used only structural design variables, indicated that the flutter effectiveness of the structural elements in the tip region was governed by their mass-balance effect, i.e., the kinetic-energy-density contribution was dominant. FASTOP therefore resized these elements to achieve a mass balance effect similar to that noted in the previous study. Since the initial values for the mass of these minimum gage structural

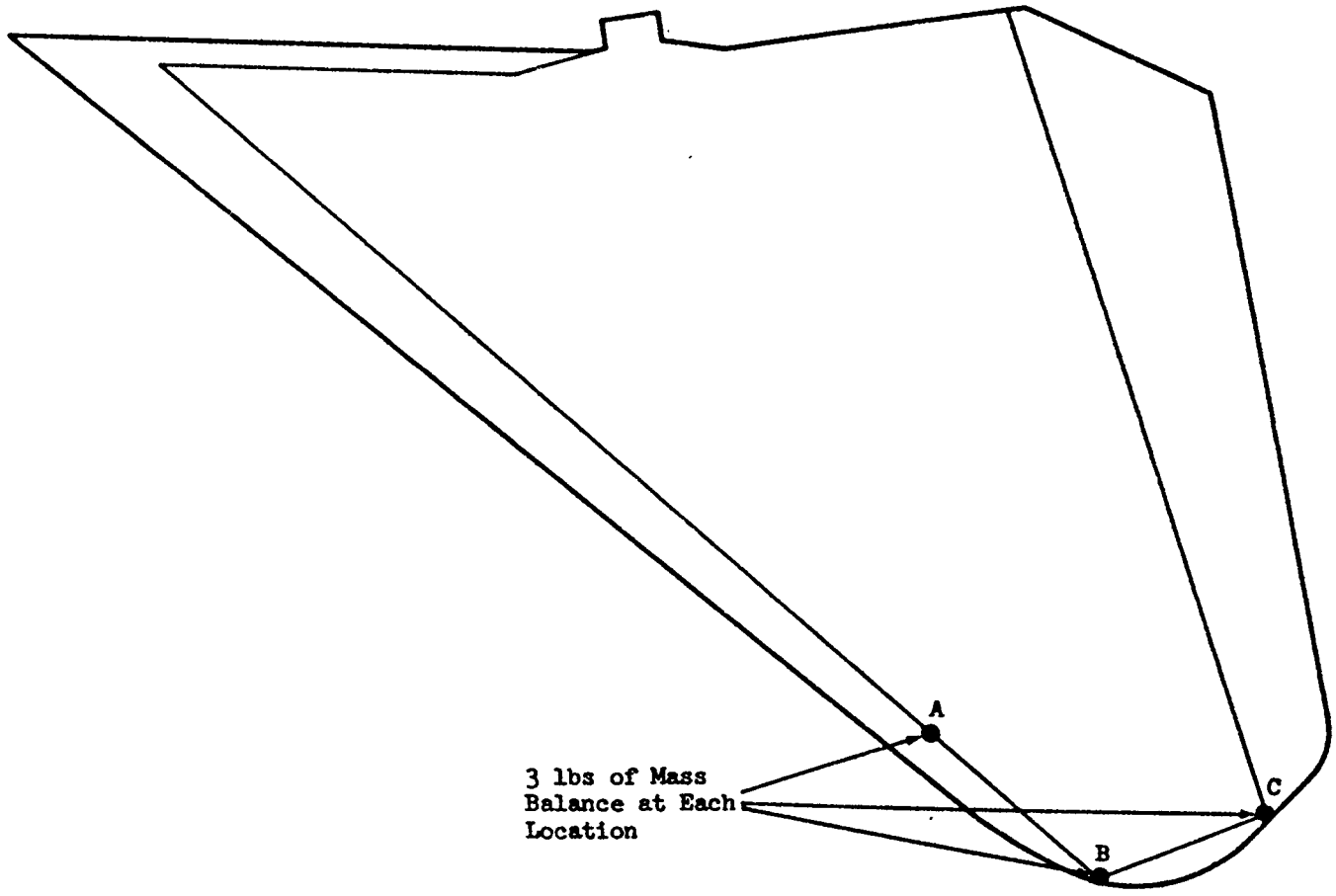

Figure 12.5 Selected Locations for All-Movable-Stabilizer Initial Mass Balance

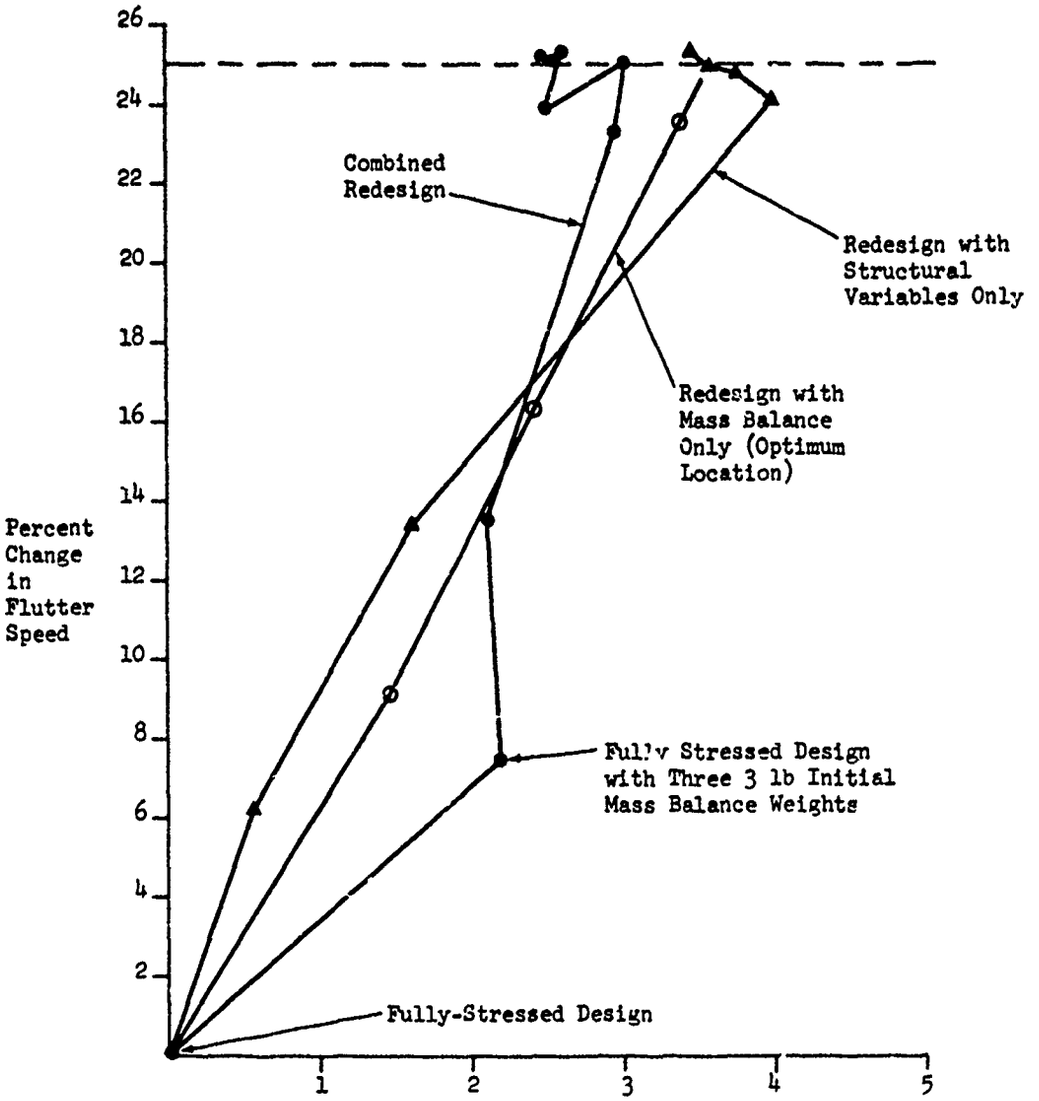

Figure 12.6 Results of All-Movable Stabilizer Redesign Study

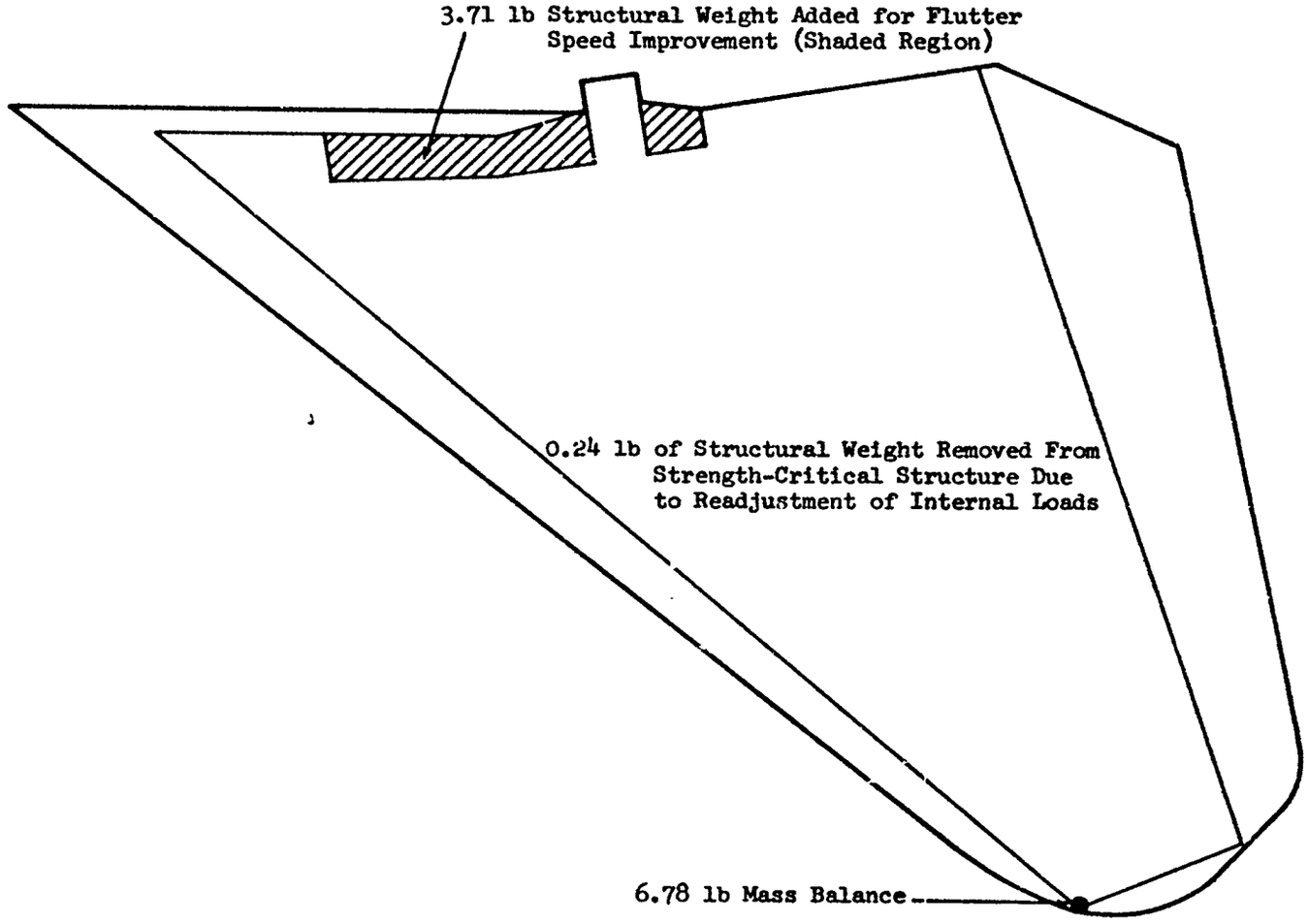

Figure 12.7 Design Changes from FSD for 25% All-Movable-Stabilizer Flutter-Speed Increase

elements was very small, it became apparent that convergence to the optimum combination of "mass balance" and structural stiffness would be slow (see Figure 12.6). Consequently, redesign was terminated before convergence was achieved. This case illustrates a fact noted in previous studies using FASTOP, namely that the convergence for flutter cases that are susceptible to mass balance is much enhanced if the user initiates redesign with arbitrary selections of mass balance in potentially effective regions of the structure.

To provide a further base of reference for the two studies described above, a final analysis was performed using mass balance alone at the most effective location indicated by FASTOP, i.e., the tip leading-edge. It was determined that 14.7 lb. of mass balance would be required to achieve the 25% flutter speed increase, compared with 10.25 lb. for the combined redesign case (see Figure 12.6).

12.2.3 Wing-with-Store

Conversion of the cantilever-structure dynamics model of the wing-with-store (see Figure 11.6) to a free-free model was achieved by including beam elements to simulate the stiffness properties of the fuselage in vertical bending. The fuselage modelling is schematically illustrated in Figure 12.8 in which it is noted that fifteen elements were used to represent the fuselage and ten beam element node points were selected as dynamic node points for vibration analysis. Thus the modified vibration model had a total of 158 dynamic degrees of freedom plus three plug (rigid body) degrees of freedom.

The preliminary gages of the finite element structures model were resized for strength in five FSD cycles using two computed subsonic aerodynamic design load distributions and one store inertial load condition. The weight of the resulting fully-stressed structure was 1340 lbs., based on the finite element idealization, and 1921 lbs., including non-optimum factors and overhanging structure. The pylon-mounted store weighed 4500 lbs. with a pitch inertia of 8×10^6 lb. in^2 about its center of gravity. The high store inertia created a critical flutter mechanism involving the first wing bending mode and the store-pitch/wing-torsion mode. A Mach 0.8, sea level flutter-critical flight condition was designated for the redesign study. The objective was to achieve a flutter speed target of 660 knots equivalent airspeed from an initial computed value of 270 knots for the fully stressed design. Wing posts and fuselage beam elements were excluded from strength/flutter redesign resulting in a total of 453 structural design variables for this study.

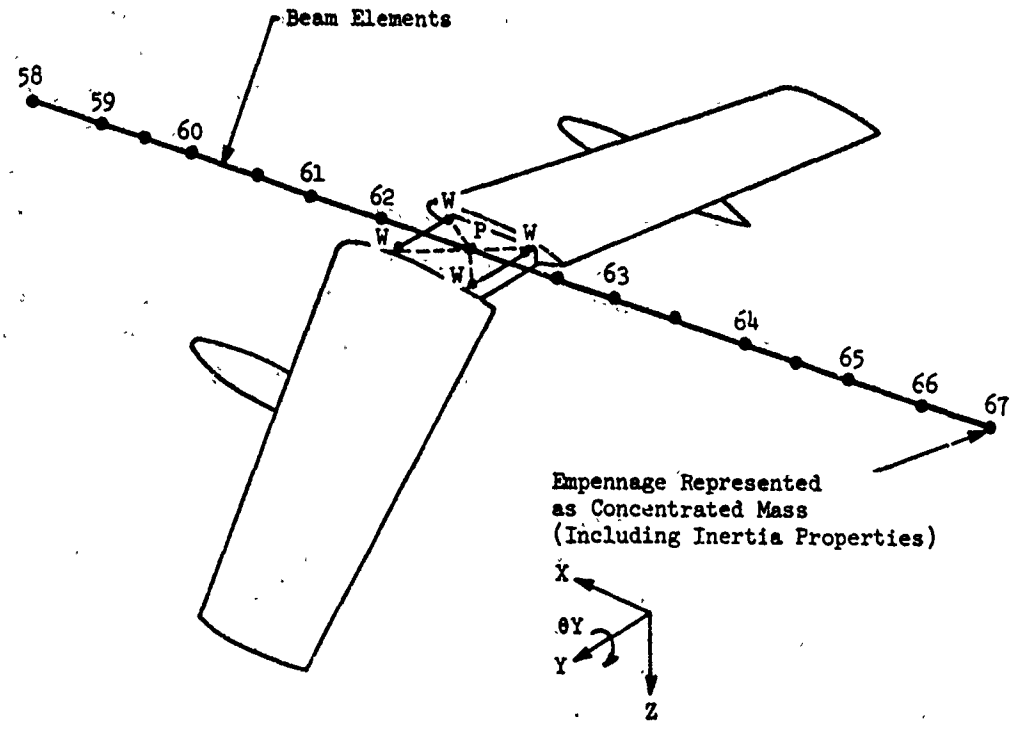

W = Wing-to-Fuselage Connection Points
P = Location of 'Plug' Mass

Note: Points W and P are Rigidly Interconnected.

Dynamic Node	Fuselage Dynamic Degrees of Freedom					
	X	Y	Z	θX	θY	θZ
58	137		138		139	
59	140		141			
60	142		143			
61	144		145			
62	146		147			
63	148		149			
64	150		151			
65	152		153			
66	154		155			
67	156		157		158	
Plug	✓		✓		✓	

Figure 12.8. Wing-with-Store Dynamic Model of Fuselage

The forward beam of the pylon support structure, connecting nodes 176 and 177 (See Figure 11.5) had the highest flutter velocity derivative in the initial design (236 knots/lb.) and the beam element which continued the forward rear connection through the lower and upper wing covers (nodes 176-175) had the second highest derivative (97 knots/lb.). The rear beam of the pylon, which had a flutter velocity derivative of -41.5 knots/lb., was not resized downward because of minimum gage constraints. As redesign proceeded, the front and rear beams of the pylon became equally flutter-effective. This change was accompanied by a noticeable change in the flutter mode shape, which initially involved components of the first wing bending mode and the store-pitch/wing-torsion mode, but later exhibited increasingly large components of the second wing bending mode as the store pitch frequency was increased. A net reduction in structural weight was achieved in the first combined flutter-strength redesign cycle (Figure 12.9) due to the fact that the initial fully stressed design was not fully converged (i.e., the stress ratios were not unity) and the subsequent strength redesign further reduced the weight of the structure in regions which were ineffective for flutter. Thus, the net weight reduction of 0.95 lb. in the first redesign cycle comprised an addition of 0.34 lb. for flutter speed improvement and a reduction of 1.29 lb. in the strength-critical regions of the structure.

Redesign for flutter appeared to be directed toward increasing the frequency of the store pitch mode and no structural elements were resized outboard of the wing store station. Resizing of wing structural elements inboard of the store station involved spar webs and the rib webs between the wing-to-pylon connection points (Figure 12.10). The resizing in the vicinity of the front wing-to-fuselage connection point accounted for a relatively small proportion of the overall weight increase. One of the most interesting results of this study was that the shear rigidity of the forward and rear spars was shown to be a more significant contributor to the overall store pitch stiffness than the wing covers.

Convergence to the final design point was achieved in eight combined flutter-strength redesign cycles (Figure 12.9), although a design very close to optimum was achieved after six cycles. The flutter speed target was achieved for only 8.42 lbs increase in weight. The distribution of this weight is tabulated below:

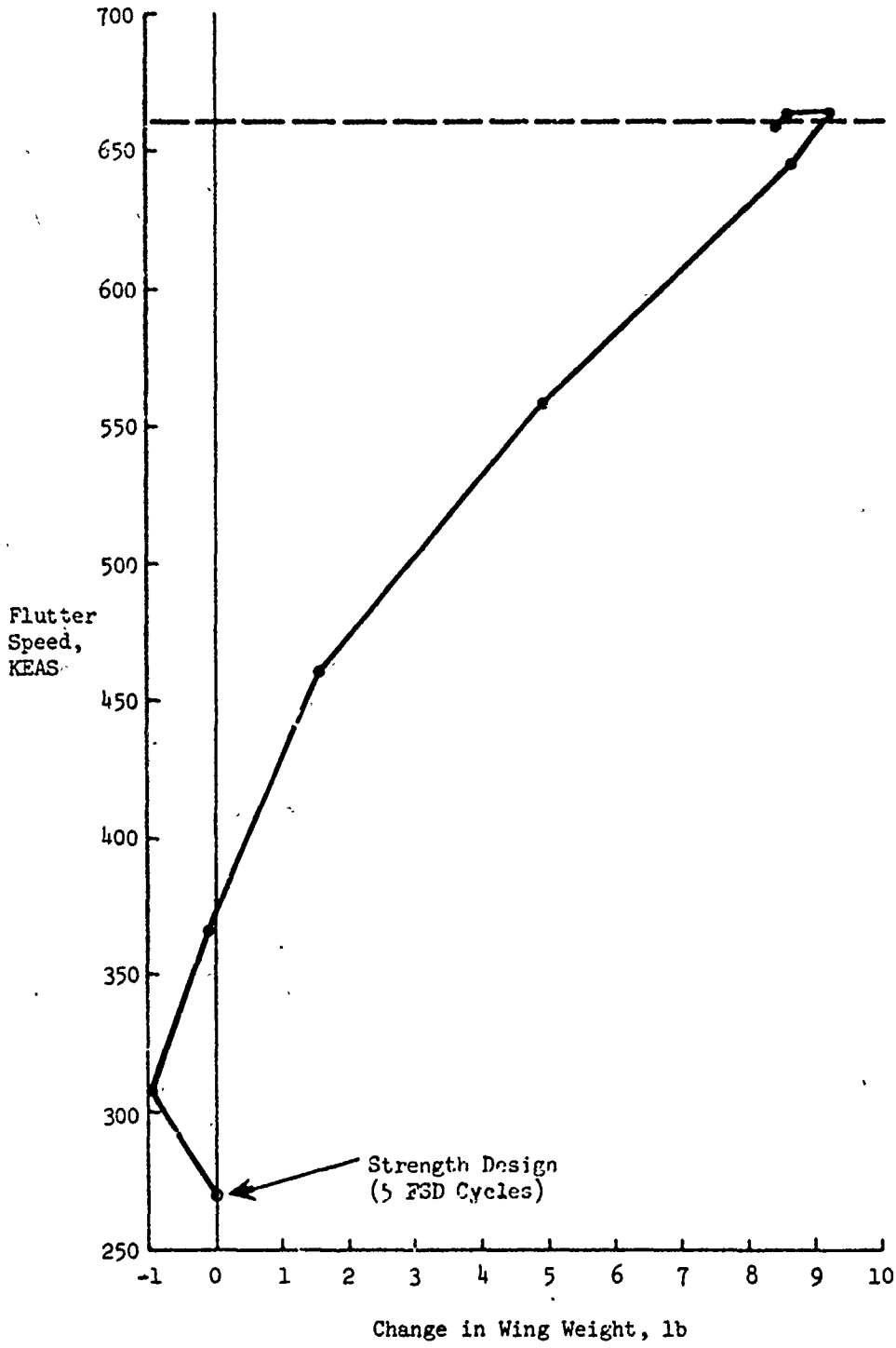

Figure 12.9 Results of Wing-with-Store Redesign Study

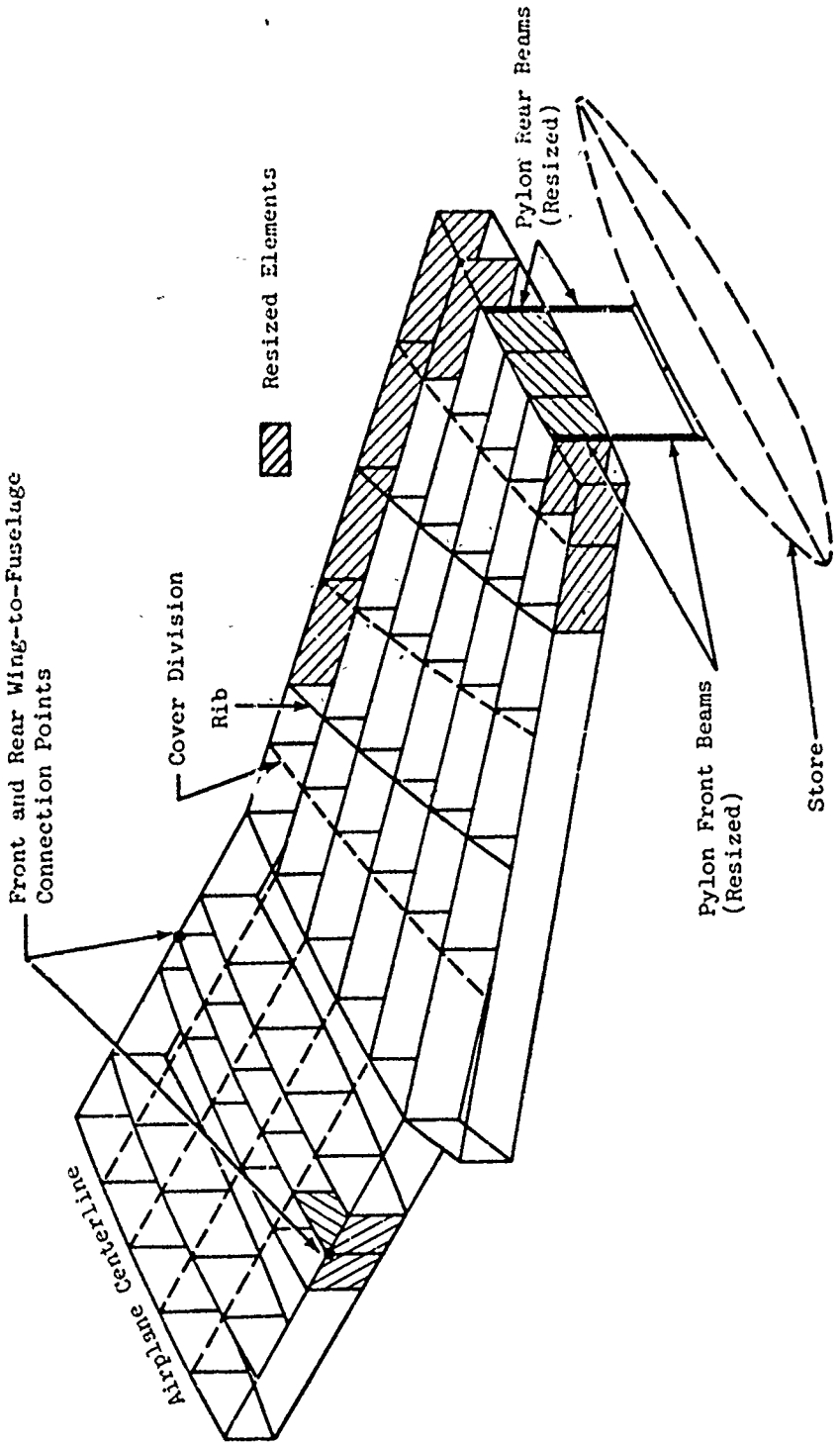

Figure 12.10. Structural Elements Resized to Achieve 390 Knot (144?) Increase in Flutter Speed, Wing-with-Store Model

Total weight increase for flutter-critical elements	=	10.35 lb.
(Weight increase for pylon alone	=	6.55 lb.)
Weight removed from strength-critical structure	=	1.93 lb.
Total weight increase from FSD starting point	=	8.42 lb.

Although the net reduction in weight of the strength-critical structure was relatively insignificant, a redistribution of cover material was noted in the inboard wing sections. Consequently strength resizing (1 FSD cycle) was accomplished in all but two of the redesign cycles. In the other two cycles, SOP was simply used to recompute a revised flexibility matrix for vibration mode calculations.

A second redesign study was initiated using both structural design variables and three mass balance design variables located at dynamic nodes 6, 9, and 55 (see Figure 11.6). Twenty pounds of mass balance was arbitrarily added at each dynamic node before initiating redesign. The flutter speed of the fully stressed design increased from 270 knots to 290 knots as a result of this mass addition. It was noted that the initial flutter-velocity derivatives of all masses were very close to zero. Consequently they were eliminated in the subsequent redesign analysis.

REFERENCES

Section 1

1-1 Kennapel, G. J., Mason, P. W., and Rosenbaum, J. D., "IDEAS, Integrated Design and Analysis System," Paper No. 670728, presented at Society of Automotive Engineers, Aeronautic and Space Engineering and Manufacturing Meeting, Los Angeles, California, October 7-11, 1967.

1-2 Grisham, A. F., "The American SST Internal Loads Analysis Methods and Procedures," Third Conference on Matrix Methods in Structural Mechanics, sponsored by AFFDL and AFIT, Wright-Patterson AFB, October 19-21, 1971.

1-3 Dwyer, W. J., Emerton, R., and Ojalvo, I., "An Automated Procedure for the Optimization of Practical Aerospace Structures, Vol. I - Theoretical Development and User's Information, Vol. II - Programmer's Manual," AFFDL-TR-70-118, April 1971.

Section 3

3-1 Dulmovits, J., "A Lifting Surface Method for Calculating Load Distributions and the Aerodynamic Influence Coefficient Matrix for Wings in Subsonic Flow," Grumman Aerospace Corporation Report No. ADR 01-02-64.1, August 1964.

3-2 Evvard, J. C., "Use of Source Distributions for Evaluating Theoretical Aerodynamics of Thin Finite Wings at Supersonic Speeds," NACA Report No. 951, 1950.

3-3 Mugler, J. P., "Calculation of Aerodynamic Loading and Twist Characteristics of a Flexible Wing at Mach Numbers Approaching 1.0 and Comparison with Experiment," NASA TR R-58, 1960.

3-4 Zlotnick, M. and Robinson, S. W., Jr., "A Simplified Mathematical Model for Calculating Aerodynamic Loading and Downwash for Wing-Fuselage Combinations with Wings of Arbitrary Planform," NACA TN 3057, 1954.

3-5 Evvard, J. C., "Distribution of Wave Drag and Lift in the Vicinity of Wing Tips at Supersonic Speeds," NACA TN 1382, 1947.

Section 4

4-1 Dwyer, W. J., Emerton, R., and Ojalvo, I., "An Automated Procedure for the Optimization of Practical Aerospace Structures, Vol. I - Theoretical Development and User's Information, Vol. II - Programmer's Manual," AFFDL-TR-70-118, April 1971.

4-2 Dwyer, W., Rosenbaum, J., Shulman, M., Pardo, H., "Fully Stressed Design of Airframe Redundant Structures," presented at the Air Force Second Conference on Matrix Methods in Structural Mechanics, October 1968.

4-3 Salvadori, M. G. and Baron, M. L., Numerical Methods in Engineering, Prentice-Hall Inc., 1959.

Section 7

7-1 Wilkinson, J. H., The Algebraic Eigenvalue Problem, Clarendon Press, Oxford, 1965.

Section 8

8-1 Hassig, H. J., "An Approximate True Damping Solution of the Flutter Equation by Determinant Iteration," Journal of Aircraft, Vol. 8, No. 11, November 1971.

8-2 Hsu, P. T., "Calculation of Pressure Distributions for Oscillating Wings of Arbitrary Planform in Subsonic Flow by the Kernel Function Method," MIT Aeroelastic and Structures Reserach Laboratory Report 64-1, October 1957.

8-3 Hildebrand, F. B., Introduction to Numberical Analysis, pp. 312-357, McGraw-Hill Co. Inc., New York, 1956.

8-4 Golub, G., "Numerical Methods for Solving Least Squares Problems," Numerische Mathematik, Vol. 7, pp. 206-216, 1965.

8-5 Householder, A. S., "Unitary Triangularization of a Nonsymmetric Matrix," Journal of the Association of Computing Machinery, Vol. 5, pp. 339-342, 1958.

8-6 Cunningham, A. M., Jr., "A Rapid and Stable Steady Subsonic Collocation Method for Solving Lifting-Surface Problems by the Use of Quadrature Integration," AIAA Paper No. 70-191, presented at the AIAA 8th Aerospace Sciences Meeting, New York, January 1970.

8-7 Zartarian, G. and Hsu, P. T., "Theoretical Studies on the Prediction of Unsteady Supersonic Airloads on Elastic Wings," Parts 1 and 2, WADC TR 56-97, February 1956.

8-8 Pines, S., Dugundji, J., Neuringer, J., "Aerodynamic Flutter Derivatives for a Flexible Wing with Supersonic and Subsonic Edges," Journal of the Aeronautical Sciences, Vol. 22, No. 5, May 1955, pp. 693-700.

8-9 Abramowitz, M. and Stegun, I. A., Handbook of Mathematical Functions with Formulas, Graphs and Mathematical Tables, National Bureau of Standards, Applied Mathematics Series 55, November 1964.

8-10 Evvard, J. C., "Distribution of Wave Drag and Lift in the Vicinity of Wing Tips at Supersonic Speed," NACA Technical Note 1382, July 1947.

8-11 Giesing, J. P., Kalman, T. P., Rodden, W. P., "Subsonic Unsteady Aerodynamics for General Configurations, Part I.-Direct Application of the Nonplanar Doublet-Lattice Method," AFFDL-TR-71-5, Part I, February 1971.

8-12 Wilkinson, J. H., The Algebraic Eigenvalue Problem, Clarendon Press, Oxford, 1965.

Section 9

9-1 Wilkinson, K., Lerner, E., and Taylor, R.F., "Practical Design of Minimum Weight Aircraft Structures for Strength and Flutter Requirements," AIAA Paper No. 74-986, presented at the AIAA 6th Aircraft Design, Flight Test, and Operations Meeting, Los Angeles, California, August 1974.

9-2 Rudisill, C.S., and Bhatia, K. G., "Optimization of Complex Structures to Satisfy Flutter Requirements," AIAA Journal, Vol. 9, No. 8, August 1971.

REFERENCES (Continued)

9-3 Siegel, S., "A Flutter Optimization Program for Aircraft Structural Design." AIAA Paper No. 72-795, presented at the AIAA 4th Aircraft Design, Flight Test, and Operations Meeting, Los Angeles, California, August 1972.

9-4 Gwin, L.B., and Taylor, R. F., "A General Method of Flutter Optimization," AIAA Journal, Vol. 11, No. 12, December 1973, pp. 1613-1617.

9-5 Zoutendijk, J., Methods of Feasible Directions, Elsevier Press, Amsterdam, Holland, 1960.

★ U. S. GOVERNMENT PRINTING OFFICE 1975 — 657-019/467

SUPPLEMENTARY

INFORMATION

DEPARTMENT OF THE AIR FORCE

WRIGHT LABORATORY (AFMC)
WRIGHT-PATTERSON AIR FORCE BASE OHIO

ERRATA AD-B009874 1 Feb 96

MEMORANDUM FOR Defence Technical Information Center
8725 John J. Kingman Road, Suite 0944
Ft. Belvoir, VA 22060-6218

FROM: WL/DORT, Bldg 22
2690 C St Ste 4
Wright-Patterson AFB, OH 45433-7411

SUBJECT: Notice of Changes in Technical Report(s) AD B009874, AD B009781, AD B029162, AD B029330.
Please change subject report(s) as follows:

AFFDL-TR-75-137, Vol 1 (AD B009874): has been cleared for public release (State A).

AFFDL-TR-75-137, Vol II (ADB009781): has been cleared for public release (State A).

AFFDL-TR-78-50, Vol I (ADB029162): has been cleared for public release (State A).

AFFDL-TR-78-50, Vol II (ADB029330): has been cleared for public release (State A).

WL-TR-95-8014 (printed in Jan 95): Distribution statement should read as C - (B208 214) Dist. authorized to US Gov Agencies and their contractors...

WL-TR-95-8015(printed in Jan 95): should read as Distribution Statement C - (15206 558) Dist. authorized to US Gov agencies and their contractors....

ERRATA
AD-B009874

Joseph A. Burke

JOSEPH A. BURKE, Team Leader
STINFO and Technical Editing
Technical Information Branch